Reviews in Mineralogy & Geochemistry
Vol. 81 pp. 489-578, 2016

Petrogenesis of the Platinum-Group Minerals

Brian O'Driscoll

School of Earth, Atmospheric & Environmental Science
The University of Manchester
Williamson Building, Oxford Road
Manchester M13 9PL
UK

brian.odriscoll@manchester.ac.uk

José María González-Jiménez

Department of Geology and Andean Geothermal Center of Excellence (CEGA)
Facultad de Ciencias Físicas y Matemáticas
Universidad de Chile
Plaza Ercilla #803, Santiago de Chile
Chile

jmgonzj@ing.uchile.cl

INTRODUCTION

The platinum-group minerals (PGM) are a diverse group of minerals that concentrate the platinum-group elements (PGE; Os, Ir, Ru, Rh, Pt, and Pd). At the time of writing, the International Mineralogical Association database includes 135 named discrete PGM phases. Much of our knowledge of the variety and the distribution of these minerals in natural systems comes from ore deposits associated with mafic and ultramafic rocks and their derivatives (see also Barnes and Ripley 2016, this volume). Concentrations of PGM can be found in layered mafic–ultramafic intrusions. Although they don't typically achieve ore grade status, supra-subduction zone upper mantle (preserved in ophiolite) lithologies (i.e., chromitite [>60 vol.% Cr-spinel], pyroxenite) characteristically host a diversity of PGM assemblages as well (Becker and Dale 2016, this volume). Occurrences of the PGM in layered intrusions, ophiolites, and several other important settings will all be described in this review.

In keeping with the general theme of this volume, the focus of this chapter is on relatively high-temperature (magmatic) settings. This is not a straightforward distinction to make, as PGM assemblages that begin as high-temperature parageneses may be modified at much lower temperatures during metamorphism, hydrothermal processes or surficial weathering (e.g., Hanley 2005). However, the vast majority of the published literature on PGM petrogenesis is based on occurrences from magmatic environments, an understandable bias given the importance of the major ore deposits that occur in some layered mafic–ultramafic intrusions, for example. For that reason, the emphasis of this review will be on high-temperature magmatic settings, with the understanding that lower temperature (sub-solidus; <600 °C) processes can modify primary PGM assemblages. The geochemical behavior of the platinum-group elements (PGE) in magmatic settings is highly chalcophile and not, as might be expected, highly siderophile. This is because most terrestrial magmatic systems are relatively oxidized, such that native Fe is not stable. A consequence of this is that the PGE have very high partition coefficients for sulfide in magmatic environments. From the high-temperature perspective, the degree of mantle melting and the manner in which magma fractionation proceeds,

1529-6466/16/0081-09$10.00 http://dx.doi.org/10.2138/rmg.2016.81.09

whether or not sulfide separation and fractionation has occurred, and the way in which late-stage (metasomatic) alteration has affected the rocks, if at all, are each potentially important processes in determining the PGM assemblage that forms. In particular, the relevance of the separation, accumulation, and crystallization of sulfide liquid (and/or arsenide liquid) in silicate magma systems, with respect to the timing of PGM crystallization, is a crucial issue.

The PGE constitute most of the highly siderophile elements (HSE; Os, Ir, Ru, Rh, Pt, Pd, Re, Au). While the HSE have and are being applied to addressing first order problems in Earth and planetary evolution, as outlined throughout this volume, outstanding concerns remain regarding the small-scale siting of the HSE in rocks. Specifically, the control exerted by the different types of PGM on bulk concentrations and relative distributions of the PGE in rock samples is presently an avenue of active investigation. Of critical but relatively unknown importance is the interplay between the high-temperature processes listed above, and the way in which these operate to produce a particular PGM assemblage. The PGE are generally considered to be relatively resistant to geochemical processes that fractionate and modify the lithophile elements in silicate and non-silicate rocks (Walker 2009). However, the petrogenetic links between the PGM and other non-silicate minerals (i.e., oxides such as chromite, base-metal sulfides, arsenides, and antimonides) remain unclear in many natural samples. One reason for this is that some of the PGE in a sample may hypothetically exist in solid solution in minerals such as sulfides or oxides, whilst others form discrete PGM. Progress in unravelling these issues has been made with the advent of high precision microbeam techniques, such as LA-ICP-MS, where trace element concentrations and isotopic information (e.g., $^{187}Os/^{188}Os$) can be collected from individual PGM, providing new information on their chronology and petrogenesis (Pearson et al. 2002; Malitch et al. 2003; Ahmed et al. 2006; Shi et al. 2007; Marchesi et al. 2011). Unfortunately, in most relevant natural materials, PGM grain sizes are too small (< 1 μm) for such analyses and uncertainties surrounding PGM crystallization processes persist.

The principal goals of this contribution are twofold: (1) to provide an overview of the principal PGM assemblages/parageneses in natural rock samples, including those from terrestrial as well as extraterrestrial environments. This includes highlighting, where possible and/or relevant, how these control whole-rock PGE budgets; (2) to provide the reader with a flavour of the processes (or combination of processes) responsible for the crystallization of PGM in different petrological environments. As noted above, this chapter is principally concerned with synthesizing observations on PGM occurrences that have been well-documented, so the emphasis is on mid-upper crustal mafic–ultramafic intrusions (including layered intrusions) and ophiolitic mantle. However, studies of secondary concentrations of PGM that are considered to be derived from high-temperature source material (i.e., placer deposits associated with ophiolites and zoned Uralian–Alaskan–Aldan-type complexes) have also contributed valuable information to our understanding of high-temperature PGM petrogenesis. For this reason, an appendix that summarizes some of the major findings of placer deposit studies is included with this chapter. The reader is also referred to reviews by Cabri and Feather (1975), Cabri (1981a, 2002) and Brenan and Mungall (2008).

PHASE RELATIONS AND ORIGIN OF THE PGM

Chemical properties of the PGM

The PGE are Group VIII transition metals, together with Fe, Cu, and Co. The PGE have melting points above that of Fe (1665 K), ranging from 1828 K for Pd to 3306 K for Os (Table 1). In their elemental form, Rh, Pd, Ir, and Pt (arranged in increasing Z) are cubic in symmetry (fcc), with Os and Ru being hexagonal (hcp). The electron configurations of the PGE are given in Table 1. They can exist in multiple valence states (0 to +8) and have

Table 1a. A compilation of some of the common natural PGM discussed in this review, organized according to mineral composition and complexity of bonding with other elements. Melting points, crystal structure and electron configuration details are also provided for the PGE. This table has been adapted and updated from Cabri (1981).

	Osmium	**Iridium**	**Ruthenium**
Melting T (K)	3306	2739	2607
Crystal structure	hcp	fcc	hcp
Electron configuration	$[Xe]4f^{14}5d^{6}6s^{2}$	$[Xe]4f^{14}5d^{7}6s^{2}$	$[Kr]4d^{7}5s^{1}$
S	Erlichmanite (OsS_2)	Xingzhongite $[(Pb,Cu,Fe)(Ir,Pt,Rh)_2S_4]$	Laurite (RuS_2)
		Kashinite $(Ir,Rh)_2S_3$	
		Cuproiridsite $CuIr_2S_4$	
As	Omeiite $[(Os,Ru)As_2]$	Iridarsenite $[(Ir,Ru)As_2]$	Anduoite $[(Ru,Os)As_2]$
			Ruthenarsenite [(Ru,Ni)As]
AsS	Osarsite [(Os,Ru)AsS]	Irarsite [(Ir,Ru,Rh,Pt)AsS]	Ruarsite (RuAsS)
Native metal	Osmium	Iridium	Ruthenium
PGE Alloys	Ir–Os	Os–Ir	
		Pt–Ir	
		Ru–Os–Ir	Os–Ir–Ru
		Chengdeite (Ir_3Fe)	

bonding behavior influenced by their overlapping *d*-orbitals. Their *d*-orbitals, in particular, are important for the formation of PGM because they consist of unpaired electrons that can form metal–metal bonds with other PGE, or covalent bonds with electron acceptors such as S. Thus, despite their differences in symmetry, the PGE can exist in solid solution with one another (Cabri 1981a), as well as combining with other siderophiles (e.g., Fe), chalcogenides (e.g., S, Te), and semi-metals (e.g., As, Sb). Native metals (minerals) composed of the PGE do not typically undergo phase transitions within temperature and/or pressure ranges of geological significance (Cabri 1981a) and the principal variable property, in addition to melting temperature (see Table 1), is the compositional range of solid solutions. Berlincourt et al. (1981) provide a detailed synthesis of the phase relations of the PGE. Examples of unary phases include the complete solid solution of Ir, Rh, Pd and Pt with Ni, and the complete solid solution of Os with Ru. More commonly, binary phases are formed between the individual PGE and each other, and elements including As, Bi, Cu, Fe, Hg, In, Ni, Pb, S, Sb, Se, Sn, and Te (see Table 1). Examples of known natural ternary and quaternary phases are also listed in Table 1. The PGE are characterized by their extreme affinity for metal phases, instead of oxides or silicates, and together with Au and Re, are referred to as the highly siderophile elements (HSE); the distribution coefficients of the PGE between metal and silicate are greater than 10^4 (Jones and Drake 1986; Holzheid et al. 2000; Fortenfant et al. 2003). The siderophilic character of the PGE is manifested by numerous occurrences (see also Brenan et al. 2016, this volume; Lorand and Luguet 2016, this volume), e.g., the high concentrations of PGE in iron meteorites, Fe–Ni metal alloys found in chondrites and the occurrence of many metal alloys as PGM (Table 1). The PGE may also have a tendency to exhibit chalcophile behavior, readily bonding with S, As, and other Group Va and VIa ligands.

Table 1b. A compilation of some of the common natural PGM discussed in this review, organized according to mineral composition and complexity of bonding with other elements. Melting points, crystal structure and electron configuration details are also provided for the PGE. This table has been adapted and updated from Cabri (1981).

	Rhodium	**Platinum**
Melting *T* (K)	2237	2041
Crystal structure	fcc	fcc
Electron configuration	$[Kr]4d^8 5s^1$	$[Xe]4f^{14}5d^9 6s^1$
S	Prassoite ($Rh_{17}S_{15}$)	Braggite (Pt,Pd,Ni)S
	Bowieite $(Rh,Ir,Pt)_2S_3$	Cooperite (PtS)
	Cuprorhodsite $(CuFe)Rh_2S_4$	Malanite $[Cu(Pt,Ir,Co)_2S_4]$
Te		Moncheite $[(Pt,Pd)(Te,Bi)_2]$
		Maslovite (PtBiTe)
As		Sperrylite ($PtAs_2$)
AsS	Hollingworthite [(Rh,Pt,Pd)AsS]	Platarsite [(Pt,Rh,Ru)AsS]
	Daomanite ($CuPtAsS_2$)	
Sb		Genkinite $[(Pt,Pd)_4Sb_3]$
		Geversite $[Pt(Sb,Bi)_2]$
		Stumpflite [Pt(Sb,Bi)]
Bi		Insizwaite $[Pt(Bi,Sb)_2]$
BiTi		Maslovite (PtBiTe)
Native metal	Rhodium (Rh)	Platinum (Pt)
PGE Alloys		Hongshiite (PtCu)
		Tetraferroplatinum (PtFe)
		Niggliite (PtSn)
		Rustenburgite $[(Pt,Pd)_3Sn]$
		Isoferroplatinum (Pt_3Fe)
		Tulameenite (Pt_2FeCu)

Extraterrestrial occurrences of the PGM

The distribution of the PGE during condensation of the solar nebula was governed by their relatively low vapor pressure (Palme 2008; Yokoyama and Walker 2016, this volume). Five of the six PGE are refractory, with condensation temperatures higher than that of Fe–Ni alloy. Only Pd, with the lowest melting temperature of the PGE, is non-refractory, condensing in solid solution with Fe–Ni. Platinum-group minerals may be found in carbonaceous chondrites (e.g., Fig. 1a,b), where they occur as refractory metal nuggets (RMN) that have traditionally been considered to be amongst the earliest condensates in the Solar System (Palme 2008). The RMN were first documented in calcium–aluminium inclusions (CAIs) in the CV3 chondrite, Allende (Palme and Wlotzka 1976; Wark and Lovering 1976). The RMN contain high but variable concentrations of the PGE (except Pd), together with Mo, W, Ni, and Fe. The presence of significant Mo

Table 1c. A compilation of some of the common natural PGM discussed in this review, organized according to mineral composition and complexity of bonding with other elements. Melting points, crystal structure and electron configuration details are also provided for the PGE. This table has been adapted and updated from Cabri (1981).

	Palladium	
Melting T (K)	1828	
Crystal structure	fcc	
Electron configuration	$[Kr]4d^{10}$	
S	Vysotskite [(Pd,Ni,Pt)S]	Vasilite $[(Pd,Cu)_{16}(S,Te)_7]$
Se	Oosterboschite $[(Pd,Cu)_7Se_3]$	Palladseite $[Pd_{17}Se_{15}]$
Te	Keithconnite $[Pd_{3-x}Te(x=0.14–0.43)]$	Merenskyite $[(Pd,Pt)(Te,Bi)_2]$
	Kotulskite [Pd(Te,Bi)]	Telluropalladinite (Pd_9Te_4)
	Telargpalite $[(Pd,Ag)_3Te]$	
As	Atheneite $[(Pd,Hg)_3As]$	Palladoarsenide (Pd_2As)
	Guanglinite $[Pd_{11}Sb_2As_2]$	Stillwaterite (Pd_8As_3)
	Majakite (PdNiAs)	
As,Sb	Arsenopalladinite $[(Pd_8(As,Sb)_3)]$	Palladodymite $[(Pd,Rh)_2As]$
	Isomertieite $(Pd_{11}Sb_2As_2)$	Mertieite-II $[Pd_8(Sb,As)_3]$
Sb	Stibiopalladinite (Pd_5Sb_2)	Sudburyite [(Pd,Ni)Sb]
SbAs	Isomertieite $(Pd_{11}Sb_2As_2)$	Mertieite-II $[Pd_8(Sb,As)_3]$
SbTe	Borovskite (Pd_3SbTe_4)	Testibiopalladite [PdTe(Sb,Te)]
Bi	Froodite $(PdBi_2)$	Sobolevskite (PdBi)
	Padmaite (PdBiSe)	Urvantsevite $[Pd(Bi,Pb)_2]$
	Polarite [Pd,(Bi,Pb)]	
BiTe	Michenerite ([Pd,Pt)BiTe]	
AsBi	Palladobismutharsenide $[Pd_2(As,Bi)]$	
Pb	Plumbopalladinite (Pd_3Pb_2)	Zvyagintsevite (Pd_3Pb)
Hg	Potarite (PdHg)	
HgTe	Temagamite (Pd_3HgTe_3)	
Native Metal	Palladium (Pd)	
PGE Alloys	Skaergaardite (PdCu)	Nielsenite $(PdCu_3)$
	Atokite $[(Pd,Pt)_3Sn]$	Cabriite Pd_2SnCu
	Palarstanide $[Pd_8(Sn,As)_3]$	Taimyrite $[(Pd,Cu,Pt)_3Sn]$
	Paolovite $[Pd_2Sn]$	Stannopalladinite $[(Pd,Cu)_3Sn_2]$

(up to 40 wt.%) and W in the RMN distinguishes them from terrestrial PGM and was originally interpreted as reflecting their formation via condensation from the solar nebula under relatively reducing conditions (possibly several orders of magnitude lower than the Iron–Wüstite f_{O_2} buffer; Simon et al. 2005), in the temperature range 1600–1400 K at ~10^{-4} bar (Palme and Wlotzka 1976; Campbell et al. 2001; Berg et al. 2009). This is because if the RMN were residues of extensive heating and vaporization, W and Mo would likely be lost as volatile oxides (Palme 2008).

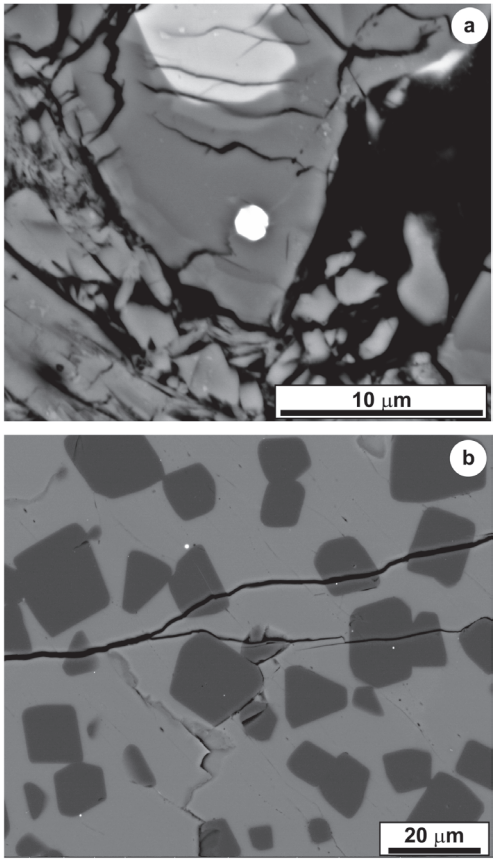

Figure 1. (a) Back scatter electron micrograph depicting Pt–Ru–Fe nugget (bright phase at image center) included in compositionally zoned melilite (Allende CV3). Image courtesy of Dr Glenn MacPherson, Smithsonian Institution (USA). (b) Numerous refractory metal nuggets (white spots) enclosed in a type B1 CAI from the Allende meteorite. The equant dark gray minerals are spinel and the light gray phase is melilite. Image courtesy of Dr Daniel Schwander, University of Mainz (Germany).

In documenting the occurrences of CAI-hosted RMN in the CV3 meteorites Allende and Leoville, El Goresy et al. (1978) noted two principal textural occurrences. The first is as isolated Pt-dominated nuggets, the second as 'Fremdlinge', a term introduced by El Goresy et al. (1978) to describe a complex opaque mineral-bearing paragenesis. In addition to RMN, Fremdlinge contain Fe–Ni metal, sulfides (e.g., Fe, Ni-dominated sulfides, MoS_2, WS_2), Ca-phosphates, and silicates (including volatile-bearing silicates such as nepheline and sodalite), oxides, and tungstates. It was originally speculated that Fremdlinge might have a presolar origin (El Goresy et al. 1978), but this has been subsequently shown to be unlikely, for the Allende examples at least, which yielded solar isotopic ratios of Mg, Fe, Mo, Ru, and W (Hutcheon et al. 1987). Isotopic data for the texturally isolated RMN are more limited (i.e., one for Ru and another for Os; Hutcheon et al. 1987 and Berg et al. 2009, respectively), but no isotopic anomalies were found. Palme et al. (1994) argued for condensation of the RMN as a single refractory metal alloy phase. They interpreted Fremdlinge as the product of oxidation and sulfidation of initially homogeneous grains, with the associated molybdenite (MoS_2) and scheelite ($CaWO_4$) being considered as secondary metasomatic products. A contrasting model suggests that since refractory metals occur in one of three different crystal structure types (*hcp* alloys of Ru and Os, *bcc* alloys of Mo and W and *fcc* alloys of Ir, Fe, and Ni), Fremdlinge may represent the product of subsequent mixing of these components (Sylvester et al. 1990). Additional studies of meteorites

including the CM2 Murchison, CV3 Allende and CM Paris chondrites (Blander et al. 1980; Berg et al. 2009; Schwander et al. 2011, 2012, 2013; Harries et al. 2012; Hewins et al. 2014) revealed that they are all observed or inferred to be associated with CAIs. Harries et al. (2012) carried out detailed crystallographic and compositional studies of RMN from the Murchison meteorite and argued that their typically homogeneous nature along with their well-defined crystal habits and crystal structures supported equilibrium condensation in the solar nebula, consistent with the proposals of Palme et al. (1994) and Berg et al. (2009). In a detailed textural and mineralogical study of CAIs from the Paris meteorite, Hewins et al. (2014) report that RMN occur exclusively inside CAI or attached to various disrupted CAI minerals, e.g., hibonite ($(Ca,Ce)(Al,Ti,Mg)_{12}O_{19}$), perovskite ($CaTiO_3$), and spinel. There is an interesting compositional variation in the RMN depending on the host mineral. Specifically, the most refractory RMN (Os and Ir ≈ 47.4 and 37.2 wt.%, respectively) are observed in hibonite. The RMN in the perovskite + Al-spinel host are Os–Ir–Mo–Ru alloys, whilst those in spinel (remote from perovskite) are enriched in Pt (i.e., up to 29 wt.%) and Rh. The RMN observed hosted in forsterite are Pt–Fe-rich alloys. The largest CAI studied by Hewins et al. (2014) contained tens of evenly distributed RMN (100 nm to < 1 μm in diameter) that appear to occur preferentially in Y-rich perovskite.

The experimental data of Schwander (2014) suggests that the condensation model may not be universally appropriate for RMN, and indicates that a silicate liquid enriched in refractory metals might have precipitated these phases (see also Cottrell and Walker 2006). This notion is supported by Rudraswami et al. (2014), who observed that RMN in cosmic spherules (collected from the Indian Ocean seafloor) formed during melting and oxidation on atmospheric entry. Croat et al. (2013) argued that if the RMN are the products of high-temperature condensation processes, they might also be expected to be present as inclusions in pre-solar graphite. Samples of the carbonaceous chondrites Murchison (CM2) and Orgueil (CI) yielded four Os-, Ru-, and Mo-rich RMN inclusions from four different pre-solar graphites. The RMN themselves are too small (30–50 nm) for isotopic analyses. However, Croat et al. (2008) presented C isotope data that indicate a pre-solar origin for the graphite, which in conjunction with the textural configuration suggests that the RMN inclusions are pre-solar too. Croat et al. (2013) consequently argued against the assumption that all isolated RMN in carbonaceous chondrites are necessarily solar in origin.

Several studies have reported the presence of RMN in martian meteorites, and attributed these to relatively late-stage processes (with respect to Solar System formation). For example, Lorand et al. (2012) have documented Fe–Os–Ir–(Ru) alloys several hundred nm in diameter associated with Ni-poor troilite in the martian meteorite NWA 2737, which they ascribed to a reduction of S in Fe-sulfides, driven by sulfur degassing. Lorand et al. (2014) also reported Ir–(Os)–As–S- and Os–S-rich compounds in the martian regolith breccia (NWA 7533), that may represent remnants of heavily bombarded ancient martian crust. The latter studies indicate that processes operating on the crusts and mantles of other planets in the Solar System are capable of forming PGM too. More generally, it is worth noting that the parent bodies of many differentiated meteorites are considered to have lower f_{O_2} than Earth, such that Fe–Ni metal may be present for the PGE to partition into (Day et al. 2016, this volume). This might result in significantly different PGM assemblages than those found on Earth.

Origin of the terrestrial PGM: Mantle melting, metasomatism, and metal transfer

The crustal abundance and distribution of the PGE in the present-day Earth are the result of a combination of processes that occurred during mantle melt extraction and the geological evolution of plate tectonics. Specifically, the way in which mantle melting has mobilized and transported the PGE is a significant factor in accounting for the distribution of these elements in natural (accessible) geological materials (see also Lorand and Luguet 2016, this

volume). Despite the overwhelming preponderance of silicate minerals, particularly olivine (55–90 vol.%) in the upper mantle (Lorand et al. 2008), there is a breadth of experimental and geochemical evidence suggesting that silicates do not significantly contribute to the overall PGE budget of the mantle (Hart and Ravizza 1996; Burton et al. 1999; Harvey et al. 2010). For example, even though the partitioning of Ir into olivine (as Ir^{2+}; Brenan et al. 2005) has been experimentally demonstrated, only trace concentrations (0.03–0.1 ppb; $ng.g^{-1}$) of the PGE have been measured in mantle olivine (Lorand et al. 2008). It has been estimated that <10% of the PGE abundances of typical mantle peridotites is controlled by their constituent silicate phases (Handler and Bennett 1999; Burton et al. 2002; Lorand et al. 2008). However, it is possible that the f_{O_2} conditions under which the substitutions above were recorded are significantly higher than those governing mantle melt production (ΔFMQ = +1.4 to 5.4 vs. –1 to –3; Ballhaus 1995). The compatibility of the PGE in olivine (i.e., Ir and Ru; Mungall and Brenan 2014) thus continues to be considered as viable, highlighting that the role of silicate in hosting mantle PGE requires further investigation. Accessory chromite is also a refractory phase during mantle melting and has been considered as a host for the PGE. The substitution of Ru^{3+} (or Ru^{4+}) and Rh^{3+} into chromite has been proposed (Capobianco and Drake 1990; Righter et al. 2004) and absolute concentrations of Ir, Ru, and Rh in the range of tens of ppb in chromite have been reported (Capobianco and Drake 1990; Righter et al. 2004; Brenan et al. 2005, 2012). In addition, concentrations of ~500 ppb Ru have been measured in komatiite chromite (Locmelis et al. 2011). However, as chromite typically occurs as an accessory phase (1–2 vol.%) in mantle peridotites, it is probably responsible for only a few percent of the bulk rock mantle PGE budget (Carlson 2005; Luguet et al. 2007). It is therefore unlikely that chromite is the dominant control on PGE in the upper mantle.

The upper mantle, particularly the sub-continental lithospheric mantle (SCLM) also commonly contains base-metal (Fe–Cu–Ni) sulfides as accessory phases. In the absence of metal phases, the PGE are chalcophilic and sulfides are widely considered to be significant carriers of PGE in the mantle (Cabri 1981a; Mitchell and Keays 1981; Barnes et al. 1985; Alard et al. 2002; Carlson 2005; Lorand et al. 2008). The abundances of the PGE in common mantle sulfide phases are typically at the ppm ($\mu g.g^{-1}$) level, three orders of magnitude higher than typical bulk rock mantle peridotite concentrations (Morgan 1986; Pattou et al. 1996; Burton et al. 2002; Lorand et al. 2008). Sulfide melt–silicate melt partition coefficients of 10^3–10^6 have been reported for the PGE (Fleet et al. 1993; Roy-Barman et al. 1998; Ballhaus et al. 2006; Mungall and Brenan 2014), signifying that it is the behavior of sulfide during mantle melting that exerts the greatest control on PGE concentration and distribution. Thus, the degree of partial melting and tectonic setting must exert considerable influence on whether sulfides and their PGE are retained in the mantle or not. High degrees of mantle melting, such as are thought to have occurred during the production of Archean komatiites and which are also manifest in some supra-subduction zones in the geological record, have the potential to liberate mantle sulfides originally held as Fe-rich monosulfide solid solution (mss). Experimental work indicates that mss is the first phase to crystallize from a sulfide liquid, followed by intermediate solid solution (iss), which crystallizes from a more fractionated Cu-rich sulfide liquid. By contrast, the low degrees of partial melting that are typical of mid-ocean ridge basalts (MORB) would favor the retention of sulfides in the mantle residue, as the melts produced are already S-saturated. Thus, MORB magmas tend to be PGE-poor (Bézos et al. 2005). However, these issues are further complicated by the fact that mantle peridotites have been observed to contain multiple sulfide populations, separable on the basis of microstructural, chemical, and isotopic criteria (see also Harvey et al. 2016, this volume). For example, numerous studies (e.g., Alard et al. 2000; Lorand and Alard 2001; Pearson et al. 2002; Bockrath et al. 2004a,b; Harvey et al. 2011) have reported Os–Ir–Ru and Rh–rich mss inclusions in olivine with depletions in the PPGE (i.e., Pt and Pd). The formation of these sulfides has been attributed to separation

of an immiscible sulfide melt fraction (i.e., droplets, tens of μm in diameter) during an early silicate melt extraction event (Holzheid 2010). The interstitial and intergranular regions of the peridotites may contain a second population of Pd–Re-enriched sulfides (Alard et al. 2002; Bockrath et al. 2004a,b; Harvey et al. 2011), whose occurrence has been attributed to relatively late-stage metasomatism. Unlike the former variety, these interstitial sulfides are more prone to subsequent mobilization and processing, as they are not 'armored' by olivine crystals. Building on the work of Alard et al. (2002), Harvey et al. (2011) carried out a detailed study of Kilbourne Hole spinel lherzolites and showed that the secondary metasomatic sulfides readily contribute their enhanced PPGE + Re (and consequently radiogenic ^{187}Os) to partial melts. By contrast, it is only via protracted and high degrees of partial melting that the silicate-hosted sulfides will be dissolved in the silicate melt, providing a mechanism by which materials enriched in the IPGE (i.e., Os, Ir, and Ru) can be included in mantle melting.

Experimental studies have suggested that the PGE are not equally soluble in base-metal sulfides (Mackovicky et al. 1986; Barnes and Francis 1995; Tredoux et al. 1995; Mungall et al. 2005). The following increase in order of the PGE partition coefficients into sulfide liquid has been suggested: Au~Os~Ir~Ru < Pt < Rh < Pd (Barnes and Francis 1995; Tredoux et al. 1995). Mackovicky et al. (1986) reported that the sulfide melt precursor of pentlandite [$(Fe,Ni)_9S_8$] and Cu-sulfide can accommodate up to 15 wt.% Pt. Borisov and Palme (2000) showed that the PGE content of mantle-derived magmas crystallizing at or below FMQ is still high enough for them to be saturated in Ru + Ir-bearing alloys, and Pt–Fe saturation is also likely (see also Mungall and Brenan 2014). Ballhaus (1995) suggested that in the shallow fertile mantle, the bulk of the IPGE reside in mss, this being governed by high sulfide/silicate partition coefficients. However, he suggested that following partial melting and the removal of sulfide with the melt, metal phases might be stabilized with decreasing f_{O_2} and f_{S_2}. Support for this comes from the detailed study of highly depleted (sulfide-free) spinel harzburgites from the Lherz massif by Luguet et al. (2007), which showed that whilst the major minerals (silicates and oxides) account for up to 30% of the bulk rock PGE budget, intergranular μm-to-sub-μm scale Ru–Os ± Ir sulfides and Pt–Ir ± Os alloys account for 50–100% of the PGE. Luguet et al. (2007) interpreted these alloys and PGE-sulfides as being residual phases that developed during complete extraction of base-metal sulfides by up to 24% partial melting of the protolith (see also Fonseca et al. 2012). The presence of PGM is not restricted to the SCLM. Luguet et al. (2003) reported Os–Ru alloys in Mid-Atlantic Ridge (MAR) sulfide-poor abyssal peridotites. Further evidence for the presence of PGM in oceanic peridotites comes from studies of ophiolite dunites, pyroxenites and chromitites (see below). It has been shown that at least some of the PGM population developed in ophiolite chromitites may be 'recycled' as xenocrystic grains during melt transport in the conduits that form the chromitite (Gonzalez-Jimenez et al. 2013a; Yang et al. 2014).

The transfer of the PGE from the mantle to crust is manifested in the variety of settings in which these precious metals are enriched. The following six sections are concerned with outlining the characteristics of the principal terrestrial settings of PGM mineralization and the diversity of the PGM observed therein. It is not possible in a review such as this to discuss every single reported example of PGM mineralization. However, we have endeavoured to be as thorough as possible with the details of important examples of ophiolites, layered mafic–ultramafic intrusions, subcontinental lithospheric mantle, Uralian–Alaskan–Aldan Complexes and Ni–Cu–PGE–sulfide deposits. Examples of less conventional PGM mineralization are also included, for breadth, but in keeping with the focus of this volume, exclusively low temperature PGM mineralization environments are not discussed in detail.

PGM IN LAYERED MAFIC–ULTRAMAFIC INTRUSIONS

Layered mafic–ultramafic intrusions (LMI) are generally taken to represent solidified magma chambers, and are typically the focal points of significant magmatic activity in anorogenic tectonic settings. The type examples of LMI are therefore associated with large igneous provinces (LIPs), which are considered to have developed during periods of significant continental break-up in the geological record. There are arguably fewer significant PGE deposits (in terms of variety of PGM) associated with LMI than there are with ophiolite chromitites and mantle peridotites (Barnes and Ripley 2016, this volume). However, there are an exceptional few LMI that contain the greatest concentrations of PGE on Earth. Indeed, the largest known layered intrusion, the Bushveld Complex (South Africa) contains >75%, >50% and >80% of the world's exploited Pt, Pd, and Rh, respectively (Naldrett 2004; Mungall and Naldrett 2008). Layered intrusions can be sub-divided on the basis of whether they represent open or closed system magma chambers. The most economically significant LMI in terms of PGE concentration predominantly contain cumulate sequences that preserve evidence for open system behavior, including the development of stratiform chromitite deposits. Type examples of such chromitites occur in the Bushveld Complex and the Stillwater Complex (Montana, USA). In both of the latter intrusions, the PGE are frequently, but not ubiquitously, associated with these chromitite seams (see below). Less commonly, closed-system LMI may also contain significant PGE enrichment (e.g., the Platinova Reef of the Skaergaard Intrusion, Greenland).

Consideration of the styles of PGE mineralization in LMI is important, in light of the issues of mantle melting discussed above. Layered intrusions are mostly the result of large degrees of partial melting of mantle that underlies continental crust, rather than the oceanic mantle sampled by ophiolite peridotites. Thus, they offer a complementary perspective on the way in which the PGE are transferred from mantle to crust relative to that observed in oceanic peridotites. Broadly speaking, the whole-rock PGE patterns associated with the most economically significant PGE-enriched LMI cumulates, including chromitites, exhibit positive slopes on chondrite-normalized plots (e.g., Fig. 2; see also Day et al. 2008; O'Driscoll et al. 2009a). This is primarily a function of the relative geochemically incompatible behavior of Pt and Pd compared to the IPGE so that magma chamber processes that form LMI cumulates concentrate the PPGE relative to their mantle source. However, it is worth mentioning that some chromitite deposits with relatively low total abundances of the PGE (e.g., the so-called sulfide-poor chromitites of the Bushveld Complex; Scoon and Teigler 1994) also have IPGE>PPGE. This highlights the danger of over-generalization in the interpretation of these deposits, i.e., layered intrusion chromitites may also exhibit PGE patterns with a negative slope on chondrite-normalized plots. Given the importance of the presence or absence of chromitite as a host lithology for PGE mineralization (*Supplementary Table* 1), it is useful to use this distinction as a criterion for sub-division of the following discussion of PGE reefs in LMI.

Chromitite-hosted layered intrusion PGM

The UG2 chromitite, Bushveld Complex. The 2054.4 ± 1.3 Ga Bushveld Complex is the largest known LMI on Earth, with an aerial extent of ~70,000 km^2 (Scoates and Friedman 2008). The stratigraphy of the Rustenburg Layered Suite of the Bushveld Complex is divided into the Marginal, Lower, Critical, Main and Upper Zones. The Upper Group 2 (UG2) chromitite occurs in the Upper Critical Zone and is the single largest PGE resource on Earth, with Pt grading at ~2.7 ppm and containing a combined $6{,}636 \times 10^6$ tons of measured, indicated and inferred ore (from D. Causey, quoted in Zientek 2012). The UG2 chromitite is broadly stratiform and is approximately 1 m thick, though it commonly comprises more than one seam. There is apparent intrusion-wide lateral and vertical heterogeneity in the absolute PGE abundances of the UG2 chromitite that is reflected in the variability of the PGM present (Schouwstra et al. 2000; Voordouw et al. 2010; Junge et al. 2014). However, where it has

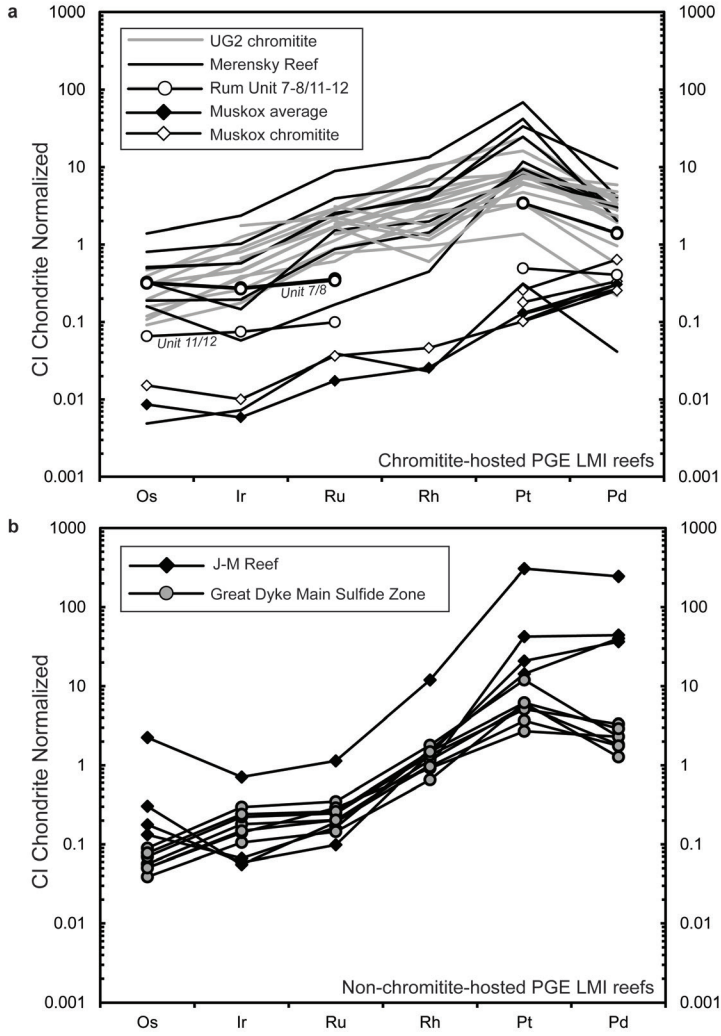

Figure 2. Chondrite-normalized PGE abundances of selected layered mafic–ultramafic intrusion PGE-ore bodies, divided into chromitite-hosted (a) and non-chromitite-hosted (b) reefs. The data plotted have been sourced as follows: UG2 chromitite (Bushveld Complex; Gain 1985, Voordouw et al. 2010, Junge et al. 2014); Merensky Reef (Bushveld Complex; Prichard et al. 2004); J-M Reef (Stillwater Complex; Godel and Barnes 2008a); Muskox chromitite reef (Barnes and Francis 1995); The Great Dyke Main Sulfide Zone (Oberthür et al. 2003; including samples from the position of the Pt peak, the Pd peak and the lowermost base-metal sulfide accumulation peak); Rum Layered Suite (the Unit 11/12 and Unit 7/8 samples are labelled; O'Driscoll et al. 2009a). Chondrite normalization values are from Naldrett and Duke (1980).

been studied closely, it appears that Pt sulfide, Pt–Pd sulfide, laurite (RuS_2), ferroplatinum (Pt,Fe), and Pt–Rh–Cu are consistently important components of the UG2 PGM population (Kinloch 1982; McLaren and De Villiers 1982; Penberthy and Merkle 1999; Schouwstra et al. 2000; Cawthorn et al. 2002; Voordouw et al. 2010; Junge et al. 2014). For example, McLaren and De Villiers (1982) documented ~6,000 PGM grains from 10 drill cores of both

the eastern and western limbs of the Bushveld. The most abundant PGM they documented were laurite, cooperite (PtS), Pt–Ir–Rh–Cu sulfide, braggite [(Pt,Pd,Ni)S], Pt–Pb–Cu sulfide, vysotskite [(Pd,Ni,Pt)S], and Pt–Fe alloy (see their Table 5 for relative distributions). In a recent study of drill core from the Karee Mine in the western limb of the Bushveld Complex, Junge et al. (2014) documented ~355 discrete PGM with grain sizes in the range <5–20 μm. The dominant phases are Pt–Fe alloys (30%), laurite (29%), cooperite–braggite (26%), and rare zvyagintsevite (Pd_3Pb) and potarite (PdHg). Petrographic examination of the PGM reveals that they typically occur at the margins of sulfide grains, which are themselves located at chromite triple junctions and grain boundaries (Junge et al. 2014). Only laurite is a commonly observed inclusion within chromite crystals, although it is more commonly found at the edges of chromite and sulfide grains. Junge et al. (2014) argued against early precipitation of laurite, suggesting that the textural relationships observed indicated co-precipitation with sulfide and chromite. A significant amount of the UG2 budget of Pd and Rh are hosted in pentlandite (maxima of 2.2 wt.% and 3 wt.%, respectively), to a much greater extent than the other PGE. Junge et al. (2014) also note the presence of rare malanite [$Cu(Pt,Ir,Co)_2S_4$], irarsite [(Ir,Ru,Rh,Pt)AsS], platarsite [(Pt,Rh,Ru)AsS], and sperrylite ($PtAs_2$). Together with laurite, Junge et al. (2014) suggest that Pt–Fe alloys and cooperite–braggite co-precipitated with chromite and sulfide, and were later modified by annealing at the postcumulus stage. Voordouw et al. (2010) carried out a detailed SEM–EDS study of the UG2 Reef from the Two Rivers Platinum Mine on the eastern limb of the Bushveld Complex. They documented >7,000 PGM which were divided among eight classes: cooperite, Pt–Pd sulfide (braggite, vysotskite), Pt–Rh–Cu sulfide, laurite, Pt–Fe alloy, PGE tellurides, PGE sulfarsenide phases, and PGE alloys. Voordouw et al. (2010) emphasized the vertical changes in PGM composition and distribution across their studied section (Fig. 3). The base of the main chromitite seam (1–2.5 m thick, at Two Rivers) contains >10 wt.% of each of Pt sulfide, laurite, Pt–Fe alloy, Pt–Pd sulfide, and Pt–Rh–Cu sulfide. The middle and top portions of this seam have >10 wt.% of the first four of these phases, but not Pt–Rh–Cu sulfide. The leader seam, a ~16 cm chromitite in the hanging wall of the UG2, contains a different PGM assemblage (Fig. 3), that is enriched in PGE–sulfarsenides and PGE alloys, relative to the main seam. The leader seam is also noteworthy for its high pentlandite and chalcopyrite ($CuFeS_2$) contents, whereas the main seam base–metal sulfide population is characterized by pyrrhotite ($Fe_{1-x}S$) and pyrite (FeS_2). Voordouw et al. (2010) conclude that the UG2 main seam represents a predominantly primary magmatic PGM assemblage, whereas the leader seam contains PGM that have been modified by secondary (metasomatic) processes. Peyerl (1982) also showed that the primary PGM mineralogy of the UG2 chromitite (i.e., Pt–Pd sulfide) may have been extensively modified (to a Pt–Fe and Pt–Pd–As–Sb-dominated mineralogy) as a result of volatile fluxing associated with emplacement of the Driekop dunite pipe in the eastern limb of the Bushveld. Given that the leader seam hosts a significant component of the mineable UG2 ore at certain localities, the observation that metasomatic processes may upgrade ore potential, by modification of the primary magmatic PGM assemblage and redistribution of the PGE, is an important one.

The Merensky Reef, Bushveld Complex. Like the UG2 horizon, the stratiform Merensky Reef occurs in the Upper Critical Zone of the Bushveld Complex, typically between 20–400 m above the UG2 chromitite. The Merensky Reef comprises 3373×10^6 tons of ore (measured, indicated and inferred), grading ~2.9 ppm Pt (from D. Causey, quoted in Zientek 2012). Strictly speaking, the bulk of the PGE mineralization does not occur within chromitite; the Merensky horizon comprises a coarse-grained (pegmatoidal) base-metal sulfide-bearing melanorite, typically on the order of 10–30 cm thick, sandwiched by an upper and a lower (1–3 cm) chromitite seam. However, those base-metal sulfides that occur in the chromitite seams contain approximately twice as much PGE as in the pegmatite (Godel et al. 2007). There has been a plethora of studies on the PGE-bearing phases of the Merensky Reef (e.g.,

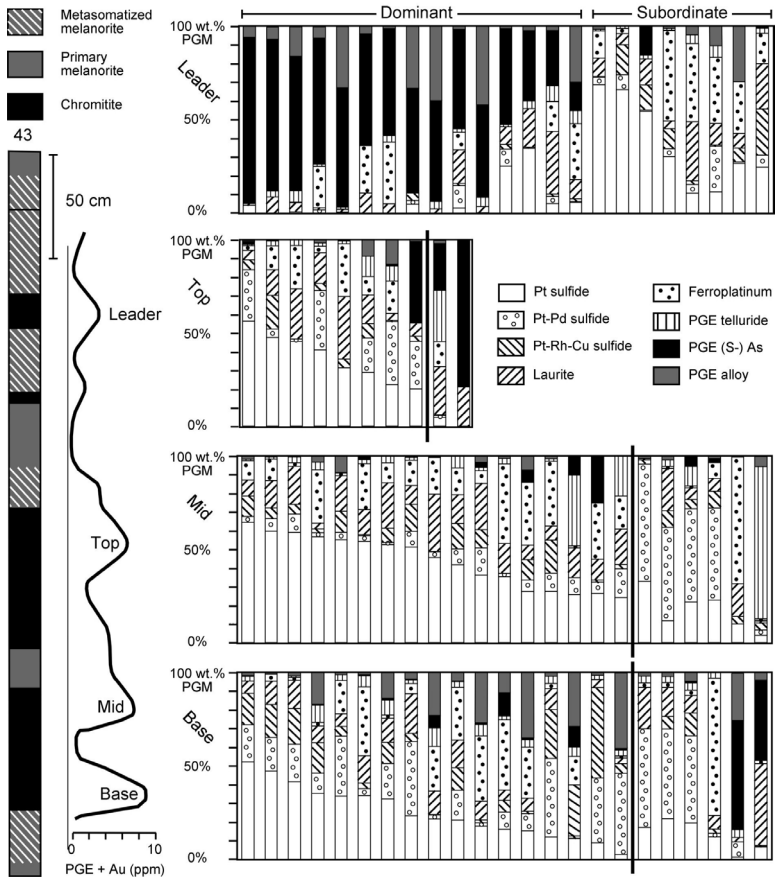

Figure 3. Stratigraphic section of the UG2 chromitite at the Two Rivers Platinum Mine, with corresponding stacked histograms illustrating the variation in whole-rock PGE abundances and PGM assemblage variation across the main seam and leader seams. This image is reproduced from Voordouw et al. 2010, having been previously published as their Figure 3. They analyzed 23 samples for each peak, except for the top of the main seam, which represents data collected from 10 samples. The image is reproduced with the permission of the author and Mineralium Deposita.

Brynard et al. 1976, Vermaak and Hendricks 1976, Kinloch 1982, Mostert et al. 1982, Peyerl 1982, Kinloch and Peyerl 1990; Prichard et al. 2004; Godel et al. 2007; Rose et al. 2011; Wirth et al. 2013) and the reader is referred to these studies for more detail than is provided here. A summary Table adapted and updated from that provided as Table II in Schouwstra et al. (2000) is provided as Table 2 here. Broadly, the dominant PGM are Pt–Fe alloys, Pt–Pd sulfides, laurite and Pt–Pd tellurides. However, like the UG2 chromitite, significant heterogeneity in the relative proportions of the PGM is observed along the lateral extent of the Merensky Reef. Some localities (i.e., at Union Mine on the western limb of the Bushveld) are dominated by (~80 vol.%) Pt–Fe alloys, whereas the Impala Mine to the south (also on the western limb of the Bushveld) is dominated (~56 vol.%) by Pt–Pd sulfides (Table 2). Mostert et al. (1982) investigated the PGM mineralogy of the Merensky Reef at the Impala platinum mines and identified 17 PGM phases in a population of 800 grains. They reported cooperite (44 vol.%), laurite (21 vol.%), moncheite ([(Pt,Pd)(Te,Bi)$_2$]; 17 vol.%), and braggite

Table 2. Volume percentage distribution of PGM in the Merensky Reef (Bushveld Complex) at a regional scale, organized by mine locality (arranged north to south for each limb)*. The bulk of the data is taken from Table 2 of Schouwstra et al. (2000), but updated with data from other sources (see table footnotes for details).

	Western Bushveld limb						
	Amandelbult	**Union**	**Boschkoppies (Bafokeng)**	**Impala Platinum****	**Rustenburg**	**Marikana*****	**Western Platinum**
PGM Groups							
Pt–Fe alloys	48.6	82.8	13.1	2	9.6	6	6.1
Pd alloys	0.2	0.4	2.3	<1	—	—	—
Pt-arsenides	4.1	0.3	39.9	2	6.4	50	51
Laurite	11.6	7	8	21	15.4	<1	—
Pt–Pd sulfides	20.7	2.3	29.4	56	31.6	17	17.3
Pt–Pd tellurides	13.3	6.7	6.5	17	33.5	21	21.4
Others	0.6	Trace	Trace	Trace	Trace	Trace	Trace
Electrum	0.9	0.5	0.7	2	3.5	4	4.1

	Eastern Bushveld limb			
	Lebowa	**Atok*****	**Two Rivers (L)#**	**Two Rivers (U)#**
PGM Groups				
Pt–Fe alloys	1.2	2	12.6	46.2
Pd alloys	Trace	—	—	—
Pt-arsenides	1.3	2	2.1	4.1
Laurite	6.8	5	9.1	7.1
Pt–Pd sulfides	70.9	85	39.1	9.0
Pt–Pd tellurides	19.1	5	33.4	29.4
Others	—	—	1.2	0.8
Electrum	0.7	—	2.5	3.3

*Data primarily from Table 2 of Schouwstra et al. (2000) (published, in turn, from mining company (Amplats) data), unless otherwise stated. **Data from Mostert et al. (1982). ***Data from Brynard et al. (1976) (in Mostert et al. 1982). Note that Lebowa and Atok are the same mine. #Data from Rose et al. (2011), for lower (L) and upper (U) occurrences of the Merensky Reef chromitite: reported in area% in that paper.

(12 vol.%) as the principal PGM present, ~84% of these minerals being associated with base-metal sulfides. More recently, Rose et al. (2011) showed that the total PGM inventory from the Two Rivers Mine in the eastern limb of the Bushveld is dominated by Pt-tellurides, Pt–Fe alloys, and minerals of the cooperite–braggite association [size of PGM, by area; maslovite ([PtBiTe]; 29.7%), isoferroplatinum ([Pt_3Fe]; 26.9%), braggite–cooperite (25.2%), and laurite (8.3%)]. Perhaps more intriguingly, a significant difference in the PGM populations of the upper and lower Merensky chromitites is also reported (see Table 2); >70% (by area) of the lower seam PGM are Pt–Pd sulfides and Pt–Pd tellurides, whereas >75% of the upper seam PGM (by area) comprise Pt–Fe alloys and Pt–Pd tellurides (Rose et al. 2011). The principal difference is thus in the respective abundances (by area) of the Pt–Pd sulfides, which comprise >48% of the PGM in the lower seam and ~16% of the upper seam PGM, and the Pt–Fe alloys; the latter comprising only ~13% of the lower seam but >45% of the upper seam. Cawthorn et al. (2002) make the point that there appears to be a greater concentration of PGE alloys in the north of the Bushveld intrusion, in comparison to the southern and eastern areas where PGE-sulfides and tellurides are more significant, an observation borne out by Table 2. Kinloch (1982) correlated the PGE character of the UG2 chromitite and the Merensky Reef at the regional scale, and showed that where the Merensky Reef shows a predominance of Pt–Pd sulfides in one section of the Bushveld, then the PGM population of the UG2 chromitite is also likely to be dominated by Pt–Pd sulfides. A similar observation holds for the distribution of Pt–Fe alloys. Kinloch (1982) interpreted this observation in terms of metasomatism of a primary magmatic PGM assemblage. He noted that close to intrusive pipe-like features (interpreted to be feeder conduits) and also to reef disturbances (i.e., the Merensky Reef potholes), Pt–Fe alloys tend to dominate the PGM assemblage. Kinloch (1982) suggested that the primary Pt–Pd sulfides had been converted to Pt–Fe alloys in these zones of enhanced volatile activity.

In general, the Merensky Reef PGM may be associated with sulfides or with primary and/or secondary silicates and occur both as inclusions within crystals and along grain boundaries (Cawthorn et al. 2002). For example, Prichard et al. (2004) note that there is no particular tendency for laurite to occur as inclusions within chromite; instead all 16 grains they observed were found in close proximity to base-metal sulfides. In their high-resolution X-ray computed tomography (CT) study of the Merensky Reef chromitites, Godel et al. (2010) reported a preponderance of PGM at chromite–silicate–sulfide triple junctions. The Merensky Reef base-metal sulfides have total average concentrations of the PGE of ~500 ppm, but given the fact that they occur in modal abundances greater than those of the PGM, their contribution to the total PGE budget of the ore deposit is deemed to be significant (Ballhaus and Ryan 1995). This generalization is supported by the observations of Godel et al. (2007), who showed that between 65% and 85% of the PGE budget of the reef is accounted for by PGM. Of the sulfides, pentlandite is the most important host for the precious metals, with total PGE concentrations of up to 600 ppm.

Several workers have carried out Re–Os [$^{187}Re \rightarrow {}^{187}Os + \beta^-$; $t_{½} = 41.6 \times 10^9$ yr] and Pt–Os [$^{190}Pt \rightarrow {}^{186}Os + \alpha$; $t_{½} = 469 \times 10^9$ yr] isotopic studies on base-metal sulfides and PGM from the Merensky Reef (Hart and Kinloch 1989; Schoenberg et al. 1999; Coggon et al. 2011a). In an extensive study, Hart and Kinloch (1989) obtained consistent and relatively radiogenic $^{187}Os/^{188}Os$ for 36 laurite grains (in the range 0.17–0.18). Additionally, they analyzed two erlichmanite (OsS_2) grains that yielded $^{187}Os/^{188}Os$ compositions of 0.11, a value consistent with that of the chondritic mantle at 2.06 Ga. Coggon et al. (2011a) analyzed several different PGM from the Merensky Reef (including laurite, cooperite, sperrylite, and Pt–Fe alloy) by LA-MC-ICPMS and found that their data defined a Pt–Os isochron with an age of 1995 ± 50 Ma, $^{186}Os/^{188}Os_{initial} = 0.11982 \pm 0.00001$ (2σ, MSWD = 1.16). The latter authors also used a single PGM grain of cooperite to calculate a ^{190}Pt–^{186}Os model age of 2024 ± 101 Ma. The model age and the isochron age are 30–59 Ma younger than the U–Pb zircon age for the Merensky Reef, explained by Coggon et al. (2011a) as reflecting late stage metasomatism of the ore body.

Petrogenesis of the Merensky Reef and the UG2 chromitite: 'Uppers' or 'Downers'?
The classic models for PGE mineralization in LMI have addressed the issue of how magmas with relatively low initial concentrations of the PGE (e.g., <5 ppb) could form crystalline (cumulate) products possessing enrichments of up to 10^3 ppm of these precious metals. In this respect, the presence of base-metal sulfides is significant. Under the conditions typical in many basalt magma chambers, the PGE have chalcophile tendencies, meaning that they will be preferentially partitioned into a sulfide phase, if present. The process by which small volumes of sulfide, envisaged to occur in magma chambers as immiscible droplets of sulfide melt, can equilibrate with many times their own volume of silicate magma so that the PGE may be 'scavenged' remains the outstanding question (see discussion of *R*-factors in Barnes and Ripley 2016, this volume). Two opposing schools of thought have dominated this debate over the past ~30 years (cf. Mungall and Naldrett 2008). Importantly, both involve transport of the PGE to the site of mineralization, from above or below. The 'downers' models invokes separation (or unmixing) of sulfide droplets from the magma, following magma mixing. These sulfides settle out through the magma column, scavenging PGE as they do so, before accumulation at the site of mineralization and exsolution of the PGM from the sulfide, typically envisaged to be at or close to the magma chamber floor. The Merensky Reef was originally interpreted in the context of the classic downers model, having developed as a result of a large scale mixing event between new and resident magma, followed by downward settling of chromite crystals and sulfide droplets through a column of magma several km thick (Campbell et al. 1983; Naldrett 1989). A revised version of the 'downers' model invokes fractional crystallization and gravity settling of chromite and sulfide droplets from a basally emplaced layer of magma only ~16 m thick (Naldrett et al. 2011). Similarly, the UG2 chromitite and attendant mineralization was traditionally considered to be the product of mixing of resident and replenishing magma, following the classic models for stratiform chromitite development proposed by Irvine (1977a,b). Building on the work of Eales (2000), Mondal and Mathez (2007) subsequently attributed the formation of the UG2 chromitite to emplacement of new magma with much of the chromitite crystal cargo already entrained.

The 'uppers' model calls for the upward percolation through the (footwall) cumulate pile of a chloride-rich aqueous fluid capable of stripping out (dissolving) PGE-enriched sulfides, before re-precipitating these as a PGE-reef at a stratigraphically higher level (cf. Boudreau and McCallum 1992a, for the Stillwater Complex J-M Reef). The 'downers' model is therefore a primary magmatic phenomenon, whereas the 'uppers' model occurs later in the solidification history of the magma chamber, when high-temperature metasomatism is more likely to be an important process. Cawthorn et al. (2002) drew attention to the Merensky Reef laurite $^{187}Os/^{188}Os$ data of Hart and Kinloch (1989), suggesting that there is no obvious overlap with the underlying anorthosite $^{187}Os/^{188}Os$ isotopic compositions and therefore there is a problem with the uppers model for the Merensky Reef. The latter authors also summarized some of the variations present in these general models, with particular relevance to the formation and concentration of the PGM in LMI. In particular, they drew attention to the ideas of Tredoux et al. (1995), which describe clustering of metal ions in magma to form PGM, followed by their entrainment in sulfide. The initial formation of the PGM as Fe–PGE alloys or discrete PGM was also suggested by Merkle (1992), Brenan and Andrews (2001) and Gornostayev et al. (2001) with later capture by either chromite (Hiemstra 1985) or sulfide (Ballhaus and Sylvester 2000). Cawthorn et al. (2002) pointed out that early formed PGM assemblages should be dominated by the IPGE, relative to the PPGE; something that does not generally hold for either the Merensky Reef or the UG2 chromitite (as described above). The latter authors referred to the study of Barnes and Maier (2002), which proposed processes involving the early development of discrete PGM, followed by their later modification involving base-metal sulfide, were responsible for the relative abundances of the PGE observed. Indeed, low temperature modification of PGM assemblages (cf. Ballhaus and Ryan 1995) has been

suggested (to temperatures as low as 80–90 °C), illustrating that for a given section of either the Merensky or UG2 horizons, the specific PGM assemblage should be considered as a combined product of the time-integrated magmatic and high-to-low temperature metasomatic processes.

Recent experimental measurements carried out by Fonseca et al. (2009) and Mungall and Brenan (2014) suggest very high sulfide/silicate partition coefficients for the PGE in the Merensky Reef and the UG2 chromitite. Specifically, Mungall and Brenan (2014) propose D^{sul}_{PGE} of $\sim 10^6$ for the Merensky Reef and the UG2 chromitite (Fonseca et al. 2009 suggest values of $\sim 10^7$ for formation of the Merensky Reef). The implication of these results is that whatever the causal mechanism for sulfide separation (and accumulation), there is no requirement for upgrading or modification of the ore deposits to explain the very high metal tenors. Instead, they are in the range of what might be expected for the high *R*-factors associated with separation of sulfide melt in both the Merensky and UG2 reefs.

The Stillwater Ultramafic Series chromitites. The Stillwater Complex (Montana, USA) is a 2705 ± 4 Ma LMI emplaced into mid-late Archean metasediments in association with a major crust-formation event (McCallum 1996). The exposed part of the complex covers 180 km^2. It comprises three series with the chromitites occurring in the lowermost Ultramafic Series, at the base of the cyclic harzburgite–orthopyroxenite units (Todd et al. 1982). The chromitite seams are named A (stratigraphically lowest) to K (stratigraphically highest). The association of the chromitite seams with the Ultramafic Series has been considered to reflect chromite crystallization from mixing of the resident magma with repetitive influxes of olivine-saturated, high-Mg melts (interpreted by some authors as boninites; Boudreau et al. 1997) into an open-system magma chamber (McCallum 1996; Horan et al. 2001). Talkington and Lipin (1986) documented the types and distribution of PGM in the (A, C, E, G, J and K) chromitites. Whole-rock abundances of the PGE range from several ppb to ~16 ppm, with Pd>Pt>Rh>Ru>Ir. The latter authors did not analyze Os, but Horan et al. (2001) subsequently reported concentrations of up to ~78 ppb in the Stillwater Ultramafic Series chromitites. The whole-rock abundances are not well accounted for by the PGM observed, which are predominantly IPGE-rich phases. Talkington and Lipin (1986) observed PGM (≤20 μm in size) both as inclusions in chromite and as interstitial phases in massive and disseminated chromitite lithologies. In the former case, inclusions contained within unfractured chromite crystals are predominantly laurite. The interstitial phases are predominantly sperrylite and isoferroplatinum. Talkington and Lipin (1986) favored a magmatic origin for the Ru–Ir–Os-rich phases, implying that PGM such as laurite precipitated relatively early, whereas they considered that Rh, Pt, and Pd may have precipitated at a later stage in the development of the chromitites. The primary rationale for this interpretation was the occurrence of laurite as inclusions within chromite crystals, and the interstitial textural position of the PPGE-rich phases. They noted the close spatial proximity of PPGE-rich PGM and interstitial sulfides, arsenides, antimonides, and mercurides, and proposed partitioning of the PPGE into an immiscible sulfide fraction at the magmatic stage, together with late-stage hydrothermal fluid processing of the primary PGM assemblage, to explain their observations.

The Rum Layered Suite chromitites. The Rum Layered Suite (NW Scotland) is a ~60 Ma open-system LMI, emplaced during the onset of opening of the Northeast Atlantic. The eastern portion of the intrusion (Eastern Layered Intrusion) contains chromitite seams at the bases of cyclic peridotite–troctolite units; each unit is considered to be the product of emplacement of a fresh batch of basaltic or picritic magma into the chamber. The chromitites are laterally extensive for 100's of meters, rarely exceeding ~2 mm in thickness and their formation has been attributed to the assimilation of feldspathic (+clinopyroxene) cumulate by replenishing picritic magmas (O'Driscoll et al. 2010). They are characterized by significant whole-rock enrichments in the PGE (ppm levels; Fig. 2a) compared to the cumulate above and below them (O'Driscoll et al. 2009a). Power et al. (2000) carried out a detailed documentation of the Rum PGM and reported a considerable abundance and diversity of mineral species. More than 70% (by number) of all

of the PGM observed (~850 grains over 5 unit boundary chromitite seams) are associated with base-metal sulfides, typically at the grain boundaries between sulfide and other mineral phases rather than as sulfide-hosted inclusions. The remainder (~28%) are either hosted in Fe-oxide and Fe-hydroxide phases or associated with silicates. One of the most remarkable features of PGE mineralization in the Rum chromitite seams is that the PGM populations are highly variable from one unit to the next, presumably reflecting the open system character of the intrusion, and perhaps the compositional heterogeneity of the replenishing magmas (Power et al. 2000). For example, at the base of the Eastern Layered Intrusion, Unit 1 contains electrum (Au,Ag) grains, but there are no reported PGM. The Unit 5/6 and 6/7 boundaries are dominated by Pt–Pd tellurides and bismuthides, whereas the Unit 11/12 chromitite seam is dominated by arsenide phases, especially sperrylite. Approximately 70% of the PGM from a chromitite seam in Unit 14 are tellurides or arsenides. The Unit 7/8 chromitite, with 374 documented PGM, is the most PGE-enriched (Fig. 4). In this case, Pt–Fe alloys and PGE sulfides (braggite and cooperite), laurite, and Pt–Pd alloys dominate the assemblage. This assemblage would appear to record a relatively high-temperature development. In this light, it is worth noting that O'Driscoll et al. (2009a) also recorded the highest whole-rock PGE concentrations from the Unit 7/8 horizon and suggested that the magma replenishing the Rum chamber at this level was particularly primitive (magnesian) in character (i.e., picritic). Power et al. (2000) argued that the tight spatial control exerted by the ~2 mm chromitite seams on the PGM abundances implied a magmatic origin, although they did not rule out localized *in situ* alteration/re-distribution of some of the phases at the postcumulus stage. On the basis of mineral compositional and textural evidence, O'Driscoll et al. (2009b, 2010) argued against the magma mixing hypothesis proposed by Power et al. (2000) and proposed that the Rum chromitite seams, sulfides, and PGM developed *in situ*. Latypov et al. (2013) expanded on the latter idea, with an *in situ* crystallization model that invoked nucleation of sulfides onto chromite crystal surfaces before scavenging the PGE from the convecting magma in the chamber. Power et al. (2003) also documented an extensive array of PGM associated with another ultramafic intrusion on the island of Rum. The PGM predominantly occur within and at the edges of disseminated base-metal sulfide grains and include paolovite (Pd_2Sn), and Pd bismuthotellurides. The ultramafic intrusion occurs as a satellite plug to the Rum Layered Suite and further highlights the potential for the Rum parental magmas to produce PGE mineralization.

Other layered intrusion chromitite-hosted PGM. It is generally accepted that magma chamber conditions and the processes that lead to the crystallization of chromitite seams in layered intrusions are also conducive to enrichment of the PGE, thus leading to high concentrations of the PGM in chromitite. The Muskox intrusion is an important LMI in the literature in this regard, as some of the classic ideas of chromitite petrogenesis were developed for the seams that occur there (Irvine 1977a,b). The Muskox intrusion is located on the northwestern edge of the Canadian Shield, and its chromitite seams are positioned in the middle of cyclic unit 21 and at the base of cyclic unit 22. The formation of these chromitites has been attributed to magma mixing in an open system magma chamber by Irvine (1977a; 1977b). No detailed documentation of the PGM has been reported in these rocks, but Barnes and Francis (1995) reported whole-rock base and precious metal concentrations throughout the Muskox stratigraphy. They showed that the enrichments of the PGE were not significant in the chromitite reef at the boundary between cyclic units 21 and 22 (i.e., 300–1000 ppb ΣPGE), compared to major chromitite-hosted PGE deposits, suggesting that chromitite PGE abundances can be quite variable from one deposit to the next. Notably, however, these PGE abundances are not dissimilar to those in the Rum chromitites. In the case of the Muskox intrusion, Barnes and Francis (1995) attributed the relatively low abundances of the PGE to a low *R*-factor, compared to that experienced by the chromitites from the Merensky or UG2 reefs (i.e., ~1,000 at the Muskox intrusion compared to >10,000 for reefs such as the Merensky Reef; see Barnes and Ripley 2016, this volume, for additional detail on the *R*-factor principle). However, it is worth noting that Day et al. (2008) reported Os concentrations of >200 ppb in unit 22 chromitite

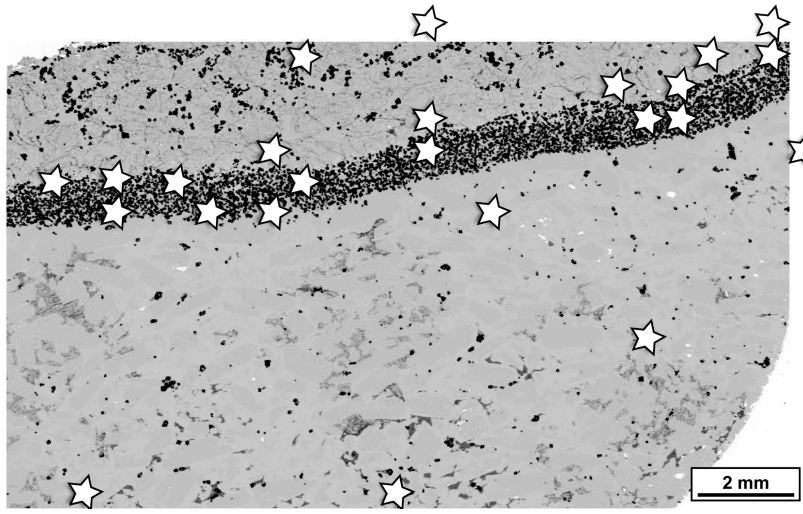

Figure 4. Grayscale QEMSCAN® image of the Unit 7–8 boundary, Rum Layered Suite. The ~2 mm thick chromitite seam running east–west across the image separates overlying Unit 8 feldspathic peridotite from the underlying Unit 7 anorthosite. The different silicate minerals are not distinguished in this image, but the distribution of Cr-spinel (colored black) in the seam and in the overlying peridotite is visible. QEMSCAN® maps samples at electron beam stepping intervals down to 1 μm and interprets the mineralogical composition of a sample at the pixel scale (see O'Driscoll et al. 2014a for further details). In the area shown by this image (adapted from O'Driscoll et al. 2014a), 31 PGM and Au/Ag-rich mineral phases were mapped by QEMSCAN® analysis (the positions of some of these are shown by the white stars). The close spatial association of these minerals with the chromitite seam is noteworthy. The white stars include both PGM and Au/Ag phases. Note that 3 grains are located out of the area of the sample.

(an order of magnitude greater than that reported by Barnes and Francis, 1995), suggesting that there may be a degree of intra-reef variability too. Other detailed PGM studies, such as those carried out by Pirrie et al. (2000) on chromitites in the ~60 Ma Mull and Skye layered intrusions (British Paleogene Igneous Province) support the general point however, that LMI-hosted (stratiform) chromitite seams tend to be enriched in PGM. Furthermore, Halkoaho et al. (1990) describe the Sompujärvi PGE Reef at the boundary between the third and fourth megacyclic unit in the Penikat layered intrusion (Finland), noting that where associated with disseminated chromite, the PGE grade is distinctly higher.

The link between chromite and PGM was explored by Finnigan et al. (2008), who carried out a series of experiments in which they documented the formation of PGM (especially IGPE-rich PGM) at the chromite-melt interface. They argued that the selective uptake of Cr^{3+} and Fe^{3+} from the melt by the growing spinel created a boundary layer across which a redox gradient developed. Finnigan et al. (2008) showed that PGE solubilities in the melt can consequently decrease dramatically (by as much as 20%) in these localized reduced (f_{O_2}) melt films, offering an explanation for the close association between the PGM and chromitite in natural environments, but also for why the PPGE are only typically enriched in chromitites that contain abundant base-metal sulfide.

Non-chromitite-hosted PGM in layered intrusions

The J-M Reef, Stillwater Complex. The J-M Reef of the Stillwater Complex contains bulk rock PGE at some of the highest grades (~18 ppm) of any deposit on Earth (Zientek et al. 2002; Godel and Barnes 2008a). Zientek (2012) reports ~149×10^6 tons of reserves and mineralized material for the deposit, grading at 3.7 ppm Pt and 12.9 ppm Pd. The mineralization occurs

within the olivine-bearing cumulate (OB-1) of the Lower Banded Series (Zientek et al. 1985). Its PGM population includes Pt- and Pd-sulfides, tellurides, and Pt–Fe alloys (Heyse 1983; Zientek and Oscarson 1986). Zientek and Oscarson (1986) reported that all of the Pt and ~20% of the Pd are contained in PGM, with pentlandite also being a significant host for Pd. Godel and Barnes (2008b) investigated the PGM phases in four different samples of J-M Reef cumulate (troctolite, anorthosite, leuconorite, and olivine melagabbronorite) and reported ~850 PGE-rich grains, which they divided into eight groups. There is variability between samples, reflecting the compositional heterogeneity of the J-M Reef in general (Figs. 5, 6). Godel and Barnes (2008b) reported that Pd–Pt sulfides and Pt–Fe alloys dominate the numbers of grains observed (~44% and ~31%, respectively) with Pd–Pt tellurides also representing a significant component (~18% of total grains). The Pd–Pt sulfides are predominantly braggite–cooperite and vysotskite, representing 59% of the total area measured across the four samples. Most of the PGM occur as vermicular-type structures within but close to the margins of base-metal sulfides, especially chalcopyrite. The Pd–Pt sulfides are also observed enclosed within secondary silicates (i.e., chlorite, amphibole) and oxide grains (magnetite; Godel and Barnes 2008b). In the latter instance Pd–Pt sulfides are recorded from the centers of secondary magnetite-bearing veins that cross-cut the base-metal sulfides, related to late Cretaceous–early Paleogene Laramide orogenesis (McCallum 1996; Fig. 5b). The Pt–Fe alloy is predominantly isoferroplatinum, which may contain up to ~5.6 wt.% Pd (Godel and Barnes 2008b). This mineral is mostly associated with base-metal sulfides, either as inclusions within pyrrhotite and pentlandite (~48% by area) or at the grain boundaries between silicate and sulfide (~39% by area). Godel and Barnes (2008b) report that the isoferroplatinum grains are relatively large compared to other PGM, with an average grain size of ~50 μm^2. A lesser number of isoferroplatinum grains (~12% by area) are observed to occur in close association with magnetite (Fig. 5a). Tellurides of Pd and Pt account for 12% by area of the total PGM population, but their contribution to the overall PGE budget is estimated at only 0.1% and 5.1%, for Pt and Pd, respectively. Telluropalladinite (Pd_9Te_4), keithconnite [$Pd_{3-x}Te_{(x=0.14-0.43)}$] and kotulskite [Pd(Te,Bi)] are the dominant PGM, typically occurring in close association with (either at the edges of or as inclusions within) secondary silicate phases. Laurite accounts for 1% (by area) of the total PGM observed by Godel and Barnes (2008b), but constitutes up to 50% of the whole-rock Os, Ir, and Ru contents. Most laurite (80% by area) is present as inclusions in base-metal sulfides (e.g., pentlandite and chalcopyrite), the rest occurring at contacts between secondary magnetite and base-metal sulfides, where they are usually smaller grains. Other PGM recorded in the J-M Reef include Pd–Pb and Pd–Cu alloys (zvyagintsevite and skaergaardite [PdCu], respectively), Au–Pd–Ag alloys, and native Pd (~3.5% by area of total PGM), all typically at the contacts between base-metal sulfides and (typically secondary) silicate phases. From the textural relationships and mineralogical associations, Godel and Barnes (2008b) proposed that the PGE, Te, Bi, and base-metals were initially contained in an immiscible sulfide liquid fraction. At least two subsequent alteration events were invoked by these authors as follows: 1) Initial desulfurization of the base-metal sulfides due to an upwardly mobile S-undersaturated silicate melt which formed the Pt–Fe alloy and some of the Pd sulfide, and 2) A low temperature (~250–465 °C) metasomatism event which led to the formation of secondary magnetite and the other Pd-alloys, including the Pd–Cu PGM. As a caveat to the latter, the observation of Barnes and Naldrett (1986) that whole-rock PGE contents correlate positively and strongly with S concentrations suggests that any S redistribution was relatively localized. In addition, the remobilization of the J-M Reef PGM assemblage at low temperatures during magnetite formation shows that such modification can occur significantly after initial crystallization.

The Picket Pin deposit occurs up stratigraphy from the J-M Reef, in the upper portion of Anorthosite subzone II (AN II), and is traceable along 22 km of strike of the Stillwater intrusion. Although there has not been a detailed mineralogical characterization of the PGM associated with this horizon, Boudreau and McCallum (1992b) report that arsenide and antimonide PGM dominate.

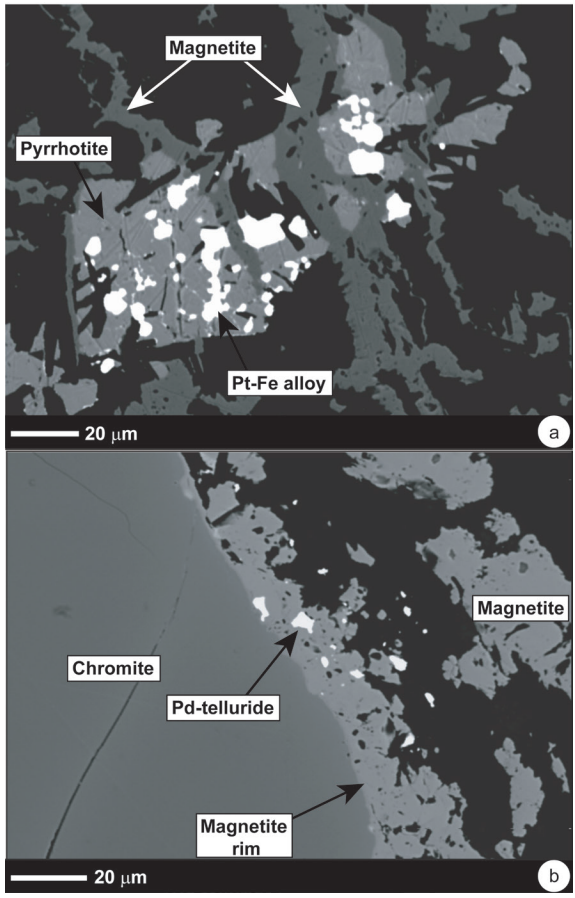

Figure 5. Textural relationships of PGM illustrated in backscatter electron micrographs of the Stillwater J-M Reef as follows: (a) Irregularly shaped bright Pt–Fe alloy grains (example arrowed) are included in pyrrhotite and crosscut by ~10 μm thick secondary magnetite veinlets (arrowed). (b) Sieve-textured magnetite rim (on Cr-spinel crystal) containing Pd-telluride inclusion. These images have previously been published in Godel and Barnes (2008b) as their Figures 6d and 8c, and are reproduced here with the permission of the authors and under the Fair Use Provision of Economic Geology.

The Main Sulfide Zone, Great Dyke. The Great Dyke (Zimbabwe) is a 2575 ± 0.7 Ma intrusion emplaced into Archean granites and greenstone belts of the Zimbabwean craton (Oberthür et al. 2002). Its lower Ultramafic Sequence contains chromitites with sub-economic concentrations of the PGE. The Main Sulfide Zone (MSZ) contains disseminated sulfide mineralization hosted predominantly in pyroxenites. The MSZ has measured, indicated and inferred resources of 2136×10^6 tons, at typical grades of 2.7 ppm Pt and 1.8 ppm Pd (from D. Causey, quoted in Zientek 2012). The MSZ is situated several meters below the transition between what are referred to as the lower Ultramafic and upper Mafic Sequences, and has economic concentrations of the PGE (Oberthür 2011) that occur as (Pt,Pd-) bismuthotellurides, PGE-arsenides, -sulfides, and sulfarsenides (Johan et al. 1989a; Oberthür et al. 1997, 1998, 2000). Oberthür et al. (2003) carried out a detailed study of a suite of mineralized bronzitites at Hartley Platinum Mine, where the MSZ is several meters thick and comprises a lower sub-economic PGE-subzone and an upper base-metal sulfide subzone. The MSZ has a fine-scale geochemical structure, whereby peaks in concentrations of different PGE and in the abundance of base-metal sulfides are stratigraphically offset from one another. As described in Oberthür (2011), the main peak in Pd concentrations occurs in the PGE subzone (plus a minor Pt peak), followed by the major Pt peak several meters above. The lower portion of the base-metal sulfide subzone overlaps with the top of the PGE subzone, and the first

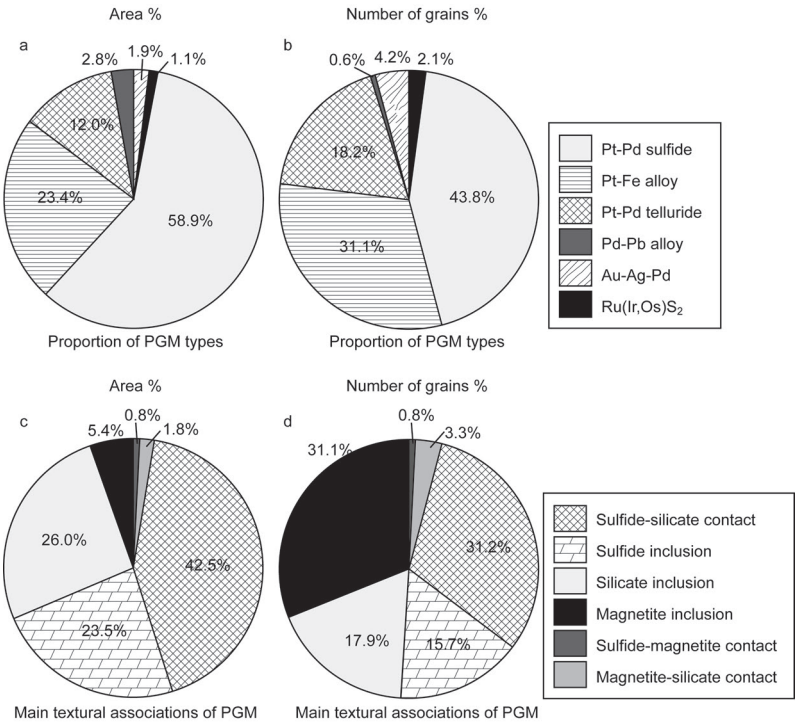

Figure 6. Pie charts illustrating the proportion of PGM observed in the four samples from the J-M Reef (troctolite, anorthosite, leuconorite, and olivine melagabbronorite with ~1 to ~5 vol.% base-metal sulfides) studied by Godel and Barnes (2008b) by area (a) and number of grains (b). The samples contain ~49 to 419 ppm bulk rock PGE (see also Fig. 2). Summary pie charts of the textural distribution of the different PGM by (c) area and (d) number of grains have been replotted using the data presented in Figures 3 and 4 of Godel and Barnes (2008b).

peak in sulfide concentration occurs <1 m above the Pt peak (Oberthür 2011). Oberthür et al. (2003) interpreted the structure of the MSZ as reflecting successive episodes of primary sulfide accumulation, PGE scavenging and fractionation. They documented 181 PGM grains throughout the MSZ (e.g., Fig. 7), predominantly Pt-rich bismuthotellurides and Pd-rich bismuthotellurides (55% and 16% of the total number of PGM grains, respectively). The most common PGM in this category are moncheite, maslovite, merenskyite [(Pd,Pt)$(Te,Bi)_2$], and michenerite [(Pd,Pt)BiTe]. Other phases recorded include sperrylite (11% by number) and cooperite/braggite (2% by number). Rarer PGM include laurite, Pt–Fe alloy, and an unnamed phase (PtSnS). Oberthür et al. (2003) also report electron microprobe data that suggest much of the Pd and Rh is hosted in pentlandite (maximum concentrations of ~2,500 ppm and 550 ppm, respectively) in the PGE subzone. In contrast, Pt is concentrated in PGM phases.

The PGM occur in discrete zones that match the geochemical zonation of the MSZ. Sperrylite occurs throughout the PGE subzone, cooperite/braggite in the lower part only and (Pt,Pd)-bismuthotellurides are concentrated at the top of the PGE-subzone. Oberthür et al. (2003) interpreted their observations as signifying that the PGE were primarily concentrated in base-metal sulfides at magmatic temperatures, referring to the observations of Ballhaus and Ryan (1995) on Merensky Reef base-metal sulfides. Subsequent expulsion of the PGE (Os, Ir, Ru, and especially Pt) occurred during recrystallization of the sulfides to pentlandite, pyrrhotite, chalcopyrite, and pyrite. Oberthür et al. (2003) suggested that Te and Bi were also

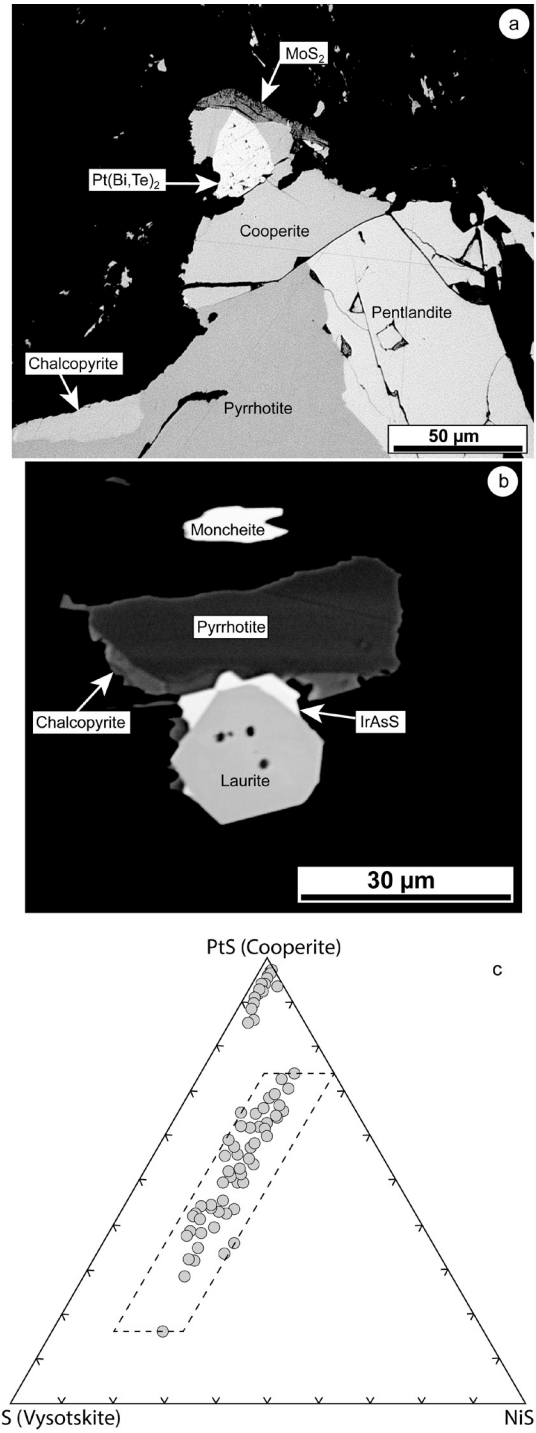

Figure 7. (a) Reflected light image (oil immersion) of braggite and moncheite grains (labelled in image) in the MSZ ore of the Great Dyke. (b) Backscatter electron micrograph of euhedral laurite grain intergrown with base-metal sulfides (chalcopyrite and pyrrhotite) from the MSZ. A grain of moncheite (labelled) also occurs. (c) Ternary (PtS–PdS–NiS mol.%) diagram illustrating the range of compositions of cooperite and braggite from pristine and altered (oxidized) MSZ base-metal sulfide ores. Panels (a) and (b) are reproduced from Figures 5a and 5e of Oberthür et al. (2003) and (c) is a reproduction of Figure 7 of that paper. All panels are reproduced with the permission of the author and of Mineralium Deposita.

expelled from the sulfide lattice at this stage, whereupon they combined with the PGE to give the observed parageneses. Low temperature (<500 °C) interstitial 'magmatic-hydrothermal' fluids were invoked by Oberthür et al. (2003) as a potentially important agent in redistributing the PGE during sulfide recrystallization, though the latter authors indicate that the precise role of metasomatism in PGM formation needs further investigation.

The Platreef, Bushveld Complex. The Bushveld Complex Platreef crops out in the northern limb of the intrusion and has measured, indicated and inferred resources of 3418×10^6 tons at grades of 2.8 ppm Pt and 3.4 ppm Pd (Mudd 2012). The stratabound (but not stratiform) Platreef is located at the base of the Rustenburg Layered Suite, in direct contact with underlying Archean metasedimentary and meta-igneous country rocks and reaches thicknesses of ~40 m. Building on earlier syntheses of the PGM populations of this economically significant deposit (e.g., Kinloch 1982; Viljoen and Schürmann 1998; Hutchinson et al. 2004), Holwell et al. (2006) carried out a detailed study of the PGM at the Sandsloot Mine in the Platreef. Base-metal sulfides (including pyrrhotite, pentlandite, chalcopyrite) are common interstitial components of the reef and are characterized as being anhedral and exhibiting a tendency to be intergrown with plagioclase and secondary phases such as actinolite, epidote and micas. Holwell et al. (2006) note that PGE grades in the reef itself are variable and are quite erratic in the footwall. They identified >1000 PGM grains in 58 polished thin sections and blocks of reef, hanging wall, and footwall samples. Nine broad groupings of the PGM were established by these authors as follows: (1) Pt/Pd tellurides; (2) Pt/Pd bismuthides; (3) Pt/Pd arsenides; (4) Pt/Pd antimonides; (5) Pt/Pd germanides; (6) PGE sulfides; (7) PGE sulfarsenides; (8) PGE alloys with Fe, Cu, Sn, Pb, and Tl; and (9) Au, and Ag bearing phases. Holwell et al. (2006) highlighted the paucity of S-dominant PGM in the Platreef at Sandsloot, in direct contrast to both the UG2 chromitite and the Merensky Reef. Overall, footwall and hanging wall PGM populations in the Platreef are dominated by Pt/Pd tellurides, alloys with lesser PGE-bearing arsenides (especially sperrylite) and antimonides. In particular, the Platreef is dominated by Pt/Pd tellurides including moncheite and kotulskite with sperrylite being common throughout the deposit too. For the most part, the PGM in the reef pyroxenites and pegmatites are surrounded by silicates or situated at silicate–sulfide grain boundaries. Holwell et al. (2006) showed that many are texturally associated with the replacement products of sulfides, such as secondary amphiboles (tremolite and actinolite). Some of the pyroxenite at the Platreef has undergone a replacement that introduced Fe-rich olivine to the rock, and these portions of the reef are characterized by a distinct PGM assemblage. Specifically, this includes Pd-tellurides and alloys and Pt–Fe alloys, as well as rare sperrylite. Another feature of note is that 55% (of the total area of PGM studied) of the Platreef hanging wall material comprises an unusual Pd-germanide with a composition close to Pd_2Ge, attributed by these authors to processing of the reef by newly replenishing Main Zone magmas. The complex PGM mineralogy of the Platreef package is likely (at least in part) a function of the interaction of parental magmas with the calc-silicate floor rocks (Schouwstra et al. 2000). Holwell et al. (2006) suggested that formation of an initial telluride-dominated PGM assemblage developed in the pore spaces of the primary cumulate texture, possibly controlled by the interaction of the intercumulus melt with primary magmatic base-metal sulfides. They argued for localized modification of the PGE-assemblage in the reef when a late-stage Fe–Pb-rich fluid, possibly derived from serpentinization of the footwall lithologies, was introduced. Holwell et al. (2006) suggested that the telluride assemblage was then converted into one dominated by Pt–Fe and Pd–Pb alloys. This interpretation was based partly on the observation that zvyagintsevite (Pd_3Pb) is unusually common in these rocks and that kotulskite has enhanced Pb contents (up to 12 wt.%), reflecting replacement of Te. Holwell et al. (2006) highlighted similarities between this process and the metasomatism considered to have modified the PGM population around the Bushveld dunite pipes and the Merensky Reef potholes (Kinloch 1982; Kinloch and Peyerl 1990). Episodes of hydrothermal fluid alteration and serpentinization are considered

to have produced the arsenide and antimonide-dominated assemblage in the footwall, based on the extremely different character of the PGM mineralization compared to that in the reef itself. For example, Holwell et al. (2006) highlighted the difference in whole-rock Pt/Pd ratios between the reef and footwall (0.79–1.94 vs. 0.54–0.98, respectively), which they argued reflected formation of the footwall from enhanced metasomatism as Pd is more mobile than Pt.

The Platinova Reef, Skaergaard Intrusion. The Skaergaard Intrusion lies at the unconformity between Precambrian gneisses and an overlying sequence of Eocene plateau lavas in Kangerdlugssuaq, southeastern Greenland. It formed via the successive emplacement of a series of magma pulses during opening of the Northeast Atlantic Ocean (~55 Ma) and is the archetypical example of the closed system fractionation of a basaltic magma (Wager and Brown 1968). Crystallization of the magma resulted in the accumulation of three different series: the Layered Series, the Marginal Border Series and the Upper Border Series. The so-called Platinova Reef occurs in the Triple Group, which constitutes the upper ~100 m of the Middle Zone of the Layered Series. The Platinova Reef is hosted in an Fe-Ti oxide-rich tholeiitic gabbro, and the associated mineralization is broadly stratiform. Inferred resources of $1{,}520 \times 10^6$ tons of ore, grading at 0.04 ppm Pt, 0.61 ppm Pd, and 0.21 ppm Au, have been reported (Mudd 2012). The base-metal sulfides of the Platinova Reef are dominated by Cu-rich minerals, contrasting with Fe–Ni–Cu sulfides that are typical of some of the PGE reefs already discussed above. The sulfides are predominantly bornite (Cu_5FeS_4), chalcocite (Cu_2S), and digenite (Cu_9S_5) and comprise ~0.05 mod.% of the reef. They occur in close textural association with Ti-magnetite/clinopyroxene grain boundaries, occasionally being intergrown with H_2O-bearing silicates (chlorite-group minerals, hornblende, actinolite, and a member of the annite–phlogopite series). The PGM assemblage has been documented in detail by Nielsen et al. (2003a–e) and is dominated (~90% of the total PGM observed) by skaergaardite (PdCu; Rudashevsky et al. 2004). Other PGM documented as both discrete grains and inclusions include keithconnite, vasilite [$(Pd,Cu)_{16}(S,Te)_7$], and zvyagintsevite. The PGM are characteristically partially or completely enclosed by the Cu–Fe sulfides (e.g., Rudashevsky et al. 2004; Godel 2013), an observation that led Andersen (2006) to suggest that the PGM are genetically related to formation of the sulfides. Rudashevsky et al. (2004) suggested that skaergaardite crystallized from a disordered Pd–Cu-rich alloy precursor that had exsolved from a Cu–Fe sulfide melt under conditions of relatively high f_{S_2} [$\log f_{S_2} > 7$ units] at ~600 °C. Unnamed Cu–Pd–Au–Pt–Fe alloys were also documented by Rudashevsky et al. (2004). In 2008, McDonald et al. also reported the occurrence of another new Pd-dominant alloy (or intermetallic), nielsenite ($PdCu_3$), in the Platinova Reef (see also Rudashevsky et al. 2009).

Karup-Møller et al. (2008) carried out an experimental study of the phase system Cu–Fe–Pd–S, at temperatures of 1000 °C, 900 °C, and 725 °C. They suggested that the skaergaardite precursor first formed as a Pd–Cu alloy at relatively high temperatures (≥1000 °C) in association with bornite (both crystallized from a metal-rich sulfide melt). In broad agreement with Rudashevsky et al. (2004), Karup-Møller et al. (2008) considered that skaergaardite (low skaergaardite; β-CuPd) formed following cooling of Pd–Cu alloy below 600 °C. These observations re-emphasize an important point already made above for the Merensky Reef PGM; that high-temperature PGM assemblages are capable of continuously reacting and re-equilibrating to significantly lower temperatures than the magmatic conditions under which they first formed. Indeed, Karup-Møller et al. (2008) suggest a lower temperature limit of 300 °C for PGM formation in the Platinova Reef. The latter authors extrapolated their observations to nielsenite formation and speculated on its high-temperature crystallization at ~1100 °C, with subsequent re-equilibration to temperatures ≤500 °C.

Other non-chromitite-hosted PGM. There are numerous layered intrusions, in addition to those named above, with non-chromitite-related PGE mineralization. Examples such as the Duluth Complex (USA) and the Sudbury Igneous Complex (Canada) are more appropriately

discussed below in the section on PGE–Ni–Cu sulfide-rich deposits, in terms of the style of PGM mineralization. Other published PGM studies include work on LMI such as the River Valley Intrusion (Canada; Holwell et al. 2014), the Freetown Layered Complex (Sierra Leone, Africa; Bowles et al. 2013), the Konttijaervi (associated with the basal contact of the Suhanko intrusion) and Kevitsa (also a Ni–Cu–PGE deposit) intrusions (northern and central Finland, respectively; Vuorelainen et al. 1982; Gervilla and Kojonen 2002), the Bird River Sill (Canada; Talkington et al. 1983), the Imandra layered intrusion (northwestern Russia; Barkov and Fleet 2004), the Ivrea-Verbano Basic Complex (lower crustal LMI, Italy; Garuti and Rinaldi 1986; Ferrario and Garuti 1990), the Munni Munni layered intrusion (western Australia; Mernagh and Hoatson 1995) and the Sompujärvi PGE Reef in the Penikat intrusion, which is not associated with chromitite, *sensu stricto* (Finland; Barkov et al. 2005). *Supplementary Table* 1 contains additional details of these intrusions. The Freetown Layered Complex and the Munni Munni layered intrusion are discussed further below.

The Freetown Layered Complex is a ~193 Ma, open-system intrusion associated with opening of the equatorial portion of the Atlantic Ocean. It comprises four major cyclic units, associated with magma replenishment events; within one of these units (Zone 3), four PGE-bearing horizons (B, C, D, and M; in order of descending stratigraphy) have been reported. Bowles et al. (2013) studied 21 thin sections of Horizon B and one of each of the others and documented a total of 169 PGM grains (Fig. 8). They noted that Horizons B and D contain Pt–Fe alloys and cooperite. The Pt–Fe alloys range in composition from isoferroplatinum to tetraferroplatinum (PtFe) and dominate the number of PGM grains observed in Horizon B (~52%; or 71% by area), with cooperite comprising ~21% of the total number of grains (and ~21% by area too). Rare tulameenite (Pt_2FeCu), bowieite [$(Rh,Ir,Pt)_2S_3$], Pt–Ir–Rh base-metal sulfides, and laurite are also present in Horizon B. Horizons C and M are dominated by Pd-bearing PGM. Horizon C contains Pd-bearing native Cu alloys (~75% of total PGM area) and nielsenite (~25% by area), with Pd-antimonide–arsenide dominating in Horizon M. Overall, a large proportion of the PGM (~35%) occur within (but close to the margins) of sulfide grains (Fig. 8c). The majority of the PGM (~50%) are associated with silicate minerals, and especially in interstitial positions to olivine, pyroxene, and plagioclase, and as inclusions within late-stage (hydrous) silicates such as amphibole, chlorite, and phlogopite (Figs. 8a,c). Bowles et al. (2013) invoked a model involving early-formed cooperite that underwent alteration (desulfurization) to Pt–Fe alloy with Pt-oxide as the final product. [It should be noted that the existence of Pt-oxide has been called into question by Hattori et al. (2010). Reference to this mineral phase here and throughout this work is solely for the purposes of acknowledging the observations of other studies, and does not bear on the views of the present authors.] The presence of arsenides and antimonides in the stratigraphically lowest layer was considered to be an effect of metasomatism. Platinum-group element mineralization in the Freetown Layered Complex probably has more in common with PGE reefs in other open system intrusions, than it does with the Platinova Reef of the Skaergaard intrusion. The study of Bowles et al. (2013) built on earlier studies (Bowles 1986; Bowles et al. 2000) of alluvial PGM from the Freetown peninsula, in which the origin of Pt–Fe alloys and Os-rich phases of the laurite–erlichmanite series was investigated by measuring their $^{187}Os/^{188}Os$ compositions, by ion microprobe. The PGM were found to have isotopic compositions extending from 0.1181 (±0.0010) to very radiogenic values of 0.2820 (±0.0040). One example of a Pt–Fe grain containing laurite inclusions with different $^{187}Os/^{188}Os$ compositions was reported, suggesting that at least some of the PGM formed in a surficial environment (Bowles 1986; Bowles et al. 2000; see also Appendix), although this was disputed by Hattori et al. (1991).

Mernagh and Hoatson (1995) described the PGM mineralogy of the Munni Munni Layered Intrusion, Western Pilbara Block (western Australia). The Munni Munni Complex is late Archean in age and its stratigraphy resembles that of the Great Dyke, discussed above.

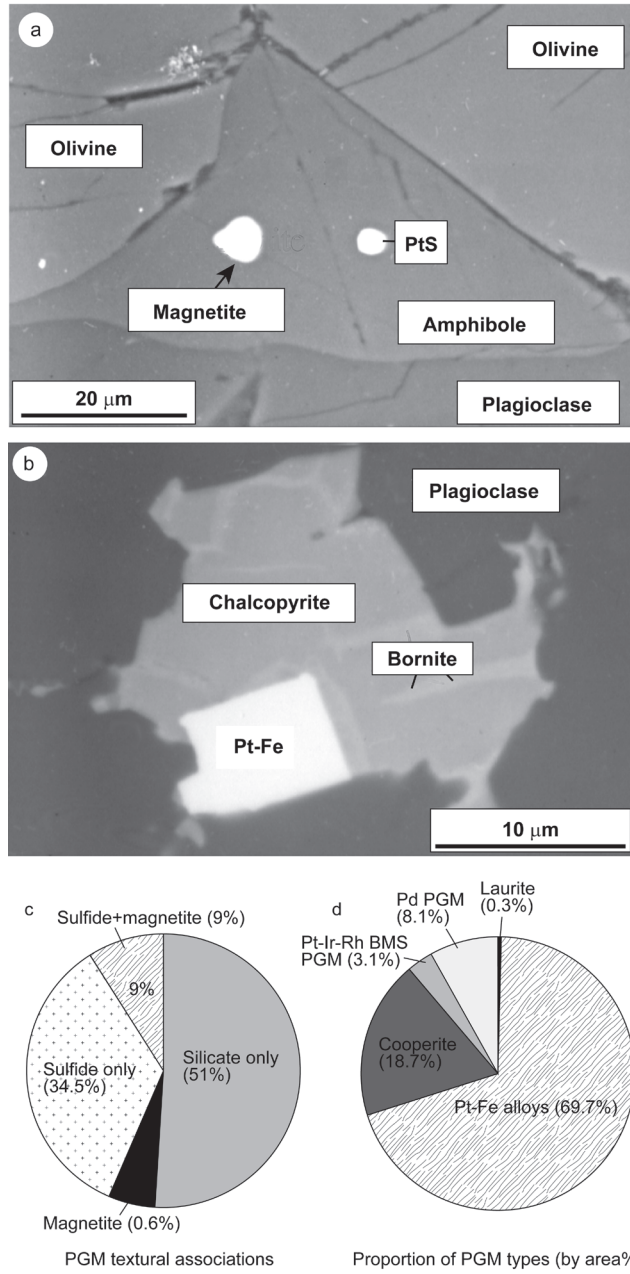

Figure 8. (a) Back scattered electron micrograph of cooperite (PtS) and magnetite (labelled) inclusions in amphibole from Horizon B in the Freetown Layered Complex. Image adapted from Figure 5c of Bowles et al. (2013). (b) Back scatter electron micrograph of Pt–Fe alloy inclusion in chalcopyrite from Horizon D, adapted from Figure 5n of Bowles et al. (2013). (c-d) Pie charts showing (c) the associations between the PGM and their host phases, and (d) the varying abundance of the types of different PGM. BMS = base-metal sulfides. Data are taken from Figures 4a and 4b of Bowles et al. (2013). Data and images are reproduced and presented with the permission of the author and Canadian Mineralogist.

It comprises a lower Ultramafic Zone (~1850-m thick), and an overlying Gabbroic Zone, ≥3600-m thick (Barnes and Hoatson 1994). Mernagh and Hoatson (1995) described the PGM (n=87) from the porphyritic websterite layer at the Ultramafic zone–Gabbroic zone contact. They found that the PGM are dominated by both Pt- and Pd-rich phases (n=45, n=42, respectively). Specific phases include sperrylite (19% of total grains), telluropalladinite (15%), potarite + atheneite [$(Pd,Hg)_3As$] (12%), moncheite (9%), platarsite (8%), and native Pt (5%), Pd (5%). With the exception of Pt–Pd sulfarsenides, all PGM were found to be <10 μm in size. Approximately 78% of the PGM were found to be associated with silicates, either as inclusions or along silicate–silicate grain boundaries. Approximately 15% of PGM occur within chalcopyrite or pentlandite. Although the PGM are thus predominantly hosted in silicate, they are still often spatially associated with base-metal sulfides. For example, PGM are commonly associated with hydrous silicate assemblages (amphibole, biotite) that appear to be a replacement product of sulfides. In addition, PGM occur in embayments or along cleavage traces of silicate (e.g., pyroxene) grains, close to where sulfides occur. Mernagh and Hoatson (1995) suggested that based on their observations, the PGM likely developed during the postcumulus replacement of primary igneous textures/mineralogy by metasomatic fluids.

PGM IN OPHIOLITES

Ophiolites are fragments of the oceanic (s.l.) crust and upper mantle, tectonically emplaced onto continental crust during orogenic events. The lowermost sections of many ophiolites offer unrivalled opportunities to study how the HSE are processed in the oceanic mantle via melt extraction, melt-percolation and metasomatism (see also Becker and Dale 2016, this volume). Ophiolite PGM are typically hosted in peridotites and chromitites, as well as placers associated with rivers draining the ophiolitic massifs (see Appendix for a description of the latter). Most of the ophiolites discussed below are considered to be derived from supra-subduction zone settings.

PGM in ophiolite peridotites

Occurrence and frequency of PGM in ophiolitic peridotites. Most mantle peridotites from ophiolites are variably serpentinized harzburgites, dunites and lherzolites. These lithologies usually contain PGE in concentrations of only a few ppb, which mostly reside in base-metal sulfides (Leblanc 1991). However, it has been shown that micrometric PGM also contribute to the PGE budget of ophiolite peridotites. For example, Augé (1988) studied PGM inclusions in accessory chromite from dunites at Tiébaghi (New Caledonia) and reported they comprise 50% laurite, ~13% native Os, ~13% unidentified $(Ir,Cu)_2S_3$, ~13% prassoite ($Rh_{17}S_{15}$), and ~13% Pt–Pd–Fe alloys. Chromite-hosted inclusions in Vourinos (Greece) dunites comprise 60% laurite and 40% Os–Ir–(Ru) alloys (*Supplementary Table* 2). Augé (1988) noted that the morphology and chemistry of the PGM in dunites from both localities are similar. Ohnestetter (1992) reported very small (<5 μm) PGM in olivine-rich pyroxenites forming the Monte Maggorie Massif (Corsica). They identified 44 PGM grains included in, and attached to, the rims of larger base-metal sulfides (pentlandite, chalcopyrite and bornite) and awaruite (Ni_3Fe). Most PGM identified at Monte Maggorie are alloys, including 32% tetraferroplatinum, 11% native Pt and Pd, 9% native Os, and <2% Ir and Cu–Pd, accompanied by 14% tellurides including merenskyite and moncheite, 9% complex amalgams of Au–Ag–Pt–Pd–Cu, 7% potarite, and <2% PdSnCu (*Supplementary Table* 2). Hutchinson et al. (1999) recorded Pt- and Pd-rich PGM in mantle peridotites of the Lizard (SW England) and Troodos (Cyprus) ophiolites. They noted that the PGM are associated with Cu-rich sulfides within poikilitic clinopyroxene-rich lenses in both mantle lherzolite (Lizard) and harzburgite that is considered to have formed just below the Moho (Troodos). The PGM identified at the Lizard are small grains (<6 μm) of laurite, sperrylite, potarite, and unidentified tellurides. At Troodos, the PGM are even smaller (<2 μm) grains of Pd–Cu, Pd–Pt–Cu, Pt–Pd, Pt tellurides and sulfides

and Pd-arsenides (Hutchinson et al. 1999). However, these authors did not report the relative abundances of each type of PGM. Kogiso et al. (2008) used X-ray fluorescence combined with microbeam analysis (micro-XRF) to search for PGM in spinel lherzolite from the Horoman peridotite complex (Japan). The analyses were conducted with a broad beam on large Fe–Ni–Cu sulfides and spinel grains and revealed several ~1 to 10 μm PGM alloy grains, including Os–Ir, Os–Ir–Pt, Pt–Au, and Pt.

Crystallization of PGM in upper mantle ophiolite peridotites. Augé (1988) interpreted the association of PGM with chromite in dunites and chromitites at Vourinos and Tiébaghi as evidence for the mineralogical control exerted by the chromite on fractionation of the PGE in the upper mantle. He proposed that discrete PGM of the IPGE group should crystallize earlier than chromite in a mantle melt. The refractory PGM could remain suspended in the melt, serving as sites upon which subsequent chromite grains could nucleate, explaining the common spatial occurrence of both together. He also noted that the similarities in PGM assemblages observed in dunite and chromitite PGM populations at Vourinos and Tiébaghi suggested that the conditions prevailing during their precipitation were similar, thereby linking the genesis of chromitites and dunites. In contrast, Hutchinson et al. (1999) suggested that the common association of PGM with base-metal sulfides in peridotites from both the Lizard and Troodos ophiolites reflects the collection of PGE from the silicate melt by the sulfide phase. The PGE are 10^4–10^5 times more compatible in sulfide than in chromite and if sulfide saturation is achieved prior to chromite crystallization in the mantle, the PGE will be scavenged by the sulfide phase. The fact that the sulfide-bearing peridotites from the Lizard ophiolite include both IPGE and PPGE-dominated PGM thus suggests that sulfur saturation was achieved, limiting the mineralogical control that the crystallization of chromite could exert on the fractionation between the two groups of PGE. Hutchinson et al. (1999) also noted the close association of the PGM with Cu-rich base-metal sulfides. They interpreted this association as reflecting the equilibration of sulfide droplets with large volumes of infiltrating silicate melts, resulting in the capture of the PGE. According to the latter authors, the fact that PGM-bearing base-metal sulfides are associated with pyroxene-rich lenses highlights the importance of melt infiltration in the peridotites. The model they proposed suggests that melt-rock reaction associated with the percolating silicate melts promoted the formation of sulfide melt droplets, which remained entrained in the partially molten peridotite matrix. These sulfide droplets equilibrated with variable volumes of infiltrating silicate melts, scavenging the available PGE. Although the exact mechanism controlling the crystallization of PGM from this early melt was not elucidated by the authors, the common presence of the PGM at the boundaries of the larger base-metal sulfides could reflect the sub-solidus exsolution of the PGE from base-metal sulfides after their crystallization. It has been demonstrated in experiments that base-metal sulfides may contain PGE in solid solution at high-T, which can be exsolved as discrete PGM upon cooling (e.g., Makovicky et al. 1986, 1988; Ballhaus and Ulmer 1995; Peregoedova and Ohnestetter 2002). The observation that PGM are commonly associated with the Cu-rich base-metal sulfides plausibly reflects either the segregation of the PGM at the latest stages of re-equilibration of the solid products of the original Fe–Ni–Cu sulfide liquid, or direct crystallization of PGM at high-*T* from the residual Cu-rich sulfide melt.

An alternative hypothesis for the formation of the PGM observed by Augé (1988) and Hutchinson et al. (1999) is that they are refractory phases already present in the peridotite, later incorporated by either crystallizing chromite or sulfide melts during their passage through the mantle. The results obtained in the experiments of Peregoedova et al. (2004) and Fonseca et al. (2012) suggest that high temperature desulfurization of PGE-bearing base-metal sulfides promotes the formation of discrete PGM, particularly Os- and Ir-bearing alloys. Fonseca et al. (2012) proposed that during partial melting of a sulfide-bearing peridotite, the extraction of sulfur into silicate melts leads to a decrease in f_{S_2} in the residue that triggers the exsolution of

Os–Ir alloys from the refractory matte (sulfide partial melt forming a solid/melt mush). Mantle base-metal sulfides may also lose S if they react with S-undersaturated melt/fluids such as those that commonly migrate through peridotites in ophiolite environments (e.g., Lorand and Conquéré 1983; Kelemen et al. 1992; Peregoedova et al. 2004). A series of small-scale melt extraction and/or melt–rock reaction events could therefore produce a sequential decrease of f_{S_2} in the mantle source region, promoting the breakdown of PGE-bearing sulfides, leading to formation of a series of residual PGM sulfides and PGE alloys. The residual PGM could remain attached to the original sulfides or be transported as discrete grains in the silicate melt. Mechanical entrainment by either chromite, as observed in Vourinos and Tiébaghi, or by migrating sulfide melts (as occurred in the Lizard and Troodos) are consequent possibilities.

Ohnenstetter (1992) ruled out a magmatic origin for the PGM identified in mantle peridotites from the Monte Maggorie Massif. It was suggested that the precipitation of the PGM was linked to a hydrothermal system created by the ascension of a fluid-enriched magma under a mid-oceanic ridge during asthenospheric upwelling. In this model, the migration of magma towards the surface as well the sudden opening of fractures may have caused a pressure drop responsible for the oversaturation of the magma in a fluid phase. The hydrothermal fluid that separated from the silicate melt could conceivably concentrate significant amounts of Pt, Pd, and Rh, together with Au, Ag, Cu, Ni, Pb, Sn, Hg, Te, and Bi. The metal-enriched hydrothermal fluid would have a relatively low viscosity, so could be injected into fractures and precipitate the PGM along cracks. It was estimated that the crystallization of the PGM from the hydrothermal fluid took place at temperatures lower than ~600 °C, based on the following criteria: (1) the crystallization of PGM after pentlandite, the latter having a maximum thermal stability of 610 °C; (2) a maximum temperature of < 470 °C for the crystallization of tetraferroplatinum co-existing with Pt–Cu and Au–Cu alloys, based on phase-equilibria data for the stability fields of binary Pt–Fe, Pt–Cu, and Au–Cu compounds; (3) a maximum temperature of < 400 °C for the crystallization of tellurides associated with the Cu-rich base-metal sulfides. Such low temperatures do not support direct crystallization from the melt, but favor metasomatic processes. Ohnestteter (1992) ruled out the potential involvement of fluids associated with the serpentinization of the hot peridotites, as the anomalous enrichments in Pt and Au (expressed in the PGM abundances) were not found to correlate with the degree of serpentinization. In addition, PGM were not typically observed in networks of serpentinized veins and fractures.

PGM in ophiolite chromitites

The mantle portion and the mantle–crust transition zone of many ophiolites host bodies of chromite of both high-Cr and high-Al type (i.e., *podiform chromitite*). These chromitites are usually characterized by relatively high abundances of all of the PGE, generally on the order of 10^1–10^3 ppb (e.g., González-Jiménez et al. 2014a,b). Differences in chromitite morphology, structural relationships, and geochemical signatures allow the recognition of three distinct chromitite types in ophiolites (González-Jiménez et al. 2014a,b). *Type I* is the most abundant and is characterized by bulk-rock enrichment in the refractory IPGE over the PPGE, independent of the bulk-rock content (usually between 10^{-3}–10^1 times CI-chondrite; Fig. 9). This type of chromitite may show a range of geometries (e.g., pods, boudins, fusiforms, veins, dikes, stockworks, and *schlieren*) and is found throughout the lower ophiolite pseudostratigraphy. *Type IIA* chromitites include concordant layers, bands, and seams, as well as less extensive discordant pods or irregular bodies that are generally confined to the shallower zones of the oceanic lithosphere. Chromitites of *Type IIA* show higher bulk-rock PGE contents than *Type I* as they are significantly enriched in Pt and Pd. The third type (*Type IIB*) of chromitite shows the same spatial distribution and PGE distributions as *Type IIA* but has a more limited range in Cr# (Cr# = Cr/Cr + Al) and a wider range of Mg# (Mg# = Mg/Mg + Fe^{2+}) that overlaps the compositional range of chromitites from LMI (Fig. 9).

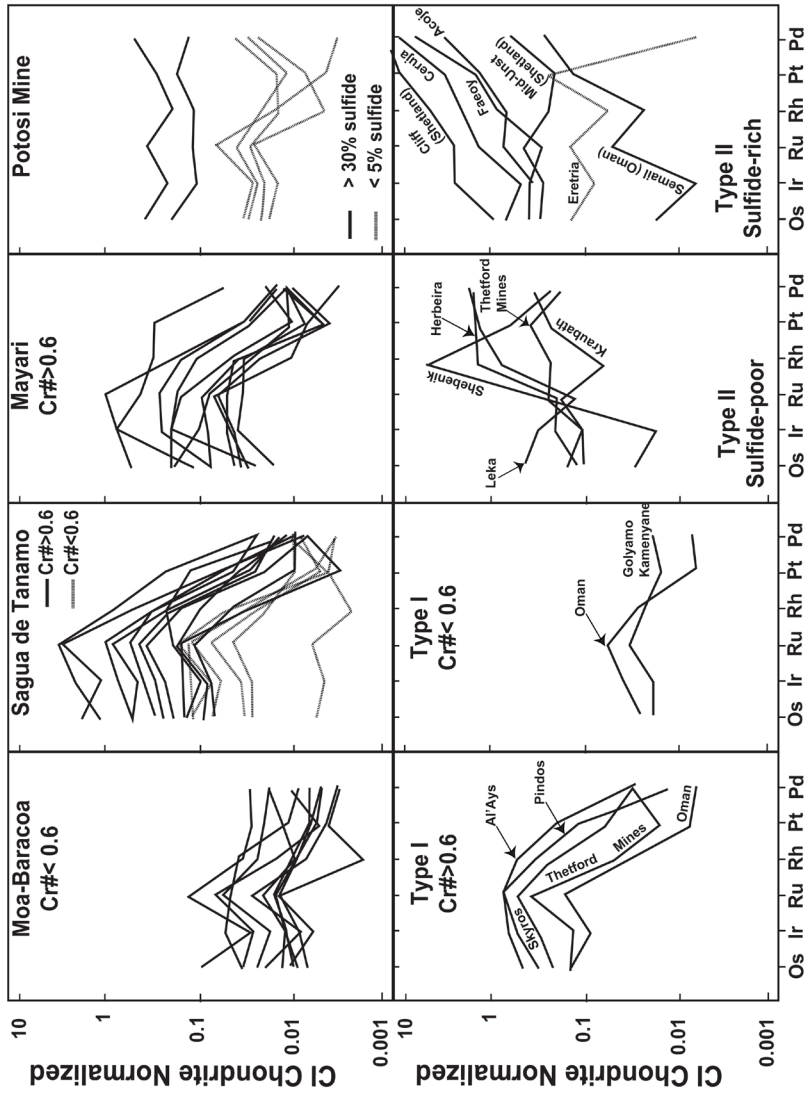

Figure 9. CI-chondrite (Naldrett and Duke 1980) normalized patterns of ophiolitic chromitites. Moa-Baracoa, Sagua de Tánamo, Mayarí and Potosí are examples of Type I chromitites with high-Cr and high-Al chromite hosted in the mantle section and Moho Transition Zone in the ophiolite belt of Mayarí-Baracoa (Proenza et al. 1999, 2001; Gervilla et al. 2005; González-Jiménez et al. 2011b). Other examples of Type I chromitites with high-Cr chromite include Al'Ays, Saudi Arabia (Prichard et al. 2008); Pindos, Greece (Economou-Eliopoulos 1993; Economou-Eliopoulos and Vacondios 1995); Oman (Ahmed and Arai 2003); Skyros Island, Greece (Economou 1983); Thetford Mines, Canada (Gauthier et al. 1990). Type I chromitites with high-Al include Golyamo Kamenyane, Bulgaria (González-Jiménez et al. 2014b) and Oman (Ahmed and Arai 2003). Data sources for sulfide-poor Type II chromitites: Herbeira, Spain (Moreno et al. 2001); Kraubath, Austria (Malitch et al. 2003); Leka, Norway (Pedersen et al. 1993), Shebenik, Albania (Kocks et al. 2007); Thetford Mines, Canada (Gauthier et al. 1990). Data sources for sulfide-rich Type II chromitites: Acoje, Philippines (Bacuta et al. 1990); Ceruja, Albania (Karaj 1992); Cliff and Mid-Unst in Shetland, Scotland (Prichard et al. 1986); Eretria, Tsangli area, Greece (Economou-Eliopoulos and Naldrett 1984) Faeoy, Finland; Haylayn Block, Oman (Lachize et al. 1991).

The *in situ* study of chromitite from a large number of ophiolites reveals that PGM are generally rare, with grain sizes typically <30 μm (Fig. 10a–f; see Ahmed and Arai 2003; González-Jiménez et al. 2014a,b, for review). In most cases, the PGM occur as inclusions in chromite grains and less frequently in the interstitial silicate matrix (unaltered or altered) between the chromite grains. Nevertheless, PGM can be also found in fractures cutting the chromite grains (where they may exhibit irregular shapes and/or alteration rims) or alteration zones around chromite edges (e.g., Fe^{2+} or Fe^{3+}-rich chromite with either porous or homogeneous textures) produced in chromite during post-magmatic alteration events such as serpentinization or metamorphism (e.g., ferrian chromite; Fig. 10e). Examples of PGM forming planar arrays (linear trails, corresponding to former grain boundaries or healed fractures) with base-metal minerals, silicates and fluid/melt inclusions have been observed. The grain morphology of PGM in ophiolitic chromitites is variable. Generally, PGM hosted in primary chromite show polygonal shapes. In contrast, those PGM found within fractures or altered zones of the chromitite may show a wide range of morphologies (i.e., subhedral or anhedral shapes, typically with internal sieve-texture and/or corroded grain boundaries) as a result of different rates of mechanical deformation or reaction with metasomatic fluids.

PGM distribution in ophiolitic chromitites. González-Jiménez et al. (2009a), and more recently González-Jiménez et al. (2014b), compiled a list of PGM in chromitites from world-wide occurrences, including reporting on the absolute number of grains found. An updated list of the PGM identified in both *Type I* and *Type II* chromitites, including previously unpublished data, is presented in *Supplementary Table* 2.

Most PGM identified in *Type I* chromitites occur in unaltered zones (i.e., cores) of chromite grains (66%), sometimes being manifest as inclusion trails. They consist predominantly of members of the laurite–erlichmanite solid solution series (76%), irarsite (9%), and Os–Ir–Ru alloys (9%). Substitution of Os by Ru in disulfides of the laurite–erlichmanite series is extensive-to-complete in most ophiolitic chromitites (Fig. 11). This is frequently reflected in the form of a range of styles of chemical zonation within single grains (Fig. 10a–d), including normal, reverse and oscillatory zonation. The coexistence of Os-poor laurite with Ru-poor, Os–Ir alloys has been reported in unaltered chromite grains, consistent with the assemblages reproduced at high-T in experiments (e.g., Brenan and Andrews 2001; Andrews and Brenan 2002). Grains of irarsite from within unaltered chromites show substitutions of Ir by Os (osarsite; OsAsS), Ru (ruarsite; RuAsS), and to a lesser extent, Rh (hollingworthite; (Rh,Pt,Pd)AsS). Rare Pt–Pd–Rh minerals observed in these unaltered zones include sperrylite and unidentified Pt–Pd–Rh alloys. Laurite–erlichmanite (18%) and irarsite (11%), characterized by S-deficiency are the most abundant PGM in the altered zones of *Type I* chromitites. Almost complete desulfurization and/or oxidation of these minerals has resulted in the formation of secondary Ru-rich Os–Ir alloys (13%) and oxides (5%) that are often observed in cracks, at the altered edges of chromite or in the serpentinized/weathered chromitite silicate matrix (Fig. 10e). Most of the remaining Pt–Pd–Rh PGM in the altered zones of chromitites comprise Pd–Cu–Sn, stibiopalladinite (Pd_5Sb_2), and sperrylite. These minerals are particularly frequent in chromitites from the metamorphosed ophiolites of Kraubath in the Austrian Alps (Thalhammer et al. 1990; Malitch et al. 2001), the Great Serpentinite Belt in Australia (Yang and Seccombe 1993), the Pampean Ranges in Argentina (Proenza et al. 2008) and the small Dobromirtsi massif in the Bulgarian Rhodopes (González-Jiménez et al. 2010). The abundance of Pt–Pd–Rh minerals in the altered zones of chromitites has been traditionally associated with the infiltration of either late magmatic or post-magmatic fluids, resulting in the localized redistribution of these PGE (e.g., Graham et al. 1996). However, it may simply reflect the physical fractionation of the PGE; Ru–Os–Ir PGM have a tendency to wet and/or nucleate along chromite surfaces while Pt–Pd–Rh PGM have a tendency to remain suspended in residual silicate melts (Matveev and Ballhaus 2002; Ballhaus et al. 2006; Finnigan et al. 2008).

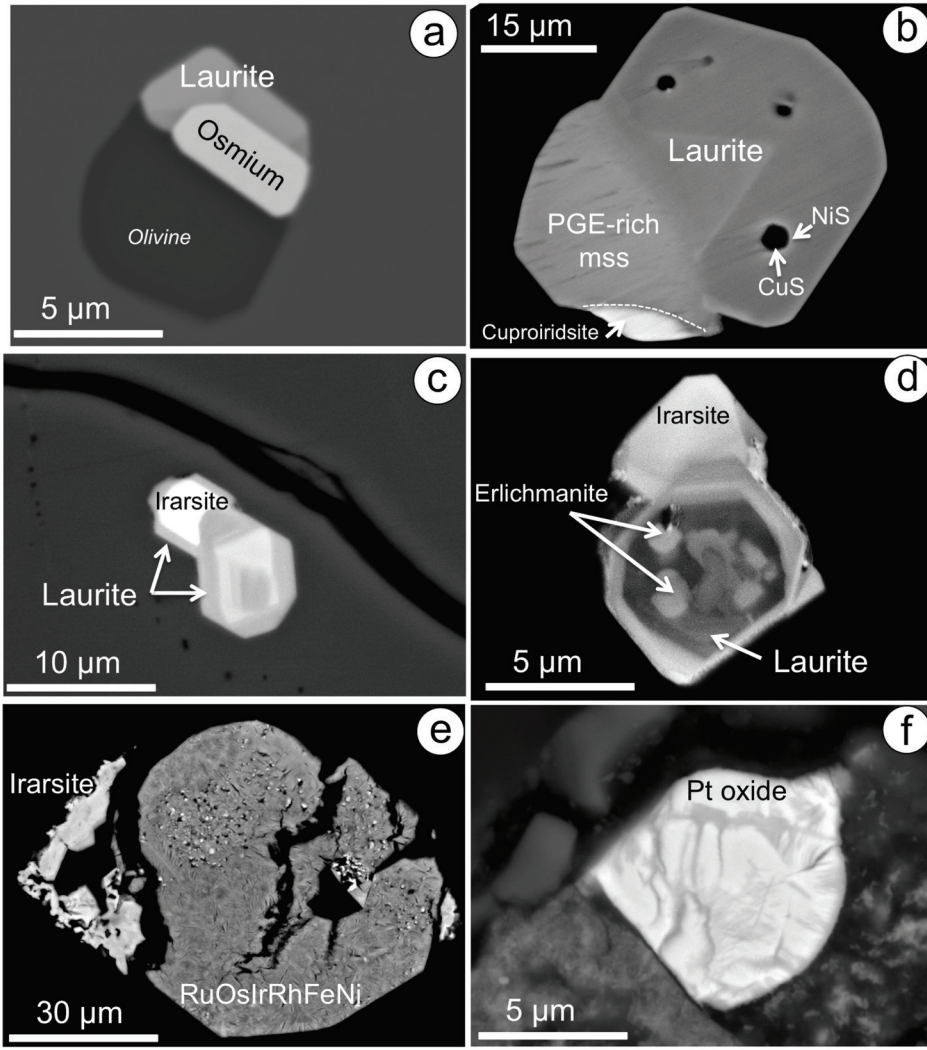

Figure 10. Images of PGM included in chromite from chromitites hosted in (a) the ultramafic complex of the Vizcaino Peninsula, Baja California Sur (Mexico), (b-e) the mantle of the Mayarí-Baracoa ophiolite belt in eastern Cuba and (f) in the silicate matrix of chromitite from the mantle-crust transition zone in the New Caledonia ophiolite. (a) Backscattered electron micrograph of a laurite and an Os-Ir grain at the edge of a silicate inclusion in chromite. (b) Backscattered electron micrograph of a composite grain made up of an intergrowth of zoned laurite with PGE-rich mss and cuproiridsite. (c) and (d) are grains of zoned laurite-erlichmanite intergrowth with irarsite (Monte Bueno chromite deposit; Gervilla et al. 2005; González-Jiménez et al. 2009b). (e) Backscattered image of partially desulfurized irarsite attached to a larger grain of a pseudomorphed Ru-Os-Ir-Rh-Fe-Ni alloy after desulfurization of laurite in a chromite crack (Tres Amigos Mine, Mayarí-Baracoa Ophiolite, Cuba). (f) Backscattered image of Pt-oxide after cooperite (Ouen Island; González-Jiménez et al. 2011a).

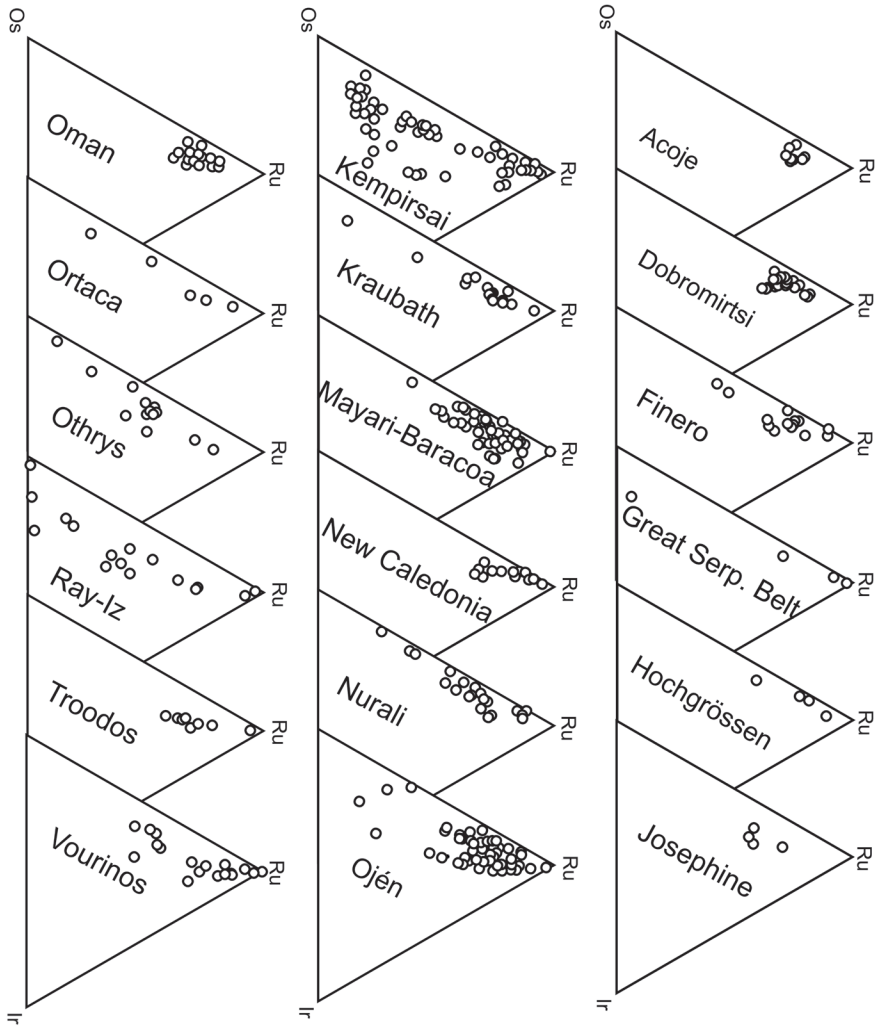

Figure 11. Composition of inclusions of the laurite–erlichmanite solid solution series in chromite grains in chromitites from different ophiolite complexes, plotted in Ru-Os-Ir (atomic %) ternary diagrams. The data for these plots are sourced as follows: Acoje block, Philippines (Bacuta et al. 1990; Orberger et al. 1988); Dobromirtsi, Rhodope Complex in southern Bulgaria (González-Jiménez et al. 2010, 2013b, 2014c); Finero (Ferrario and Garuti 1990; Garuti and Zaccarini 1994); Great Serpentinite Belt, Australia (Yang and Seccombe 1993); Hochgrössen (Thalhammer et al. 1990; Malitch et al. 2003); Josephine (Stockman and Hlava 1984); Kempirsai, Kazakhstan (Melcher et al. 1997); Kraubath, Austria (Thalhammer et al. 1990; Malitch et al. 2003); Mayarí-Baracoa, eastern Cuba (including Moa-Baracoa, Sagua de Tánamo and Mayarí; Gervilla et al. 2005; González-Jiménez et al. 2011b); New Caledonia (including Tiébaghi, Massif du Sud, Ouen and Pirogues; Augé 1988; Augé et al. 1998; González-Jiménez et al. 2011a); Nurali, Russia (Zaccarini et al. 2004b; Grieco et al. 2006); Ojén, southern Spain (Torres-Ruiz et al. 1996; Gutiérrez-Narbona et al. 2003; González-Jiménez et al. 2013a) Oman (Augé 1987; Ahmed and Arai 2003); Ortaca, southeastern Turkey (Uysal et al. 2005); Othrys, Greece (Garuti et al. 1999a); Ray-Iz, Russia (Garuti et al. 1999b); Troodos, Cyprus (Legendre and Augé 1986; Augé and Johan 1988; McElduff and Stumpfl 1990), Vourinos, Greece (Augé 1985; Augé 1988; Garuti and Zaccarini 1997).

In accord with their whole-rock enrichment in the PPGE, *Type II* chromitites show a preponderance of Pt, Pd, and Rh PGM (Fig. 9). Most *Type II* chromitites described are associated with metamorphosed ophiolites and the Pt–Pd–Rh PGM are situated near chromite rims (usually altered) or in the interstitial silicate matrix (63%), rather than in the unaltered portions (i.e., chromite crystal cores). These features make it difficult to interpret the fractionation of the PGE in terms of high-temperature magmatic processes. In their recent review, González-Jiménez et al. (2014b) showed that sperrylite (29%), stibiopalladinite (10%) and isoferroplatinum (8%), and members of the solid solution series cooperite–braggite are the most common minerals in the unaltered cores of chromite. The Pt–Pd–Rh ± base-metal alloys (23%), isoferroplatinum (12%), sperrylite (9%), and Pt-oxides (derived from the alteration of Pt-sulfides such as malanite) are the most abundant PGM in the altered zones of the chromitite. In chromitites that have been altered by high-temperature hydrothermal fluids (i.e., Ouen Island, New Caledonia), grains of isoferroplatinum in a chlorite-dominated interstitial matrix show corroded outlines and enrichment in Pd, whereas malanite in a serpentine-rich matrix is partially corroded and S-poor due to desulfurization. When in contact with chlorite, the malanite has rims of Pt-oxide (González-Jiménez et al. 2011a). The Os–Ir–Ru PGM are the same as those that predominate in *Type I* chromitites, whether they are observed as inclusions in chromite or they occur in the groundmass: laurite–erlichmanite, Os–Ir–Ru alloys and irarsite. As observed in *Type I* chromitites, when IPGE-rich sulfides occur in the altered silicate matrix they show evidence of post-magmatic desulfurization or oxidation, such as corroded outlines, a S-deficiency or rims of Pt-group alloys/oxides.

Re–Os isotopes in ophiolitic chromitite PGM. The Re–Os isotope systematics of PGM from ophiolitic chromitites were initially examined on individual grains separated mechanically from chromitite samples and more recently on polished thin sections and blocks, using N-TIMS (Walker et al. 1996; Malitch et al. 2003), ion probe (Ahmed et al. 2006), and LA-MC-ICPMS (Pearson et al. 2007; Shi et al. 2007; González-Jiménez et al. 2014b and references therein). The PGM in ophiolite chromitites generally yield relatively low $^{187}Re/^{188}Os$ ratios and show a significant dispersion in $^{187}Os/^{188}Os$ ratios (Fig. 12). The *in situ* LA-MC-ICPMS analysis of Re–Os isotopes of PGM included in unaltered chromite grains have revealed significant heterogeneity in the Os compositions of PGM inclusions within single chromite grains, separated several mm apart. This isotopic heterogeneity is observed within composite aggregates of the PGM smaller than 50 μm in diameter and even within single zoned laurite grains (e.g., Marchesi et al. 2011; Gonzalez-Jimenez et al. 2012a). Although Re-depletion model ages (T_{RD}) of some chromitite-hosted PGM broadly coincide with the timing of known tectonomagmatic mantle or crust-forming events (e.g., Shi et al. 2007; Marchesi et al. 2011; Belousova et al. 2015; McGowan et al. 2015), more commonly chromitite-hosted PGM yield T_{RD} ages older than the supposed age of formation of the host chromitite/ophiolite (Fig. 12). For example, the ~21 Ma chromitites of the Ojen massif in southern Spain contain PGM that yield T_{RD} ages of ~1.4 Ga, and the Group II Os-Ir alloys analyzed by Shi et al. (2007) in the chromitites of the Mesozoic Donqiao ophiolitic massif reveal a range of T_{RD} between 1130 and 240 Ma, with age peaks at ~870, 930, 1089, 1100, and 1130 Ma. Interestingly, González-Jiménez et al. (2013a) observed that grains of laurite and base-metal minerals (including sulfides and arsenides) in chromitite and in the host peridotite of the Ojen massif (southwestern Spain) have similar values and ranges of heterogeneity in Os isotopes. Most laurites ($n = 104$) and base-metal minerals ($n = 27$) have $^{187}Os/^{188}Os$ between 0.1181 ± 0.000003 and 0.1364 ± 0.0006, roughly matching those of the base-metal sulfides of the peridotite (0.1159 ± 0.0007 to 0.1374 ± 0.0014; $n = 33$). González-Jiménez et al. (2014a) proposed that the presence of multiple populations of PGM in the chromitites reflects the combination of (1) direct crystallization of PGM from the basaltic parental melts of the chromitites and (2) entrainment of some older PGM present in the peridotite during the migration of such a melt through the source/host mantle.

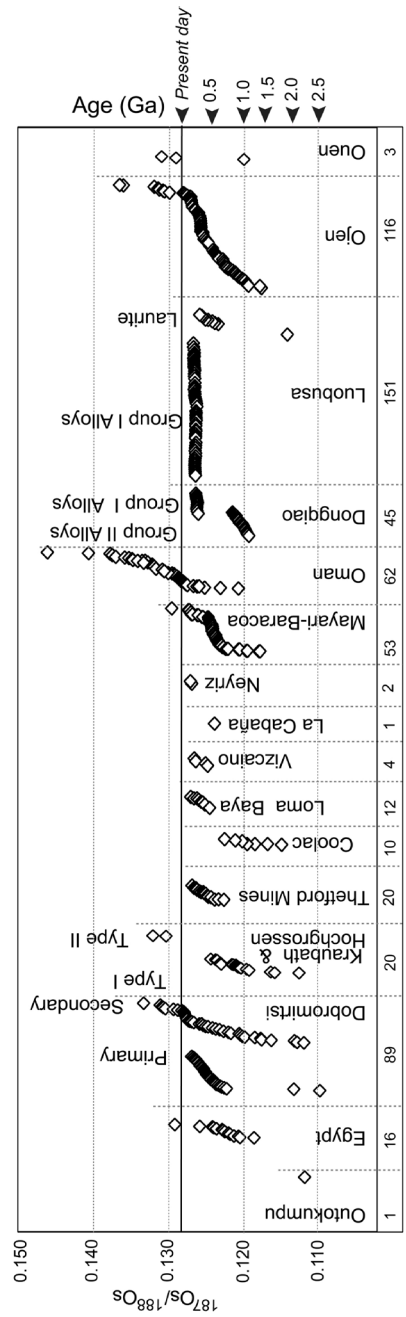

Figure 12. $^{187}Os/^{188}Os$ isotopic ratios and corresponding T_{RD} model ages for PGM analyzed *in situ* in chromitites from ophiolite-type ultramafic complexes; updated after González-Jiménez et al. 2014a. Data sources: Coolac Serpentinite Belt, Australia (Belousova et al. 2015); Dobromirtsi (Bulgaria; González-Jiménez et al. 2013a, 2014c); Eastern Desert, Egypt (Ahmed et al. 2006); Hochgrössen and Kraubath massifs, Austria (Malitch 2004; Malitch et al. 2003); La Cabaña (this study); Loma Baya, Guerrero State, Mexico (González-Jiménez et al. 2014b); Luobusa and Donqiao, Tibet (Shi et al. 2007; McGowan et al. 2015); Mayarí-Baracoa, eastern Cuba (Marchesi et al. 2011; González-Jiménez et al. 2012a); Neyiríz (this study); Ojén (González-Jiménez et al. 2013a); Ouen Island (González-Jiménez et al. 2014b); Outokumpu ophiolite, Finland (Walker et al. 1996); Thetford Mines, Canada (this study); Vizcaino, California State, Mexico (this study).

The analysis of Re–Os isotopes of individual PGM from highly metamorphosed chromitites yields somewhat contradictory results. González-Jiménez et al. (2012b) observed that in highly metamorphosed chromitites of the Dobromirtsi peridotite (Central Rhodope Complex, Bulgaria), laurite grains wholly enclosed in unaltered chromite have $^{187}Os/^{188}Os$ compositions very distinct from the secondary laurite in the altered zones (Fig. 12). Given the low $^{187}Re/^{188}Os$ compositions in both populations (<0.024), these authors suggested that the wider range of $^{187}Os/^{188}Os$ observed in the secondary laurite population formed by interaction with fluids of variable $^{187}Os/^{188}Os$ composition during metamorphism. Malitch et al. (2014) analyzed a similar assemblage of PGM containing laurite ± Os–Ir alloy ± Ru-pentlandite in chromitites from the Shetland Ophiolite Complex (Scotland), but they did not observe a comparable dispersion of $^{187}Os/^{188}Os$ values. Instead, the latter authors note that the PGM in the Shetland chromitites exhibit unusually homogeneous $^{187}Os/^{188}Os$ that they interpreted as evidence for the resistant nature of the $^{187}Re–^{188}Os$ system in Os-rich minerals to metamorphic alteration. González-Jiménez et al. (2014a) suggested that polyphase metamorphism might not just disperse the $^{187}Os/^{188}Os$ signatures of individual PGM, but may act to homogenize them also. Following this line of reasoning, alteration of the Shetland PGM may have occurred in a closed system and was not directly related to metamorphism but to a separate 'auto-hydrothermal' event, perhaps during the late stages of magmatic evolution of the chromitite ore system (cf. Derbyshire et al. 2013). González-Jiménez et al. (2011a) proposed a similar scenario to explain the origin of secondary 'desulfurized' PGM sulfides within 'primary hydrous silicates' in the chromitites of Ouen Island, New Caledonia.

Petrogenesis of PGM during chromitite formation in the upper mantle. As noted above, *Type I* ophiolitic chromitites usually contain two types of PGM assemblage (*Supplementary Table* 2): (1) *inclusions in chromite* composed of almost exclusively Os-, Ir-, and Ru-rich PGM, which are commonly associated with small amounts of Ni–Fe–Cu sulfide (even in the same inclusion); (2) *an interstitial assemblage* consisting mainly of PPGE-rich minerals. The latter assemblage may also contain secondary Os–Ir–Ru PGM, produced following alteration of primary PGM via hydrothermal alteration or weathering. The PGM included in chromite may therefore be considered as primary, as these grains are 'shielded' from post-magmatic alteration.

The origin of these two assemblages in chromitite has been the subject of much debate during the last four decades (see González-Jiménez et al. 2014a for review). Some authors have suggested that PGE-rich chromitites could result from a PGE-rich melt produced following high-degree partial melting of a PGE-enriched mantle source (e.g., Prichard et al. 2008). However, experimental data (e.g., Ballhaus et al. 2006; Finnigan et al. 2008) show that the PGE-enrichment in chromite and the fractionation between IPGE and PPGE could simply reflect the local effect of chromite crystallization in PGE-bearing S-undersaturated melts. Gijbels et al. (1974) and Naldrett and Cabri (1976) suggested that the PGE could enter the structure of chromite at high temperature and subsequently be exsolved as discrete PGM upon cooling. Later experimental work showed that Os, Ir, Ru, and Rh could substitute in the chromite structure at high temperature and suitable f_{O_2} (Capobianco 1998; Capobianco and Drake 1990; Capobianco et al. 1994; Righter and Downs 2001; Righter et al. 2004). Although later experiments indicated that such high values of f_{O_2} are probably unrealistic at mantle conditions (Brenan et al. 2012), the potential role of high-temperature formation of inclusions of Os-, Ir- and Ru-rich PGM in chromite is worth further discussion. Another problem with the idea is that the textures exhibited by the PGM are not typical of exsolution (e.g., they don't occur along the crystallographic planes of the chromite). Instead, chromite-hosted PGM are characteristically euhedral and faceted, as shown by multiple studies employing optical (conventional reflected light microscopy, SEM) and laser ablation techniques.

An important alternative model suggests that both sub-μm and visible PGM grains form initially as nano-size metal clusters (cf. Tredoux et al. 1995; Helmy et al. 2013), which later

coarsen to larger PGM. Coarsening presumably takes place by diffusion-driven, solid-state Ostwald ripening, similar to that observed for native Au nanoparticles in pyrite (Reich et al. 2006). Micronuggets of PGM have been reported for chromites from a range of settings (Ballhaus and Sylvester 2000; Sattari et al. 2002; Locmelis et al. 2011; Pagé et al. 2012). However, their thermal behavior in the chromite matrix is not well understood due to a lack of experimental data on their physical and chemical properties. Coarsening of nano-scale metal clusters could operate at the sub-μm scale in chromite at high-temperature when diffusion is easier. However, macroscopic PGM that exhibit chemical and Os isotopic zoning characterized by precipitation–dissolution microstructures (e.g., Fig. 10) are better explained by the involvement of fluid/melts during mineral growth.

Locmelis et al. (2011) and subsequently Pagé et al. (2012) conducted laser ablation ICP-MS analysis on komatiite chromites and observed an almost homogeneous distribution of Ru and sub-μm Ir-bearing alloys, which they took to imply that Ru exists in solid solution in chromite at high temperatures. However, they did not carry out high-resolution transmission electron microscopy (HRTEM) to test the potential existence of native Ru particles at near atomic scales. It is possible that the LA-ICP-MS technique, with typical beam diameters of ~20–40 μm, does not operate at sufficiently high resolution to detect nano-scale PGM. This might in turn imply a different range of stability of Ru nanoparticles relative to metal nanoparticles of the other PGE. In light of this, the linear correlations observed between Os+Ir+Ru and Cr# in chromites from natural samples and experiments might simply reflect nugget fractionation, rather than PGE substitution in the crystal lattice of chromite (Ballhaus et al. 2006).

Precipitation of metallic nanoparticles of the PGE from silicate melts has been documented in a series of experiments (Mungall 2005; Finnigan et al. 2008). As described above, local reduction of f_{O_2} at the edges of chromite crystals may cause the saturation of the most easily oxidized PGE (Os, Ir, Ru) in the form of metallic nanoparticles (Finnigan et al. 2008). These results are comparable to those obtained by Matveev and Ballhaus (2002), Bockrath et al. (2004b) and Ballhaus et al. (2006), who also reported the nucleation of abundant nanoparticles of Os–Ir–Ru alloys on chromite surfaces. They also crystallized fewer but much larger-sized metallic alloys of Pt and Pd in the silicate glass. These experimental results clearly demonstrate that the precipitation of chromite may cause fractionation of the PGE from one another, as it provides a nucleation substrate for the most refractory IPGE alloys. Nugget formation is likely only possible at S-undersaturated conditions. These experimental constraints are also consistent with the observation that natural chromitites precipitated from S-undersaturated arc melts in the upper mantle contain an assemblage of Os-, Ir-, and Ru-rich PGM included in chromite crystals and another mostly dominated by Pt- and Pd-rich PGM in the interstitial silicate matrix (e.g., González-Jiménez et al. 2014a). Another excellent and historically significant example of this sort of distribution of the PGM (i.e., Os-, Ir-, and Ru-rich phases in chromite, and Pd-rich phases in interstitial sulfarsenides and arsenides, is described from Heazlewood, Tasmania (Peck and Keays 1990).

A similar mechanism of chromitite genesis can be assumed for the formation of PGM in the *Type II* chromitites. In this model, ascending basaltic melts crystallize IPGE-rich chromitites in the lower parts of the mantle through which they migrate, producing Pt- and Pd-rich fractionated melts (Fig. 13). The fractionated melts would migrate upwards giving rise to Pt- and Pd-rich chromitites in the uppermost mantle portion or the lower crustal (cumulate) section of the ophiolite. Usually, *Type II* chromitites have much lower Mg# than *Type I* chromitites, which is taken as evidence that they crystallized from melts that underwent higher degrees of fractionation. This might also induce sulfur saturation relatively early during magmatic evolution, explaining the coexistence of oscillatory zoned laurite with Pt-rich alloys, Pt±Rh±Ir sulfides and Ni–Cu–Fe (e.g., Ouen Island and Pirogues in the New Caledonia ophiolite; Augé and Maurizot 1995; González-Jiménez et al. 2011a).

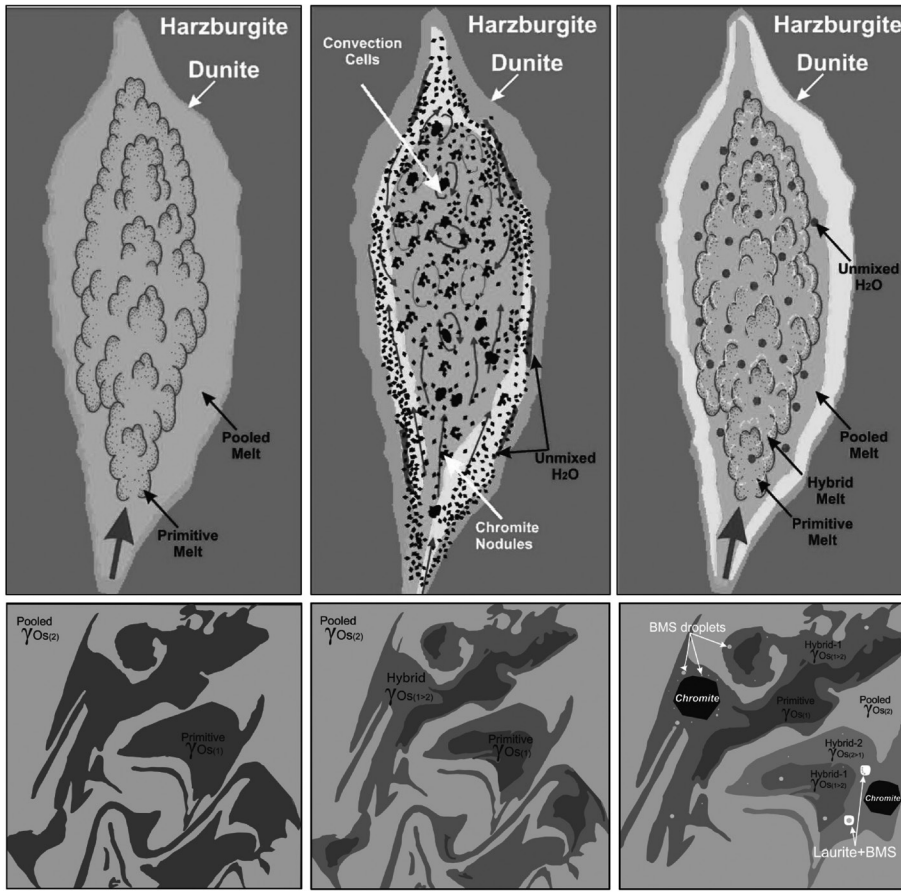

Figure 13. Sketches illustrating how chromite and PGM crystallize from hybrid melts, following the mixing/mingling of magmas with different degrees of fractionation. The sketches also show how Os isotope heterogeneity can develop in the upper mantle conduits where podiform chromitites are considered to form. These conduits can be centimeters to tens of meters wide, but are typically on the order of tens of centimeters to several meters wide. Details are given in the main text. The parameter γ_{Os} signifies the percent deviation of $^{187}Os/^{188}Os$ from a chondritic reference at the time of formation, and BMS is base-metal sulfide.

Many PGM inclusions in chromite exhibit euhedral morphologies, an observation originally interpreted as evidence for their direct precipitation from fluids or melts before chromite crystallization (e.g., Constantinides et al. 1980; Legendre 1982; Stockman and Hlava 1984; Augé 1985). The mechanical trapping of PGM-saturated melt droplets by chromite was suggested by Melcher et al. (1997). In this scenario, fast-growing chromite can mechanically trap molten inclusions, explaining the drop-like textures that the inclusions sometimes exhibit. Melcher et al. (1997) also suggested that even euhedral inclusions may have originated as melt inclusions, suggesting that they filled negative crystal cavities in the chromite host.

During the 1980s and 1990s the formation of chromitite was interpreted as the result of a simple mechanism of fractional crystallization of basaltic melt. In this model, the PGM represented early refractory minerals crystallized before chromite. The coexistence of PGM alloys, sulfides, and sulfarsenides simply reflected different stages of the cooling history of the chromitite body. The PGM alloys crystallized first at higher temperature and under lowest f_{S_2},

which increased upon cooling to give rise to a series of PGM sulfides and/or Ni–Cu–Fe sulfides (Stockman and Hlava 1984; Augé and Johan 1988; Leblanc 1991; Torres-Ruiz et al. 1996; Augé et al. 1998; Garuti et al. 1999a). The results obtained in subsequent experiments (Brenan and Andrews 2001; Andrews and Brenan 2002; Bockrath et al. 2004b) showed that Os-free laurite (RuS_2) may co-precipitate in equilibrium with Os–Ir alloys at the T–f_{S_2}–f_{O_2}–P conditions prevailing during the crystallization of chromitites in the upper mantle [1200–1300 °C, log f_{S_2} from –2 to –1.3, and ~0.5 GPa]. Furthermore, a simple trajectory of cooling does not explain why many chromitite bodies contain PGM with a range of patterns of compositional zoning, including normal, reverse, and oscillatory zonation (Fig. 10a–d; González-Jiménez et al. 2009b). Fractional crystallization also doesn't explain the wide dispersion of $^{187}Os/^{188}Os$ isotope compositions amongst individual PGM (and base-metal sulfides) that coexist within single grains of chromite or intra-crystal Os isotopic heterogeneity in oscillatory-zoned laurites (Ahmed et al. 2006; Marchesi et al. 2011; González-Jiménez et al. 2012a). Crystallization of chromitite by melt mixing (or mingling) in open conduits in the upper mantle may create a heterogeneous environment with variations in T–f_{O_2}–f_{S_2}–a_{As} over short time spans (González-Jiménez et al. 2014a,b). Local changes in f_{O_2} during crystallization of chromite could cause the precipitation of small metallic nanoparticles of PGM, which could then attach to the surface of chromite in equilibrium with the ambient silicate melt, as has been observed experimentally (Fig. 14; Matveev and Ballhaus 2002; Ballhaus et al. 2006; Finnigan et al. 2008). The influx of fluids/melts into the open conduit, producing sudden changes of f_{S_2} and/or a_{As} could destabilize discrete alloys, leading to the formation of PGE-sulfides or PGE-sulfarsenides (e.g., Bockrath et al. 2004b). Such a dynamic environment could also promote the immiscible segregation of droplets of sulfide melt, producing the base-metal sulfides commonly associated with the PGM in chromite (Garuti et al. 1999b) which could scavenge any PGE remaining in the melt (Moreno et al. 1999; Proenza et al. 2001; González-Jiménez et al. 2012a).

Incorporation of PGM from the host peridotite: an alternative model? As noted above, some ophiolite chromitites contain PGM with T_{RD} ages much older than the supposed age of formation of their host chromitite/ophiolite. For example, Luobusa chromitite 'Group II' alloys yield T_{RD} ages (≥1.1 Ga) much older than the age of formation of the ophiolite (177 ± 31 Ma; Zhou et al. 2002), which has led to them being considered as xenocrystic in the chromitites (Shi et al. 2007). The latter authors stated that 'Group II alloys were scavenged from the surrounding oceanic lithospheric mantle during melt-rock reaction'. The model of Shi et al. suggests that not all PGM hosted in ophiolitic chromitites necessarily form by direct precipitation from their parental melts. According to González-Jiménez et al. (2014b), incorporation of PGM present in the host peridotite might explain the ancient (> 1 Ga) T_{RD} ages of some chromitite-hosted PGM from Phanerozoic ophiolites (Figs. 12, 13). González-Jiménez et al. (2014b) suggested that such heterogeneity in $^{187}Os/^{188}Os$ signatures of PGM could reflect '*…a series of small-scale events of melt extraction and melt-rock reaction that has produced a progressive but stepped sequence of decreasing f_{S_2} in the mantle, promoting the breakdown of their PGE-bearing base-metal sulfides into 'residual' laurites, and to a major extent Os–Ir alloys…*'. The latter authors invoked this as a process to explain '*…the broad coincidence of the T_{RD} ages of many PGM with known magmatic events related to ophiolite formation*'. Some PGM could therefore reside in the mantle for hundreds of millions of years, explaining the coexistence of PGM with ages close to that of the chromitite/ophiolite host and those with older ages. Chromitite-hosted PGM also show similar ranges in $^{187}Os/^{188}Os$ as peridotite-hosted base-metal sulfides. According to Gonzalez-Jiménez et al. (2014b), Os may be transported as submicroscopic Os-bearing alloys which could later react with S to form sulfides like laurite in water- and volatile-rich melts at high temperature, low pressure and low f_{S_2} (cf. Bockrath et al. 2004a). This is an alternative mechanism that may produce contemporaneous PGM and chromite, where the PGM preserve older Os signatures from their host mantle, analogous to partial recent recrystallization of zircons that can also preserve older $^{176}Hf/^{177}Hf$ isotope signatures (cf. Belousova et al. 2015; McGowan et al. 2015).

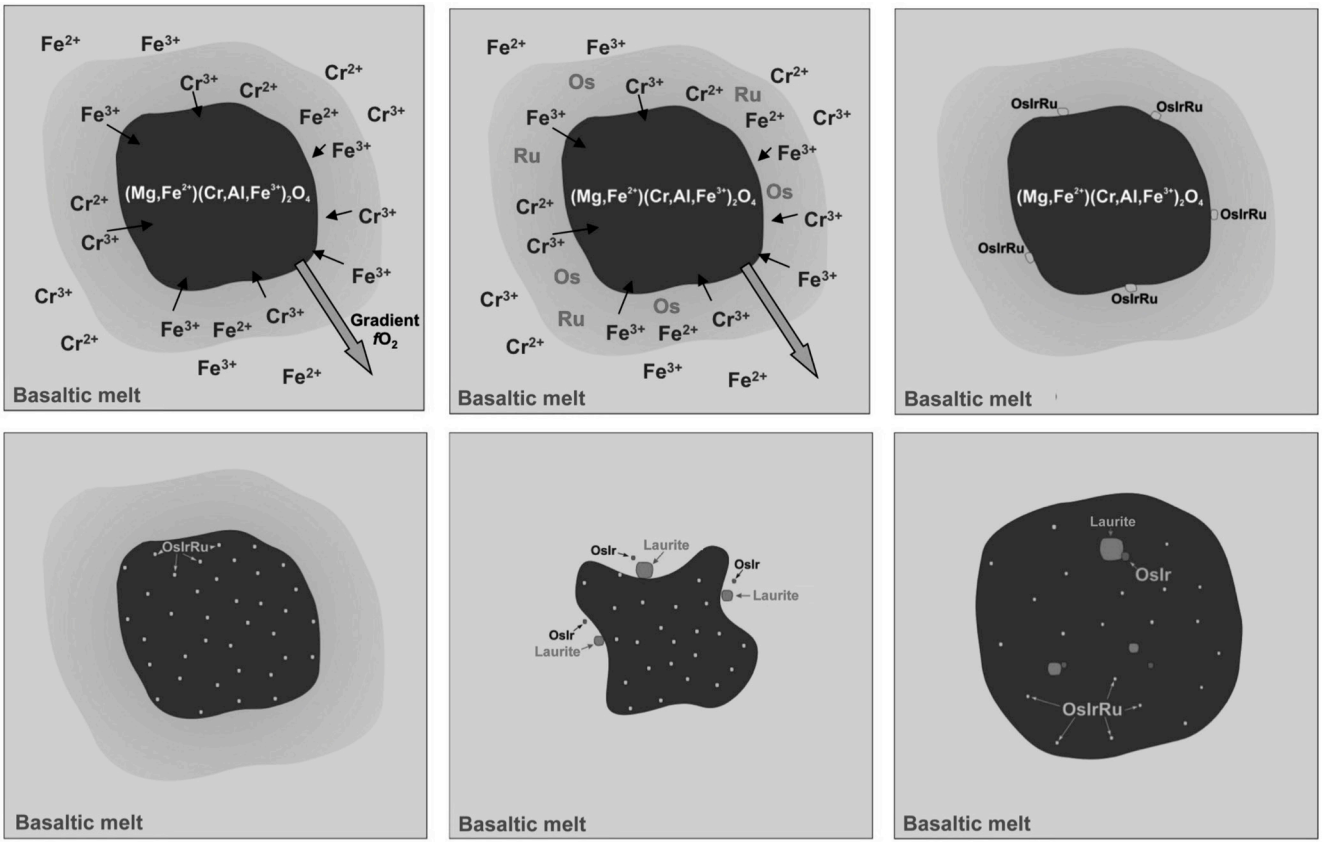

Figure 14. Sketches showing the localized (grain-scale) effect that chromite crystallization may have on PGE fractionation and PGM formation. Details are given in the main text (see also Finnigan et al. 2008).

PGM in sulfide-rich ophiolite lithologies

The association of massive base-metal sulfide ores with mafic and ultramafic rocks is an uncommon feature of ophiolites. The sulfide-rich ores may be either of magmatic or hydrothermal origin and located in any part of the ophiolite stratigraphy. Magmatic base-metal sulfides representing up to 5% by volume of the rock have been described in the crustal portions of some ophiolites, including the sheeted dike complex of Faeoy, Norway (Barnes et al. 1988; Boyd et al. 1988), the layered gabbros of the Haylayn block in Oman (Lachize et al. 1991) and the pyroxenite cumulates of ophiolites of south western Oregon, USA (Foose 1985). Horizons more enriched in magmatic sulfides than this have been described in dunite seams and pods of the mantle–crust transition and upper mantle at Ceruja (Albania; Karaj 1992), Unst (Shetland; Prichard and Lord 1993; O'Driscoll et al. 2012; Derbyshire et al. 2013), and chromite-rich dunites (including chromitites) at Acoje (Philippines; Bacuta et al. 1990), Potosí (eastern Cuba; Proenza et al. 2001) and northen Oman (Negishi et al. 2013).

Overall, sulfide mineralized lithologies exhibit enrichment in PPGE over IPGE, represented by steep positive chondrite-normalized PGE patterns (Fig. 9), irrespective of the relative PGE abundances. This has been interpreted as reflecting immiscible segregation of sulfide melts after extensive fractionation of the silicate melt. However, Proenza et al. (2001) showed that the origin of the PGE-rich sulfide mineralization associated with the chromitites at Potosí (Cuba) was associated with the modification of the chromite ores by the late intrusion of olivine-norite and gabbro dikes. According to these authors, the interaction between pre-existing, sulfide-poor chromitite and the intruding volatile-rich melts drove brecciation, partial dissolution, and recrystallization (coarsening) of chromite. The sulfide assemblage formed by fractionation of an immiscible sulfide melt that segregated from the volatile-rich silicate melt; the segregation process itself has been attributed to the reaction between the intruding melts and the host chromite (Proenza et al. 2001). Evidence for the magmatic nature of the sulfide mineralization comes from sulfur isotopes ($\delta^{34}S$), which range from –0.4‰ to +0.9‰. According to Proenza et al. (2001), the variable extent of the melt–rock reaction produced chromite ores with variable sulfide ratios, which preferentially collected the relatively incompatible PPGE.

Massive sulfides interpreted as hydrothermal precipitates, related to serpentinization of the host rocks, have been reported in the Tsangli area, Eritrea (Greece; Economou and Naldrett 1984), and in the serpentinized harzburgites and dunites of the Limassol Forest (Cyprus; Foose et al. 1985; Thalhammer et al. 1986). Unlike magmatic ores, hydrothermal sulfides show relatively flat PGE patterns, with a depletion in Pt in the sulfide-rich chromitite ores described from Eretria (Fig. 9). A detailed PGM documentation of sulfide-rich ophiolite peridotites has only been provided for the Shetland Ophiolite Complex (Prichard et al. 1994; Derbyshire et al. 2013) and the pertinent details are summarized as follows:

1. Some sulfide-rich dunites on the island of Unst have >1 ppm Pt+Pd (O'Driscoll et al. 2012). These lithologies contain stibiopalladinite, sperrylite, geversite [$Pt(Sb,Bi)_2$], genkinite [$(Pt,Pd)_4Sb_3$], Pt–Fe–Cu alloys, hongshiite (PtCu) and Pt–Pd ochres. Antimonides of Pd occur in silicates surrounding the clusters of sulfide, in fractures cross-cutting the chromite grains, as rims to breithauptite (NiSb), or in Ni–Fe alloy rims on heazlewoodite or pentlandite. Geversite and the Pt–Fe–Cu alloys were found in a chlorite rim surrounding a cluster of sulfides associated with chromite grains.
2. Sulfide-bearing wehrlites and pyroxenites contain grains of sperrylite, Pd-antimonides and Pt-ochres, located at the margins of aggregates composed of chalcopyrite (replaced by bornite) and pyrrhotite (hosted within clinopyroxene).
3. Gabbro-hosted wehrlite in the uppermost part of the dunite transition zone (i.e., immediately below the geophysical Moho) of the Shetland Ophiolite is rich in base-metal sulfides (pyrrhotite, pentlandite, pyrite, chalcopyrite ± gersdorffite [NiAsS], and niccolite [NiAs]). Prichard et al. (1994) reported one grain (~5 μm) of sperrylite at the junction between wehrlite and pyroxene layers.

Prichard et al. (1994) interpreted the close spatial association of Pt- and Pd-rich PGM and base-metal sulfides as evidence that the precipitation of the PGM occurred after the collection of the PGE from a silicate melt by an immiscible sulfide fraction. They suggested that the Pt preferentially entered the structure of chalcopyrite whereas pyrrhotite and pentlandite incorporated Pd more easily. On cooling and alteration, these PGE were released from the sulfides and recrystallized as PGM in close proximity to the sulfides. Although there is evidence to suggest that Pd exists in solid solution in pentlandite, the balance of evidence suggests that incorporation of Pt into chalcopyrite and Pd into pyrrhotite as suggested by Prichard et al. (1994) is less likely.

PGM IN PERIDOTITES OF THE SUBCONTINENTAL LITHOSPHERIC MANTLE

The subcontinental lithospheric mantle (SCLM) formed in the mid-late Archean and constitutes the lower part of the continental lithosphere (see also Aulbach et al. 2016, this volume, and Luguet and Reisberg 2016, this volume). By providing stable continental cratons on an Earth floored by oceanic crust, the SCLM has facilitated a significant reorganization of plate tectonics over geological time (Griffin et al. 2013). Micrometric PGM have been identified in tectonically emplaced peridotite massifs and mantle xenoliths, both considered to represent SCLM materials.

Subcontinental lithospheric mantle peridotite massifs

Mineralogical distribution and petrogenesis of PGM in peridotite massifs. Sub-μm PGM grains have been identified in lherzolites of the Lherz massif (southern France; Luguet et al. 2007; Lorand et al. 2010; König et al. 2015) The PGM identified in these studies are micronuggets (0.5–0.3 μm diameter) and occur as inclusions in or at the margins of larger base-metal sulfides. The PGM consist primarily of the laurite–erlichmanite solid solution series, Pt–Ir–Os-rich alloys, and Pt–Pd–Te–Ni minerals of the moncheite–merenskyite series. Other PGM found in these peridotites include sperrylite, minerals of the malanite–cuprorhodsite [$(Cu,Fe)Rh_2S_4$] solid solution series, braggite, unidentified Pt–Cu alloys, Pt–Fe alloys, and Au. Lorand et al. (2010) also identified smaller PGM during ablation runs of base-metal sulfides using LA-ICP-MS.

In the Lherz peridotites, laurite occurs with Pt–Ir–Os alloys and members of the malanite–cuprorhodsite series in base-metal sulfide-poor, and base-metal sulfide-free harzburgites. The Pt- and Pd-rich bismuthotellurides are predominantly found in lherzolite and to a lesser extent in clinopyroxene-bearing harzburgite. Thus, the relative abundances of bismuthotellurides and base-metal sulfides increase significantly in the relatively fertile rocks (i.e., lherzolites and clinopyroxene-bearing harzburgite), whilst that of laurite drops. Lorand et al. (2010) interpreted the textural relationships between the PGM and base-metal sulfide in the different rock types as the result of mixing between refractory PGM (laurite/Pt–Ir–Os alloys) inherited from older refractory SCLM and late-stage metasomatic sulfides precipitated from a melt of tholeiitic composition. The formation of laurite and Pt–Ir–Os alloy is attributed to a series of partial melting events of the (~2 Ga) SCLM, that removed base-metal sulfide and left behind refractory PGM that were stable under S-undersaturated conditions. These PGM were subsequently mechanically collected by droplets of sulfide melt during refertilization reactions that converted the harzburgite protolith to lherzolite (see also Riches and Rogers, 2011). According to Lorand et al. (2010), the textural relationships and the positive correlation between base-metal sulfide and the abundance of Pt–Pd–Te–Bi minerals in the lherzolite indicate that these minerals are cogenetic and that their origin is related to the process of refertilization, which also added chalcogenes and semi-metals like Se, As, Sb, Te, and Bi.

Marchesi et al. (2010) identified sulfide-hosted Pt-rich nuggets up to several μm across in peridotites of the Ronda massif (southern Spain). These Pt-rich minerals were inferred by inspection of time-resolved signals collected during laser ablation ICP-MS analyses.

SCLM peridotite xenoliths

Mineralogical distribution and petrogenesis of PGM in mantle peridotite xenoliths. As with the Pt-rich nuggets identified by Marchesi et al. (2010) in the Ronda massif, discrete Pt-rich minerals also occasionally occur within the base-metal sulfides found in mantle xenoliths. Examples include mantle xenoliths that have sampled the SCLM beneath the Massif Central in France (Lorand and Alard 2001), the South China Block in Taiwan (Wang et al. 2009), Central Iberia (Fig. 15; González-Jiménez et al. 2014c) and those associated with kimberlitic olivine from the Siberian lithospheric mantle (Griffin et al. 2002). The Pt-rich micronuggets that are found are generally considered to have formed at relatively low-temperature during sub-solidus decomposition of the base-metal sulfide.

Lorand and Alard (2001) and Alard et al. (2002) noted that in some cases the PGM micronuggets associated with base-metal sulfides in mantle xenoliths are too small to be properly identified by LA-ICP-MS. Alard et al. (2011) used a Scanning Nuclear Microprobe to analyze sulfides in mantle xenolith material from Montferrier (southern France) and detected micronuggets of sperrylite. According to Alard et al. (2011), the sperrylite crystallized at temperatures below or near 900ºC (i.e., below the solidus of the sulfide) from volatile-rich fluids that refertilized the Montferrier mantle. The fact that Alard et al. (2011) were able to detect micronuggets of sperrylite included in the Monteferrier sulfides highlights the advantages of the Scanning Nuclear Microprobe relative to conventional techniques for identifying PGM. As reported by these authors, this instrument analyses a greater volume of the sulfide grain (imaged down to ~70 μm depth) and can be very useful for identifying sulfide-hosted PGM. In contrast, LA-ICP-MS analyses are commonly carried out on areas of ~50 mm in diameter (e.g., thick sections, polished blocks) and depths ranging between 40–60 μm, so may not provide sufficient coverage for PGM inclusion identification. The paucity of documentation of PGM nano-scale grains in the literature might be a problem of volume sampling using LA-ICP-

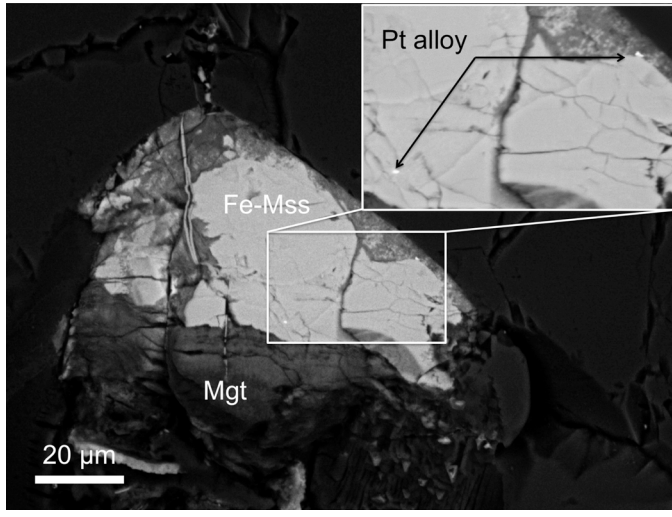

Figure 15. Images of Pt-alloy micronuggets in Fe-rich mss and magnetite (Mgt), interstitial to olivine in a mantle (lherzolite) xenolith from the Calatrava Volcanic Field, central Spain.

MS, as well as a function of the limitations of conventional SEM microscopy. Therefore, the presence of PGM micronuggets in base-metal sulfides could be more frequent than reported, as also suggested by recent experimental results where PGM nanograins were crystallized from sulfide melts prior to larger base-metal sulfides (Helmy et al. 2013).

PGM IN CONCENTRICALLY ZONED URALIAN–ALASKAN–ALDAN-TYPE COMPLEXES

Concentrically zoned, Uralian–Alaskan–Aldan-type complexes (CUAAC) are intrusions of relatively small size and elliptical shape, typically with a concentrically zoned structure where dunite is embedded in an envelope comprising pyroxenite ± wehrlite ± hornblendite ± magnetitite, passing outwards into gabbroic rocks (*Supplementary Table* 3). Minor associated lithologies include chromitite and magnetitite, and there are reported occurrences of gabbro/diorite, monzonite, monzodiorite, and hornbende–feldspar ± quartz ± biotite pegmatite. Concentrically zoned complexes occur within narrow structural belts of several hundreds of km length and develop at convergent margin settings (Uralian–Alaskan-type) or at the periphery of stable cratons (Aldan-type). Intrusions hosted in orogenic belts in Russia are referred to as Uralian-type (cf. Noble and Taylor 1960; Taylor 1967; Foley et al. 1997; Garuti et al. 1997, 2002, 2003; Malitch and Thalhammer 2002; Augé et al. 2005a), whereas those located in similar tectonic settings in southeastern Alaska (and more generally the North American Cordillera) are termed Alaskan-type (Findlay 1969; Himmelberg et al. 1986; Nixon et al. 1990; Patton et al. 1994; Himmelberg and Loney 1995; Fedortchouk et al. 2010). Examples of CUAAC have also been reported from all over the world (e.g., Australia, Colombia, Ecuador, Egypt, Madagascar, and Papua New Guinea), and can collectively be termed Uralian–Alaskan-type complexes (see Johan 2002 and *Supplementary Table* 3). Zoned Aldan-type complexes are located in the Aldan Province (southern Siberian Craton) and from the Koryak–Kamchatka belt and the Aluchin Horst (Chukota Pensinsula in eastern Russia; Podlipskiy et al. 1999; Gornostayev et al. 1999, 2000; Malitch and Kostoyanov 1999; Malitch et al. 2011a,b,c; Scheka et al. 2004; Tolstykh et al. 2004; Nazimova et al. 2011).

Most authors agree that CUAAC from both orogenic belts and stable cratonic platforms crystallize from mantle-derived melts. Geochemical and petrological studies of zoned complexes indicate parental melts characterized by low a_{SiO_2}, giving rise to intrusions rich in clinopyroxene with little or no orthopyroxene. Most authors suggest that the parental melts of the CUAAC were generated in supra-subduction zones, or within marginal continental crust. From the standpoint of PGE geochemistry, an important feature of CUAAC rocks is positive anomalies of Pt and Ir with negative anomalies of Ru and/or Pd producing 'M' shaped patterns on standard chondrite-normalized PGE diagrams (Fig. 16). This characteristic distribution of the PGE distinguishes CUAAC from ophiolites and layered mafic–ultramafic intrusions. Nevertheless, the PGE patterns of CUAAC are variable from one locality to another. The PGE mineralization in CUAAC dominantly occurs as lodes, associated with chromitite, dunite–pyroxenite and/or concentrations of base-metal sulfides. Another distinctive characteristic is that streams draining CUAAC form placers of alluvial PGM that may attain local economic importance (see Appendix). Such occurrences constituted the main source of Pt up until the early twentieth century, when the PGE deposits in the Bushveld Complex were discovered. Broad overviews of PGE-mineralization in selected examples of CUAAC are provided by Yuan (2001), Johan (2002) and Economou-Eliopoulos (2010). In general, the bulk of the literature on PGE in CUAAC does not provide detailed information on the textural and compositional characteristics of PGM; many authors simply refer to the relative abundances of the PGM in terms of high- and low-temperature assemblages. *Supplementary Table* 3 summarizes CUAAC PGM information, as reported in the literature.

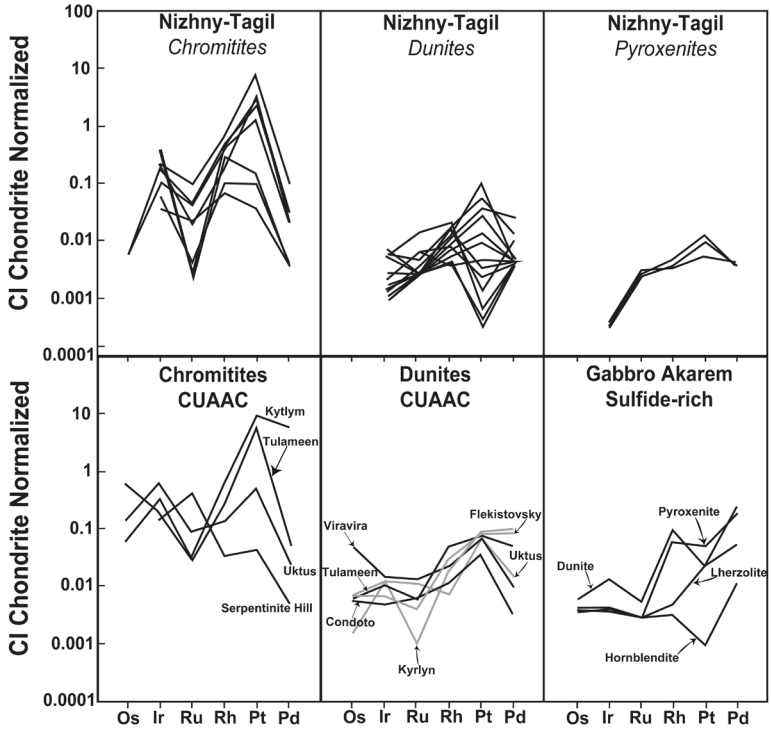

Figure 16. CI-chondrite (Naldrett and Duke 1980) normalized patterns of different rock types from CUAAC. Data plotted in the top three graphs correspond to rocks from the Nizhny Tagil zoned complex in the Urals (Augé et al. 2005a; Malitch et al. 2011c). Average PGE concentration data for chromitites and dunites from other CUAAC are presented as follows: the Kytlym, Uktus Flekistovsky and Kyrlyn complexes of the Urals (Garuti et al. 1997, 2003; Zaccarini et al. 2011), Serpentinite Hill in Tasmania (Brown et al. 1998), Tulameen in British Columbia, Canada (Nixon et al. 1990) and Viravira and Condoto in Colombia (Tistl 1994). Data for sulfide-rich rocks of the Gabbro Akarem complex are from Helmy and Mogessie (2001).

PGM in dunite, pyroxenite and gabbro

PGM in peridotites and mafic rocks of CUAAC. Accessory PGM are found dispersed in dunites (Alto Condoto, Colombia; Kondyor and Galmoenan, Russia), or other mafic lithologies, including pyroxenites and gabbros (Galmoenan, Russia), and magnetite-rich clinopyroxenites (Kachkanar, Russia; Fifield, Australia). The PGM identified by Tistl (1994) in the dunites of the zoned complex of Alto Condoto are mainly Pt–Fe alloys (possibly isoferroplatinum) containing lamellae of native Os (*Supplementary Table* 3). Tistl (1994) reported a second type of primary PGM mineralization (Viravira-type) within fragments of largely serpentinized, orthopyroxene-bearing peridotites (dunite, harzburgite, lherzolite) hosted in high-Mg basalts. The PGM associated with dunite in the Kondyor massif are Pt–Fe alloys located in the interstices of chromite, olivine, and pyroxene aggregates (Rudashevsky et al. 1982; Ukhanov et al. 1997; Cabri et al. 1998). Primary accessory PGM in dunites, pyroxenites and gabbros at Galmoenan are isoferroplatinum, native Os, native Ir, and sulfides of the laurite–erlichmanite solid solution series (*Supplementary Table* 3). Low-temperature alteration of this PGM assemblage produced a secondary paragenesis dominated by tetraferroplatinum, tulameenite, hongshiite, unidentified Pt–Cu, sperrylite, and sulfarsenides of the irarsite–hollingworthite solid solution series

(*Supplementary Table* 3). The main PGM phase in the magnetite-bearing clinopyroxenite of the Kachkanar (Gusevogorsk deposit) is the Pt–Fe alloy isoferroplatinum (Razin and Yurkina 1971; Fominmykh et al. 1974; Bezigov et al. 1975) containing Os–Ir alloys, 'drop-like' inclusions of cooperite, euhedral crystals of laurite, and erlichmanite and Ir- and Rh-rich sulfides including bowieite and kashinite [$(Ir,Rh)_2S_3$]. Other PGM identified in the Gusevogorsk deposit (associated with base-metal sulfides dispersed in the peridotite) include unidentified Pd–Pt–Fe alloys, Pd–Cu, Hg_3Pd_2, braggite, vysotskite, atheneite, mertieite-I [$Pd_{11}(Sb,As)_4$] and Pd-rich tellurides (*Supplementary Table* 3). Johan et al. (1989b) and Slansky et al. (1991) reported primary PGE mineralization in magnetite-bearing pyroxenites (the 'P-unit' of Suppel and Barron 1986) of the Fifield complexes, consisting of isoferroplatinum, tetraferroplatinum, erlichmanite, cooperite, and cuprorhodsite–malanite. The latter assemblage is locally replaced by secondary geversite, sperrylite, and stumpflite [Pt(Sb,Bi)].

Crystallization of primary PGM in peridotites and mafic rocks of CUAAC. Tistl (1994) suggested that PGM crystallization in the Alto Condoto Complex was coeval with, but independent of, chromite crystallization. He proposed that cogenetic assemblages of PGM and chromite result from mechanical trapping of PGM grains by contemporaneous crystallizing chromite. In this model, the most important factor governing PGM precipitation, particularly Pt–Fe alloys, is the crystallization of olivine from the silicate melt. This follows from the experimental works of Amossé et al. (2000), arguing that the crystallization of olivine leads to an increase of melt f_{O_2}, which lowers the solubility of Pt and Ir, but inhibits formation of PGM formed from Ru, Rh, and Pd since these PGE cannot form stable minerals at these *P–T* conditions. Tistl (1994) suggested that the presence of common crystallographic growth defects in the Alto Condoto PGM points to rapid growth of these minerals, potentially driven by volatile exsolution from the melt (causing a decrease in the crystallization temperature), or by changes in f_{O_2} and/or f_{S_2}. Rapid tectonic movements, causing a decrease in pressure and superheating of the melt, could promote such changes. Thus, formation of the Alto Condoto dunite was initially characterized by early crystallization of Pt–Fe alloys, chromite and olivine. Continued crystal fractionation of chromite and olivine (principally controlled by f_{S_2}, according to Tistl 1994) drove magma evolution and the precipitation of PGE sulfides. In the model suggested for the Alto Condoto Complex by Tistl (1994), the singular Pt enrichment of the ultramafic and mafic rocks is thus not associated with especially high Pt in the parental melts or the mantle source.

Johan et al. (1989b) suggested that the intergrowth of Pt–Fe alloys + erlichmanite, isoferroplatinum + cooperite, or erlichmanite + cooperite associated with the magnetite-bearing pyroxenites at Fifield reflects a progressive increase of f_{S_2} during different stages of cooling of the silicate melt. They proposed that erlichmanite and the Pt–Fe alloys would crystallize first at relatively high temperature and lowest f_{S_2}; down temperature increases in f_{S_2} would give rise to a suite of PGE sulfides such as cooperite and cuprorhodsite–malanite. They suggested that the presence of the equilibrium $OsS_2 + PtS_2$ association implies a maximum temperature of about 860°C for the crystallization of PGM in the ore-forming system. In their model, crystallization of the PGM is probably related to the appearance of a reducing fluid during the final stages of evolution of the so-called P-units, which develop in the most oxidized pyroxenites of the Fifield complexes.

Chromitite-hosted PGM in CUAAC

Occurrence and frequency of PGM in chromitites of CUAAC. The PGM associated with CUAAC-hosted chromitites have mainly been documented from several massifs of the Russian Platinum Belts (Fig. 17; *Supplementary Table* 3; Ural Mountains; Nizhny Tagil, Uktus, Volvosky, Kytlym, Kachkanar, and Koryak–Kamchatka [Galmoenan]), the Tulameen massif in British Columbia (Canada), Yubdo (Ethiopia), and Kondyor (Russian Aldan Shield). The chromitites associated with these massifs are usually small bodies (~tens of cm long and several

cm thick) hosted in dunite. However, Augé et al. (2005a) observed larger (100 × 5 m) *schlieren* of disseminated chromite and similarly-sized bodies of chromitite within the ultramafic unit of the Nizhny Tagil Complex. These may be brecciated, net-textured or massive. Brecciated chromitites contain autoliths of the host dunite, suggesting that chromitite is younger (Augé et al. 2005a). Zaccarini et al. (2011) reported a composite chromitite/amphibolite clinopyroxenite vein with anomalously high PGM concentrations at Butyrin in the Kytlym massif. Chromitite-hosted PGM in CUAAC are usually micrometric grains (< 50 μm) positioned in one of three manners: (1) inclusions in chromite crystals, (2) at chromite–silicate grain boundaries and (3) more rarely, in the silicate matrix.

A characteristic feature of CUAAC chromitites is their positive anomalies of Pt plus Ir and negative Ru and Pd anomalies on chondrite-normalized PGE diagrams, yielding diagnostic 'M'-shaped patterns (Fig. 16), as noted above. Nevertheless, the PGE patterns of CUAAC exhibit additional variability depending on locality. For example, Garuti et al. (2003) identified three distinctive PGE patterns in chromitites of the Utkus Complex, which they linked to variation in the chemical composition of chromite in the chromitites. They devised a classification scheme, in which their type I chromitites are characterized by PGE normalized-chondrite patterns with a negative slope due to enrichment of the IPGE over the PPGE. Chromite in this case is magnesiochromite with low $Fe^{3+}/(Fe^{3}+Fe^{2+})=0.23–0.35$. The principal PGM include laurite, kashinite, and cuproiridsite ($CuIr_2S_4$); secondary phases are irarsite and tolovkite (IrSbS). Their type II chromitites exhibit a PGE distribution pattern characterized by an M-like shape with marked positive anomalies of Pt and Ir; the chromite here is magnesiochromite with higher $Fe^{3+}/(Fe^{3+}+Fe^{2+})$ ratios (0.40–0.44). Type II chromitites contain abundant primary isoferroplatinum associated with native Os, erlichmanite, cuproiridsite, and cuprorhodsite, coexisting with free grains of malanite and cooperite. Isoferroplatinum is commonly replaced by tulameenite, whereas the Ir- and Rh-bearing PGM are transformed to unnamed Rh_4S_3 and Ir–Fe, accompanied by potarite. The third, type III chromitites contain Fe-rich chromites ($Fe^{3+}/(Fe^{3+}+Fe^{2+})=0.59$) and exhibit PGE patterns with an M-like shape similar to that of type II chromitites, but with higher Pt and Rh abundances. The PGM assemblage in type III chromitites consists of irarsite, tulameenite, RhSbS, PtPdCu, and PdCu alloys.

The mineralogy of PGM in chromitites of the CUAAC is monotonous, typified by a predominance of Pt-rich PGM and a paucity of Os–Ir–Ru-rich PGM (Figs. 17 and 18). Alloys of the Pt–Fe–Ni–Cu system are by the far the most abundant. Isoferroplatinum is the most common alloy followed, in order of abundance, by tetraferroplatinum, tulameenite, and more rarely Fe-bearing native Pt, Fe + Ni-bearing native Pt and hongshiite, as well other unidentified alloys with variable proportions of Pt/(Fe+Ni+Cu) (Fig. 18). The Pt–Fe alloys often host inclusions of native Os or Ir; the latter can also be found as isolated inclusions in chromite. The coexistence of these alloys along with sulfides of the laurite–erlichmanite solid solution series has been described in chromitites of most CUAAC. Other rare PGM include sulfides such as cooperite, cuproiridsite, cuprorhodsite, and kashinite, and Ir–Rh–Pt sulfarsenides such as irarsite, hollingworthite and platarsite, sperrylite, geversite, and RhNiAs (possibly zaccariniite; Vymazalová et al. 2012).

Secondary low-*T* assemblages of PGM are generally formed by metasomatic replacement of pre-existing PGM and localized remobilization of the PGE during serpentinization and regional metamorphism (e.g., Nixon et al. 1990). The Pt–Fe alloys are commonly replaced by rims of Cu-rich alloys like tulameenite and/or As- and Sb-rich minerals such as sulfarsenides of Ir–Pt–Rh (irarsite–platarsite–hollingworthite), arsenides (sperrylite) or antimonides (geversite and genkinite), and more rarely by PGE antimonides and reported occurrences of Pt-oxides. Other relatively rare secondary minerals identified in chromitites of the Galmoenan massif in the Koryak–Kamchatka Platinum belt include bismuthides like froodite ($PdBi_2$) or sobolevskite (PdBi) and stumpflite (*Supplementary Table* 3).

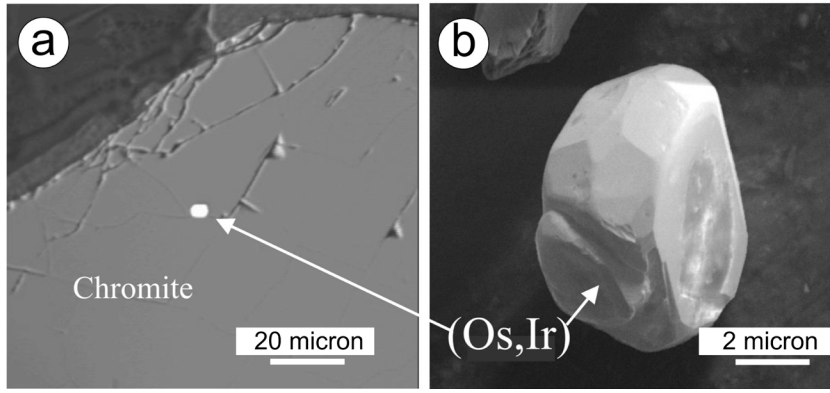

Figure 17. Images of Os-Ir alloy grains (a) *in situ* and (b) liberated by mechanical processing from chromitites of the Guli massif (adapted from Malitch et al. (2011b) Redox conditions of formation of osmium-rich minerals from the Guli massif, Russia. Geochemistry International, Vol. 49, p. 726–730, with the permission of the author and publisher).

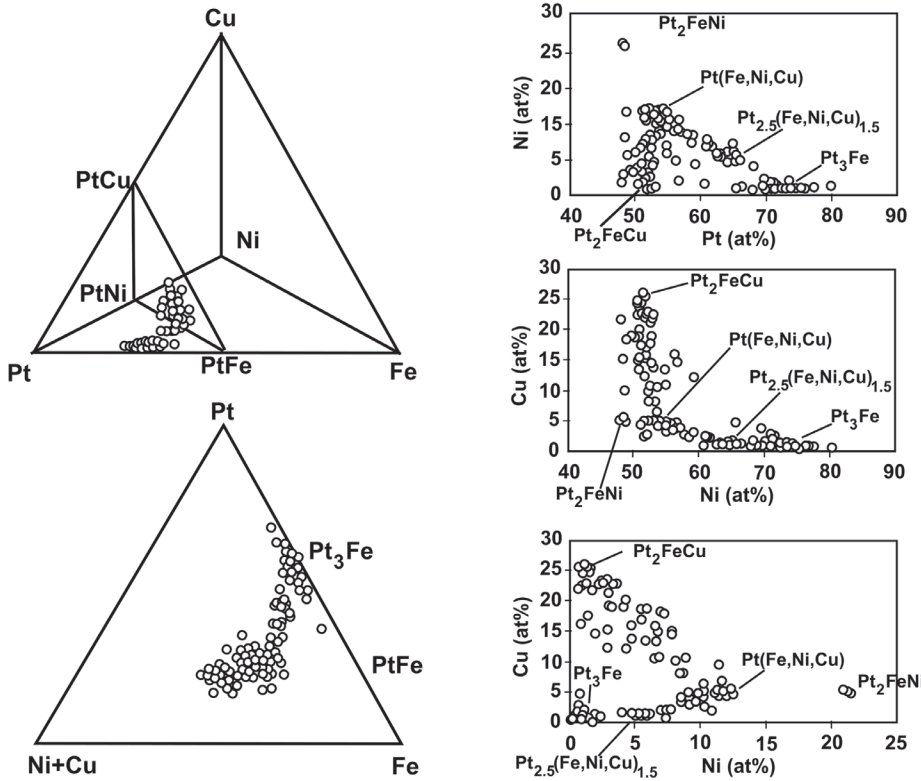

Figure 18. Compositional variation of Pt-alloys hosted in chromitites from the concentrically zoned complexes of the Urals (Kytlym and Uktus). These plots are adapted, replotted and redrawn from Garuti et al. (2002).

Crystallization of primary PGM during chromitite formation in CUAAC. As noted above, CUAAC chromitites may contain a primary PGM assemblage formed at high-temperatures and/or a secondary one developed at low-temperatures during late-stage magmatic or post-magmatic events. The high-temperature PGM assemblage is usually found as inclusions in chromite. However, Augé et al. (2005a) also reported primary PGM attached to the edges of chromite grains or forming the interstitial groundmass to these grains in chromitites of the Nizhny Tagil Complex. Nixon et al. (1990) observed a similar PGM-chromite relationship in chromitites of the Tulameen Complex, suggesting that it may be a common characteristic of CUAAC chromitites in general.

Malitch and Thalhammer (2002) reported the first (and only, to our knowledge) Os-isotope dataset from Os-rich minerals in CUAAC-hosted chromitite. Two grains of native Os from the chromitites of the Jurassic Kondyor massif (analyzed by N-TIMS) yielded $^{187}Os/^{188}Os$ values of 0.1248 and 0.1252. The authors interpreted these relatively low $^{187}Os/^{188}Os$ compositions as indicative of a mantle source for the PGE, suggesting the PGM have a magmatic origin. Nixon et al. (1990) also suggested that euhedral Pt–Fe alloys locked in chromite grains of the Tulameen chromitites were high-temperature segregations that formed in an early phase of crystallization from primitive mantle-derived silicate melts. Using the thermodynamic and experimental data obtained by Hill and Roeder (1974) and Amossé et al. (1990), Nixon et al. (1990) estimated an increase in f_{O_2} associated with the crystallization of chromite would significantly drop the solubility of Pt in the surrounding melt, favoring the precipitation of Pt–Fe alloys. The latter authors estimated the co-precipitation of Pt–Fe alloys and chromite occurred within the range ~1300–1200 °C and at –6 log f_{O_2}.

The latter model contrasts with that proposed by Garuti et al. (2003) who explained the abundance of Pt–Fe alloys in Uktus Complex chromitites (Fig. 18) as being related to changes in the activity of FeO in the melt, rather than f_{O_2}. Garuti and co-workers suggested, based on experimental results on the solubility of Pt in basaltic melts (e.g., Borisov and Palme 1997, 2000; Amossé et al. 1990), that the precipitation of Pt–Fe alloys may take place independently of the true variation in f_{O_2} and may reflect an increase in FeO activity during magma fractionation. Garuti et al. (2003) suggested that the low silica activity of the melts that produce the CUAAC could favor the crystallization of olivine, resulting in an increase in the Fe_2O_3 and Fe_3O_4 activity of the melt. They concluded that under these conditions, fractionation produces increasing amounts of Fe^{2+} and Fe^{3+} in the melt that may be incorporated into the crystallizing chromite; as a result the chromite would show an increasing oxidation ratio ($Fe^{3+}/[Fe^{3+}+Fe^{2+}]$) as is observed in the Uktus chromitites. The observations of Garuti et al. (2003) are noteworthy since the effect on chromite composition of changing FeO activity in the melt is similar to that of increasing the melt f_{O_2}. Co-precipitation of Fe-rich chromite and Pt–Fe alloys in CUAAC chromitites may thus be a result of the critical undersaturation in SiO_2 of the primitive melt. Another interesting observation made by Garuti et al. (2003) on the Uktus chromitites is that the precipitation of Pt–Fe alloys appears to have occurred only during the crystallization of chromite under conditions of high f_{O_2}, as evidenced by chromite with $Fe^{3+}/(Fe^{3+}+Fe^{2+}) > 0.4$. In contrast, these authors did not observe crystallization of Pt-rich phases in chromite with a low Fe-oxidation ratio (i.e., < 0.3). Chromites with low ratios would be expected to crystallize in the early stages of magmatic fractionation where the melt is characterized by lower FeO activity, so the latter scenario was interpreted as meaning that the Pt remained in the silicate liquid and other Ru–Os–Ir minerals like laurite or Ir-sulfides were the only PGM that crystallized.

Augé et al. (2005a) attributed the abundance of Pt-rich PGM in the chromitites of the Nizhny Tagil and Kachkanar Complexes to mechanical processes that concentrated both chromite and PGM. On the basis of their observations, they concluded that there is no evidence to support a Pt-rich melt/fluid as being important in the formation of PGM in CUAAC. They suggested that the observed chromite breccias and networks of massive chromite in the Nizhny Tagil and Kachkanar CUAAC are indicative of the formation of chromitites via dynamic accumulation

of chromite in cavities in magma conduits. According to Augé et al. (2005a), the PGM would be incorporated in crystallizing chromite crystals or remain attached to them due to their strong affinity for the oxide rather than the silicate melt. The effectiveness of chromite to accumulate a higher concentration of PGM would be determined by the ratio of the mass of silicate melt to the mass of chromite in contact with the ascending melt (i.e., the CR-factor, which is analogous to the sulfide mineralization *R*-factor, defined by Campbell and Naldrett, 1979). Where the CR-factor is high (i.e., a relatively low proportion of chromite in contact with a large volume of melt crystallizing the PGM), the efficiency of the mechanical collection of the PGM is at a maximum and the concentration of PGE (or concentration of PGM grains) will be high. In contrast, a low CR-factor produces PGE- or PGM-poor chromitites, as seen in some ophiolites. The Augé et al. (2005a) model requires the existence of melts that already contain PGM, i.e., it does not explain the crystallization of PGM; it invokes a previous mechanism to lower the solubility of the PGE in the melt and crystallize PGM that are subsequently 'physically' accumulated.

Okrugin (2011) proposed an alternative model for the origin of PGM in CUAAC, including chromitite-hosted PGM. His model is based on studies of PGM parageneses from both chromitites and placer deposits, associated with the CUAAC of the Aldan Shield. Okrugin suggested that fractional crystallization of olivine from a picritic melt would result in the formation of a residual melt enriched in Cr, the PGE, and other metals, as well as easily fusible and volatile elements. He suggested that over the course of slow fractional crystallization, the latent heat of olivine crystallization could drive the residual melt to an immiscibility field through a superliquidus path. On reaching the immiscibility field, this residual melt would separate into two immiscible melts; a lighter SiO_2-rich one and a denser Cr-rich oxide one. In a fluid-saturated parental melt, a Cr-rich oxide melt would be separated from the silicate melt based on the density contrast; upon cooling the crystallization of such a melt would lead to the formation of the chromitites. Okrugin (2011) proposed that the high PGE content of chromitites (relative to the host dunites) could be explained by the initial accumulation of PGE in the dense Cr-rich oxide melt. The preferential partitioning of the PGE into this Cr-rich oxide melt is the result of the chromite ionic-structure vs. the ionic-molecular nature of the silicate melt. Metallic nanoclusters of PGM accumulate in the Cr-rich oxide melt, stabilized by outside 'envelopes' of ligands of semi-metals (e.g., S, As, Sb, Te). According to Okrugin (2011), the coalescence and subsequent crystallization of such clusters leads to the formation of various PGM assemblages consisting mainly of alloys, often intimately intergrown with sulfides, arsenides, and other PGE and ligand compounds. The crystallization of the different PGM assemblages observed in the chromitites results from the progressive separation of a series of immiscible melts enriched in PGE after chromite crystallization. This is because crystallization of Cr-rich oxide melts leads to the concentration of PGE in the residual melt, since PGE are less soluble in chromite than in the melt. The characteristic Pt-enrichment observed in the chromitites of CUAAC is thus assumed to reflect the initial IPGE/PPGE ratio of the parental melt.

PGM and sulfide mineralization in CUAAC

The association of PGM and sulfide mineralization in CUAAC. The association of disseminated and massive base-metal sulfides with PGM is an unusual feature in CUAAC. This association has only been described in a couple of zoned complexes in North America (Salt Chuck in Alaska and Turnagain in British Columbia), the Central Urals (Vokosvsky Complex) and from the Eastern Desert in Egypt (i.e., Gabbro Akarem and the Genina Gharbia mafic–ultramafic intrusions) (*Supplementary Table* 3).

At the Salt Chuck complex, the PGM are associated with 15 vol.% bornite and chalcopyrite in biotite-bearing magnetite clinopyroxenite and gabbro (Loney and Himmelberg 1992), which are confined to fault zones. This sulfide mineralization was mined intermittently from 1905 to 1941 and produced about 300,000 metric tonnes of sulfide ore, estimated to have averaged 0.95 wt.% Cu, 19.91 g Au, 7.04 g Ag, and 26.1 g Pd, per tonne (Gault 1945; Holt et al. 1948). Watkinson and Melling

(1989) identified isolated grains of PGM associated with the sulfides, consisting mainly of kotulskite (PdTe) intergrown with hessite (Ag_2Te). Other assemblages consisting of temagamite (Pd_3HgTe_3) and isolated grains of Au-rich sperrylite + kotulskite + Pd_6AsSb, temagamite + Au, and kotulskite + temagamite + merenskyite were observed.

The main occurrences of massive to semi-massive Fe–Ni–Cu sulfide ores in the Turnagain complex are hosted by wehrlite and clinopyroxenite and rarely in serpentinized dunite (Nixon 1997). The base-metal sulfides are envisaged to have formed from immiscible sulfide melt that segregated from silicate magma (Clark 1975). Jackson-Brown et al. (2014) identified clinopyroxenites and hornblendites with up to 5 vol.% sulfides including chalcopyrite and pyrrhotite with minor pyrite and pentlandite, in addition to a variety of arsenides, As–Sb sulfides and PGM. The PGM include sperrylite and sudburyite [(Pd,Ni)Sb], with minor Pd-rich melonite ($NiTe_2$), hongshiite, testibiopalladinite [PdTe(Sb,Te)], and genkinite. The PGM form small (<40 μm across) inclusions in chalcopyrite, pyrrhotite, pentlandite, cobaltite (CoAsS), and silicates. Sperrylite and sudburyite also form veins and rims on the edges of base-metal sulfides.

Zaccarini et al. (2004a) observed abundant grains of vysotskite associated with patches (50–300 μm) of chalcopyrite (± bornite, ± carrollite; $CuCo_2S_4$) rimmed by magnetite and disseminated in serpentinized olivine- and apatite-rich rocks, from the zoned complex of Volkovsky in the Central Urals. Vysotskite has been replaced along its grain boundaries by stillwaterite (Pd_8As_3) and unidentified Pd–As–Te (törnroosite? [$Pd_{11}As_2Te_2$]) PGM. Zaccarini et al. (2004a) also reported large patches of kotulskite (~20 μm) intergrown with electrum and an unidentified mineral with a composition close to $Pd_3(As,Te)$.

At the Genina Gharbia mafic–ultramafic intrusion, Helmy (2004) described michenerite and melonite–merenskyite, associated with hessite, altaite (PbTe), tsumoite (BiTe), sylvanite [$(Ag,Au)Te_2$], and native Te, located mainly at sulfide–silicate grain contacts and as inclusions in altered silicates. Palladium-bearing bismuthian melonite is the most abundant PGM and forms: (1) isolated euhedral (<30 μm) inclusions in pyrrhotite and pentlandite; (2) polyphase aggregates (30–50 μm) with hessite, michenerite, altaite, and tsumoite at the contact between sulfides and silicates; (3) grains of variable size (15–70 μm) associated with altaite and tsumoite embedded in secondary silicates (mainly quartz and epidote). Helmy (2004) described melonite associated with native Te within cracks in violarite ($Fe^{2+}Ni_2^{3+}S_4$) and forming composite grains with hessite and altaite at the contacts between sulfides and silicates. Merenskyite was observed at the contacts between pyrrhotite and epidote and, more rarely, in hessite associated with fractured pyrrhotite.

The PGM associated with Ni–Cu–Fe sulfides from Gabbro Akarem are native Pd and bismuthotellurides (*Supplementary Table* 3). Helmy and Mogessie (2001) described ~85 grains of merenskyite enclosed in pyrrhotite together with several grains of michenerite at chalcopyrite–silicate (serpentine and chlorite) contacts. Palladium-bearing bismuthian melonite forms small subhedral crystals (10–20 μm) associated with hessite, often along cracks within sulfides and at the contacts between the sulfides and silicates.

Petrogenesis of the PGM-sulfide association in CUAAC. Gault (1945) interpreted the assemblage of PGM + sulfide at Salt Chuck (Alaska, USA) as the product of infiltrating 'ore-bearing' fluids along the contacts between fractured magnetite-rich clinopyroxenite and gabbro. He suggested the preferential concentration of chalcopyrite in the main faults of the massif was due to the infiltration of Cu-bearing fluids along these structures. Mertie (1969) suggested that the ubiquitous occurrence of sulfides in microfractures was evidence for the precipitation of sulfides from circulating hydrothermal solutions. The disseminated character of the sulfides and PGM, together with the predominantly igneous textures exhibited by the host rocks, suggests crystallization of these minerals from late-stage magmatic fluids during an intrusive event (Loney and Himmelberg 1992). The latter authors suggested that the

veins and fractures observed by Gault (1945) and Mertie (1969) were formed during this late magmatic event. Loney and Himmelberg (1992) argued for a two-stage process, involving the initial (magmatic-stage) development of disseminated sulfides and PGE, largely in the gabbroic part of the zoned complex. A subsequent magmatic-hydrothermal stage remobilized and concentrated the PGE in veins and fractures in the magnetite-bearing clinopyroxenite primarily close to the contact between the magnetite-bearing clinopyroxenite and gabbro. Watkinson and Melling (1992) suggested that the formation of PGM was associated with the post-magmatic infiltration of a Cl-bearing hydrothermal fluid enriched in PGE and Cu, which replaced the magmatic sulfides.

Nixon (1997) interpreted the formation of base-metal sulfides in the Turnagain intrusion as being products related to the separation of immiscible sulfide melt from a silicate melt. His interpretation is based on the fact that the sulfides are interstitial to silicates and show bleb-like textures in disseminated zones, or coalesce to form continuous networks enclosing cumulus silicate crystals. The net-textured sulfides locally occlude silicates altogether to form massive accumulations. Jackson-Brown et al. (2014) noted that the abundance of base-metal sulfides in the Turnagain intrusion differs from most Alaskan-type intrusions and Scheel (2007) suggested that the relative abundances of sulfide here (relative to other CUAAC) was a result of assimilation of crustal sulfur by the parental melt. Jackson-Brown et al. (2014) suggested that formation of the PGM was associated with the intrusion of a Cu–Pt–Pd-bearing melt phase that crystallized separately from the earlier (Ni–Co enriched) main dunite–wehrlite units.

Zaccarini et al. (2004a) recognized three stages of PGM formation in the Volkovsky Complex (Central Urals, Russia) that they related to chemical changes during fractional crystallization and cooling of the ore system. According to these authors, high initial f_{S_2} in the melt caused the crystallization of vysotskite and chalcopyrite. This was followed by continued cooling that promoted the exsolution of kotulskite from vysotskite and electrum from both vysotskite and chalcopyrite. According to Zaccarini et al. (2004a), the occurrence of arsenotellurides and kotulskite in the outer rims of the sulfide blebs indicates that the melt became enriched in Te and As after the first stage. In the final stage, Te activity in the melt decreased significantly and enrichment in As led to the formation of stillwaterite that overgrows arsenotellurides. The observation that stillwaterite often forms intergrowths with magnetite (itself associated with secondary silicates) led Zaccarini et al. (2004a) to suggest that the final stage was characterized by high a_{As}, coinciding with the serpentinization of the silicates under relatively oxidizing conditions.

Helmy (2004) also proposed a three-stage model to account for the petrogenesis of PGM in the Genina Gharbia intrusion (Eastern Desert, Egypt). In the first stage, sulfide saturation was achieved in the silicate melt due to fractional crystallization. Base-metal sulfides were precipitated in an interstitial network around early-formed olivine and pyroxene in harzburgite and lherzolite. All of the PGE were incorporated into sulfides and sulfarsenides (mainly pentlandite and cobaltite–gersdorffite). At an advanced stage of magma fractionation, additional sulfur and other semi-metals were added to the melt from the surrounding metasediments. The base and noble metals were subsequently separated and concentrated in a highly evolved H_2O-rich fluid that formed in equilibrium with the parental melt to the gabbros. Sulfides, PGM, and other tellurides then crystallized from this metal-rich fluid at lower temperature. The post-magmatic stage is characterized by localized ductile deformation, which remobilized metals and concentrated them along shear zones.

Helmy and Mogessie (2001) estimated a crystallization temperature for the lherzolites at Gabbro Akarem between 912–888 °C, using two-pyroxene geothermometry. They suggested that this temperature range is the upper limit for the segregation of immiscible sulfide liquid following crystallization of olivine and orthopyroxene. The identification of troilite (FeS) + smythite [$(Fe,Ni)_9S_{11}$ or $(Fe,Ni)_{13}S_{16}$] intergrowths at Gabbro Akarem (Sideek

and El Goresy 1996) led Helmy and Mogessie (2001) to propose extensive equilibration from magmatic temperatures down to low temperatures (~75 °C). The latter authors suggested that the initial stages of cooling of the immiscible sulfide melt were dominated by the early segregation of merenskyite now found as inclusions in pyrrhotite, whereas the final stages were dominated by the crystallization of michenerite identified at the contacts between chalcopyrite and silicates. Helmy and Mogessie (2001) also suggested that the infiltration of low-temperature hydrothermal solutions could be responsible for the mobilization of Pd and Au that contributed to the formation of merenskyite and electrum in serpentine veins that crosscut the olivine grains.

PGM IN Ni-SULFIDE DEPOSITS

Komatiite-associations

Komatiites are ultramafic volcanic rocks that crystallize from melts with MgO contents >18 wt.% that are considered to be essentially free of volatiles (Arndt 2008). In general, ultramafic rocks with 10–15 wt.% MgO that are demonstrably derived from anhydrous komatiitic parental melts are referred to as komatiitic basalts. Although most komatiites are restricted to Archean and early Proterozoic greenstone belts, they have rarely been reported from rocks of the Phanerozoic Eon. Relatively young komatiites include those found on Gorgona Island in Colombia (Gansser et al. 1979; Echeverria 1980; Arndt 1994; Arndt et al. 1997) and the Triassic lavas described from the Otrhys ophiolite complex in Greece (Cameron et al. 1979; Cameron and Nisbet 1982; Paraskevoupoulos and Economou 1986; Tsikouras et al. 2008). Komatiites are typically considered to be S-undersaturated at the comparatively high temperatures of their eruption (1450–1600 °C; Lesher et al. 1984; Fiorentini et al. 2010). However, the assimilation of crustal material can substantially change their nature (e.g., S-content and degree of polymerization) and promote sulfur saturation, potentially leading to the formation of magmatic Ni-sulfide deposits (Lesher et al. 1984; Lesher 1989; Barnes 2006). Komatiite-hosted ores have been classified using a variety of criteria (see Lesher and Keays 2002 for a review). In the present contribution, we consider two principal groups for the sake of simplicity: (1) sulfide-rich (deposits in lava channels, i.e., type 1 of Lesher and Keays 2002) and (2) sulfide-poor (stratiform layers in differentiated sills or lava lakes, i.e., type 3 of Lesher and Keays 2002), in a similar manner to Fiorentini et al. (2004, 2007) and Locmelis et al. (2009, 2011, 2013).

Mineralogy and petrogenesis of PGM in sulfide-poor komatiites. PGE-rich, sulfide-poor mineralization in komatiites has been described in differentiated sills and/or lava lakes formed by the strong *in situ* fractionation of ultramafic melts. These sills and lava lakes are generally associated with complementary cumulates. This kind of PGE mineralization, 'type 3' in the classification of Lesher and Keays (2002), is generally interpreted as the result of precipitation from sulfide melts that were segregated in cotectic proportions with olivine when an initially S-undersaturated komatiite melt underwent extensive closed-system fractionation. Reported examples of PGM associated with this type of mineralization include the Boston Creek Sill (Abitibi greenstone belt in Ontario, Canda; Stone et al. 1992; Fiorentini et al. 2004), the atypical stratiform mineralization of the Wiluna cumulate body (east Yilgarn craton; Fiorentini et al. 2004, 2007) and Mount Clifford (Locmelis et al. 2009; western Australia).

The PGM identified in the Boston Creek Sill are merenskyite, bismuthian kotulskite, merteite I, unidentified Pd–Ag sulfide, sperrylite, and an unidentified Rh–Pt sulfarsenide. According to Stone et al. (1992), the PGM occur as grains <15 μm in diameter associated with Cu–Fe sulfides, native Au, electrum, a suite of Ag minerals, and secondary silicates derived from the alteration of Fe–Ti oxides in pyroxenite. Stone et al. (1992) suggested that the mineralogy, textures, and spatial associations of the PGM indicate the importance of secondary processes in their formation. The anhedral, sutured, and elongate shapes of the PGM at grain boundaries with secondary silicates were interpreted as reflecting remobilization of the PGE during growth of the secondary silicates.

Stone et al. (1992) proposed that Pd and Pt were remobilized and concentrated in the pyroxenites by hydrothermal fluids during the metasomatic transformation of the primary cumulate, during either cooling of the flow or later greenschist-facies metamorphism.

Fiorentini et al. (2004) suggested that inclusions of Ir–Os(±Pt) were present in chromitites hosted in komatiitic basalt flows from the greenstone belts of Abitibi (Theo's, Fred's, and Boston Creek flows) and Agnew-Wiluna (Wiluna). Though not observed directly, the presence of these inclusions was inferred from peaks for Ir, Pt, and Os in time-integrated depth profiles generated during laser ablation ICP-MS analyses of chromite grains. Fiorentini et al. (2007) subsequently re-examined a suite of chromite-free pyroxenites and melagabbros from the upper mafic section overlying the peridotitic cumulates at Wiluna, using an SEM equipped with an automated image analyzer optimized for PGM detection. In this study, they identified >70 PGM grains, none of which formed part of the same paragenesis as sulfide, i.e., the PGM were only found in sulfide-poor/free intervals. The most frequent PGM they identified were small (1–3 μm) alloy grains, including 24 grains of unidentified Pt–Pd–Cu alloys, and 10 grains of isoferroplatinum, fully embedded in clinopyroxene crystals. In addition, they identified 31 grains of sperrylite in zones of oikocrystic pyroxene in pyroxenite and 12 grains of unidentified Pd-bearing bismutotelluride in small veinlets at the edges of clinopyroxene crystals in melagabbro. According to Fiorentini et al. (2007), the fact that all of the PGM in oikocrystic pyroxenites are bleb-shaped and occur as clusters of very closely spaced grains hosted within clinopyroxene indicates that the crystallization of the PGM took place coevally with the onset of pyroxene crystallization. Because the amount of sulfide at Wiluna is very small, they hypothesized that PGE saturation was driven purely by fractional crystallization of silicate and oxides in a S-undersaturated melt. They suggested that clinopyroxene catalyzed the nucleation of PGM, similar to the role of chromite in chromite-saturated melts.

Locmelis et al. (2009) identified 66 grains of PGM in the komatiitic (dunite) cumulates at Mount Clifford, approximately 150 km south of Agnew-Wiluna (Wiluna). According to Locmelis et al. (2009), all of the PGM are hosted in serpentine and rarely intergrown with sulfides (pentlandite or millerite), magnetite, and nickel arsenides that formed during the alteration. The PGM are small (<5 μm) and occur as clusters with very heterogeneous internal textures. The minute size of the grains coupled with their chemical heterogeneity makes their accurate identification challenging. Locmelis and co-workers classified these PGM into three compositional types: (1) Pd-antimonides (Pt-free and Pt-bearing), (2) Pt-dominated PGM and (3) Pt-bearing Ni-antimonides. According to Locmelis et al. (2009), the association of a PGE-rich zone with a reversal in the Mg/Fe ratio of the host cumulates, as well as offsets in peak concentrations of Pt, Pd, and Cu-S peaks for whole-rock compositions indicates a primary magmatic origin for the PGM mineralization, rather than a secondary origin associated with hydrothermal alteration. They suggest a model in which the formation of the different PGM was the result of a combination of processes, including early sulfide segregation at low *R*-factor values producing Ni- and IPGE-rich olivine, partial re-dissolution and removal of most of this sulfide component during a major replenishment event and subsequent overprinting by a mobile Pt–Pd–Cu-rich fluid derived from highly differentiated trapped liquid.

Mineralogy and petrogenesis of PGM in sulfide-rich komatiites. Proterozoic komatiite–basalt sulfide-rich PGE deposits, such as those of the Raglan Ni–Cu–(PGE) deposit (Quebec, Canada), exhibit the highest PGE grades (cf. Seabrook et al. 2004). Two well-studied examples of PGM-bearing komatiite-related sulfide deposits are the ~2.7 Ga Kambalda Ni–Cu sulfide deposit of western Australia and ~2.9 Ga O'Toole Ni deposit in Brazil. These styles of mineralization fall within the 'type 1' classification of Lesher and Keays (2002), as outlined above, and are discussed further below.

At Kambalda, the PGM are associated with lenses of massive and disseminated sulfide formed after the immiscible segregation of sulfide melts from evolving silicate melts. The PGM associated with these orebodies are <20 μm in size and are Pt–Pd-rich. Sperrylite

and moncheite are most abundant, followed by the Pd-rich PGM, including: sudburyite, merenskyite, stibiopalladinite, palladoarsenide (Pd_2As), michenerite and testibiopalladinite. Other rare PGM include unidentified minerals of Pd combined with As or Sb. Sperrylite is very abundant in bodies of chalcopyrite-bearing massive sulfide. In contrast, moncheite and the other Pd-rich PGM are observed in veins in the massive and matrix ores, within stringers of sulfides in the footwall rocks, or associated with late-stage hydrothermal veins (Hudson and Donaldson 1984). The association of sperrylite with primary chalcopyrite suggests that it was formed during the magmatic event that segregated the massive sulfide ore (Hudson 1986). In contrast, the association of the other PGM with late-stage veins suggests a post-magmatic origin for the PGM, perhaps linked to the infiltration of hydrothermal fluids during shearing and deformation associated with metamorphism. Lesher and Keays (1984) interpreted the footwall stringers, which are enriched in Pd and Cu, as a product of hydrothermal remobilization. Hudson and Donaldson (1984) suggested that hydrothermal fluids carrying Te, As, and Sb would have infiltrated the massive and net-textured sulfide ore, releasing PGE from the sulfides and producing discrete telluride-, arsenide-, and antimonide-dominated PGM.

The O'Toole deposit in the Morro do Ferro Greenstone Belt (Brazil) is a Cu–Ni–Co sulfide lens made up of 65% pyrrhotite, 30% pentlandite, and 5% chalcopyrite with accessory cobaltite–gersdorffite and sphalerite (Marchetto 1990). According to Marchetto (1990), cobaltite and gersdorffite may contain small (generally <10 μm) inclusions of PGM; the most frequent (i.e., 203/372 grains) is a mineral with a composition varying between kotulskite and melonite, followed by irarsite (123 grains) and sperrylite (20 grains). Other PGM include omeiite [$(Os,Ru)As_2$], osarsite, and a series of unidentified PGM: $OsAs_5$, OsRhAsS, RuTeAs, OsRuAs, and a complex Os–Re–As–Te–Fe–Y–Rh mineral. Marchetto (1990) observed that some portions of oxidized material from the weathered top of the O'Toole deposit also contain PGM. Here, sperrylite is the most common, followed by irarsite and kotulskite–melonite and a single grain of native Pt. Marchetto (1990) suggested that the PGM crystallized early in the first stage of cumulate formation, after the crystallization of magnetite but before the onset of sulfide and arsenide crystallization. This explains why irarsite, sperrylite, and kotulskite–melonite occur frequently as small inclusions in the cores of cobaltite–gersdorffite grains. It was also suggested that since pyrrhotite locally replaces cobaltite– gersdorffite, pyrrhotite likely also crystallized later than the PGM and their host cobaltite–gersdorffite. After deposition and crystallization, the ores underwent regional metamorphism under upper greenschist and low-temperature amphibolite facies conditions. Together with the subsequent weathering of the sequence, this metamorphism may have modified the relative abundances of the PGM (Marchetto 1990; De Almeida et al. 2007).

It should be noted that PGE mineralization associated with arsenide enrichment has also been reported from some komatiite localities. For example, the Rosie Ni Prospect in the Duketon greenstone belt (Yilgarn craton, western Australia) contains a suite of sulfides and sulfarsenides together with sperrylite, melonite, and bismuthotellurides (Godel et al. 2012). In addition, Hanley (2007) documented Pt- and Pd-rich arsenides at the Dundonald Beach South locality (Abitibi Sub-province, Ontario, Canada). In both of the latter studies, early segregation of a PGE-rich arsenide melt phase was proposed. By contrast, Prichard et al. (2013a) proposed a hydrothermal origin for PGE mineralization associated with arsenides in the Spotted Quoll Nickel ore deposit (Forrestania greenstone belt, western Australia).

Magmatic Ni–(±Cu–±PGE)–Sulfide Deposits in non-komatiitic rocks

Non-komatiitic sulfide ore deposits with significant concentrations of Ni (±Cu, ±PGE) occur in a variety of mafic and ultramafic magmatic associations (Naldrett and Duke 1980; Naldrett 2004; Eckstrand and Hulbert 2007). The parental melts are sourced from the upper mantle and their sulfide component is derived from either the initial S content of the magma and/or from the crustal rocks through which the magma passes. In either case, ore formation is envisaged to proceed via accumulation of an immiscible sulfide fraction, before crystallization

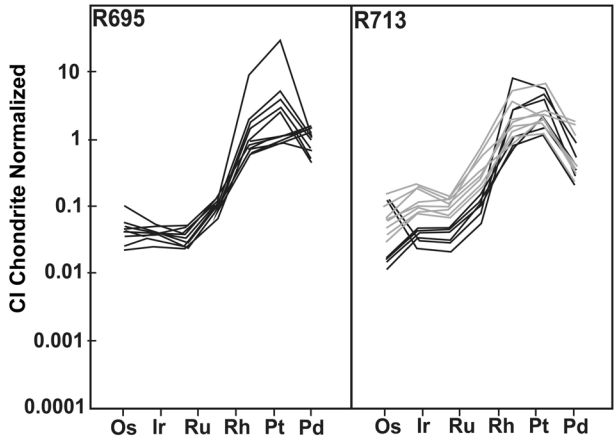

Figure 19. CI-chondrite (Naldrett and Duke 1980) normalized patterns of samples from drill cores R695 and R713, representative of the upper part of the Keivitsansarvi deposit (Kevitsa; after Gervilla and Kojonen 2002). Gray lines correspond to samples containing arsenides and sulfarsenides.

and differentiation of the sulfide liquid. There is some overlap with LMI environments (e.g., Sudbury and Muskox, Canada; Duluth, USA; Kevitsa, Finland, Fig. 19). In general, however, LMI Ni-sulfide deposits are not recognized as being amongst the world's major PGE resources; a feature that might be related to dilutional effects on the ore forming process (i.e., low *R*-factor; Naldrett 1989, 2004). There are relatively few non-komatiite-associated Ni-sulfide ore deposits with significant PGE-enrichments; these are typically associated with mafic–ultramafic sills, stocks or 'tube-like' intrusions. In fact, a wide range in PGE-contents is observed in non-komatiite-associated Ni-sulfide ore deposits, with highly enriched deposits such as that at Noril'sk-Talnakh (Russia) at one end of the spectrum and relatively PGE-poor deposits such as Jinchuan (China) at the other end. Several examples are described in more detail below, presented in no particular order.

The Noril'sk-Talnakh Ni-sulfide deposit. The most economically significant Ni-sulfide deposit that is unrelated to komatiite magmatism (or associated with an LMI) and that also contains appreciable PGE-mineralization is the Ni–Cu sulfide-enriched suite of intrusions at Noril'sk-Talnakh in western Siberia (Russia). The ore deposits are associated with the Siberian flood basalt province and, in particular, with a suite of elongate sill-like mafic intrusions (referred to as chonoliths) that underlie the 3.5 km thick lava sequence. The sills comprise a sequence of olivine-bearing dolerite–gabbro units that can be several 100s-m thick with lengths of several km. Noril'sk is exceptionally enriched in the PPGE and is the world's second leading producer of Pd (after the UG2 chromitite) as well as producing significant quantities of Pt. The nature and distribution of the PGM in the Noril'sk, Talnakh and Oktyabr'sk deposits are similar (Genkin 1968; Genkin et al. 1981; Genkin and Evstigneeva 1986; Vymazalová et al. 2009). The PGM have not commonly been documented from the disseminated ores of Noril'sk, but isoferroplatinum and cooperite have been reported as being typical (Genkin and Evstigneeva 1986; Vymazalová et al. 2009). More detail exists on the PGM assemblages in the massive sulfide ores that occur as sheets and lenses at the bases of the sills. In general, there is an increase in PGE content with an increase in the concentration of Cu-Fe sulfides (chalcopyrite, talnakhite [$Cu_9(Fe,Ni)_8S_{16}$], mooihoekite ($Cu_9Fe_9S_{16}$), and putoranite [$Cu_9(Fe,Ni)S_{16}$]), but not with pyrrhotite concentration. The PGM in the massive sulfide ores generally exhibit irregular textural features, occurring

either as individual grains or clusters of grains of varying size. They are characterized by a considerable range in chemical composition; common minerals include tetraferroplatinum and a diverse assemblage of Pd-dominant PGM (e.g., atokite [$(Pd,Pt)_3Sn$], cabriite (Pd_2SnCu), froodite, insizwaite [$Pt(Bi,Sb)_2$], isomertieite ($Pd_{11}Sb_2As_2$), majakite (PdNiAs), maslovite, michenerite, palarstanide [$Pd_8(Sn,As)_3$], palladoarsenide, paolovite, sobolevskite, stannopalladinite [$(Pd,Cu)_3Sn_2$], pašavaite ($Pd_3Pb_2Te_2$), stibiopalladinite, and taimyrite [$(Pd,Cu,Pt)_3Sn$]) along with an unusually rich variety of Pd–Pb minerals (plumbopalladinite (Pd_3Pb_2), polarite [Pd,(Bi,Pb)], urvantsevite [$Pd(Bi,Pb)_2$], and zvyagintsevite). A key feature of the massive ore-hosted PGM at Noril'sk is the wide development of ternary compounds of Pd, Sn, and Cu. Palladium- and Pt-sulfides, bismuthotellurides, and tellurides (braggite, cooperite, kharaelakhite [$(Pt,Cu,Pb,Fe,Ni)_9S_8$], kotulskite, merenskyite, telargpalite [$(Pd,Ag)_3Te$] and vysotskite) are more typical of vein-hosted and breccia ores that form at sill upper contacts. Genkin and Evstigneeva (1986; their Table 1) provide a detailed list of Noril'sk PGM. These authors envisaged a progressive (three-stage) process as being responsible for the PGM parageneses at Noril'sk. The earliest stage of crystallization, directly from the sulfide melt fraction, is typified by the early-formed PGM, isoferroplatinum and cooperite, in the disseminated ores. Genkin and Evstigneeva (1986) suggested that the PGM in the massive sulfides were concentrated by a residual Cu–volatile-rich liquid that evolved after separation of the sulfide melt fraction. Incorporation of the PGM into the sulfides was envisaged to be a relatively late-stage metasomatic process as this residual liquid permeated the interstitial spaces between sulfides and microfractures in sulfide grains. The presence of the Cl-bearing sulfide djerfisherite [$(K,Na)_6(Fe,Cu,Ni)_{25}S_{26}Cl$] and a Pd–Bi chloride in the mineral assemblage was used to develop this model. The existence of compositionally zoned intergrowths and clusters of PGM in the massive and vein-hosted ores at Noril'sk suggests that metasomatism and modification of primary PGM assemblages occurred well below the solidus, possibly related to the presence of hydrothermal chloride solutions (Genkin and Evstigneeva 1986).

However, the model proposed by Naldrett (2004) and Czamanske et al. (1992) is generally considered to supersede the older model of Genkin and Evstigneeva (1986). Naldrett (2004; see also Barnes and Ripley 2016, this volume) highlighted the widespread evidence for assimilation of country rock and proposed that thermochemical erosion of coal measures provided the S that triggered sulfide saturation at Noril'sk. Separation and differentiation of the sulfides, via concentration in hydrodynamic traps, formed the large ore deposits.

The Aguablanca Ni–Cu–(PGE) sulfide deposit. The exotic Aguablanca ore deposit is an economic Ni–Cu sulfide orebody (6.6 Mt at 0.6% Ni and 0.4% Cu) associated with a sub-vertically oriented magmatic breccia, located in the northern portion of the Aguablanca calc-alkaline mafic intrusion (SW Spain; Piña et al. 2008, 2012). Ages from U–Pb dating of zircon indicate that the Aguablanca stock was emplaced at ca. 340 Ma ago when an Andean-type magmatic arc developed during the Hercycinian orogeny in the Ossa Morena Zone (Piña et al. 2008 and references therein). This tectonic setting is very unusual for this type of ore body, but structural and gravity data show that the deposit occurs as a funnel-like body of mineralized breccia, adjacent to the Cherneca ductile shear zone (a Variscan sinistral transpressional structure). The orientation of the breccia zone, possibly representing a feeder zone to the stock, corresponds to that expected for tensional fractures formed within the strain field of the Cherneca shear zone. Piña et al. (2010) distinguished two different events as being important for the origin and emplacement of the Aguablanca deposit, (1) initial ore-forming processes associated with magma emplacement in the crust, assimilation of crustal S, and segregation/gravitational settling of sulfide melt (a scenario similar to most plutonic Ni–Cu sulfide ores), and (2) later-stage emplacement of the Ni–Cu sulfide-bearing rocks by multiple melt injections. The melt injections are envisaged as being controlled by successive opening of tensional fractures related to the Cherneca shear zone. Three types

of ores were ultimately produced: semi-massive, disseminated, and veined chalcopyrite-rich ore. Piña et al. (2008) interpreted the semi-massive ore, comprising pyrrhotite and pentlandite with minor amounts of chalcopyrite, as a cumulate of mss enriched in Os–Ir–Ru–Rh and poor in Pd–Pt–Au–Cu. In contrast, the chalcopyrite veins rich in Cu–Pd–Au–(Pt) crystallized from a residual Cu-rich melt formed after the crystallization of the mss. The disseminated ore consists of equal proportions of pyrrhotite, pentlandite and chalcopyrite and represents *in situ* crystallization of the original sulfide melt.

PGM are present in all ore-types, although they are most abundant (71%) in the semi-massive and the chalcopyrite-veined (21%) ores, relative to the disseminated (8%) ore (Ortega et al. 2004; Piña et al. 2004). Most of the PGM are rounded and lath-like inclusions in pyrrhotite and pentlandite, although they can be also found along sulfide–silicate and sulfide–sulfide grain boundaries. Only a small proportion of the PGM occur as inclusions in matrix silicates. The PGM assemblage includes, in decreasing order of abundance, merenskyite, melonite, michenerite, moncheite, and sperrylite (Fig. 20a–d). The mode of occurrence and the composition of the PGM suggest that they are magmatic rather than hydrothermal. The positive correlation between the total PGE and S contents in whole-rock samples suggests that the PGE were initially collected by the immiscible sulfide liquid and later exsolved from the mss upon cooling. The fractionation of the IPGE and PPGE between the different ore types, and therefore the formation of distinct PGM, is likely directly controlled by the partition coefficients between the PGE and the sulfide phase.

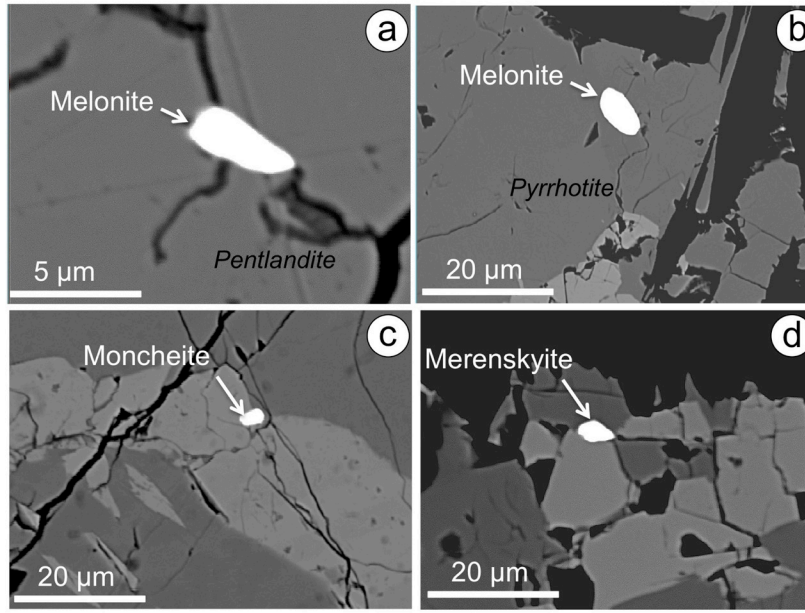

Figure 20. Images of PGM included in sulfides of the Ni ± (Cu ± PGE) sulfide deposits of Aguablanca in southwestern Spain (image courtesy of Dr Rubén Piña).

The Jinchuan intrusion, northern China. Prichard et al. (2013b) described ~140 PGM grains from fresh and altered samples of olivine–sulfide liquid cumulate from the Jinchuan intrusion, North China Craton. Jinchuan is ~832 Ma (Zhang et al. 2010) and is estimated to

be the third largest Ni–Cu(–PGE) deposit on Earth. The intrusion is sheet-like in geometry, ~200 m thick and is structurally subdivided into the west, west-central, and eastern subchambers by a series of northeast trending strike-slip faults. It intrudes Paleoproterozoic migmatites, gneisses, and marbles of the Longshoushan Group. Prichard et al. (2013b) studied samples of peridotite (lherzolites and dunites). They found that although a sample of relatively fresh dunite contained the highest abundances of Pt, the types of minerals hosting Pt were unclear. In particular, Prichard et al. (2013b) reported concentrations of ~3 ppm Pt in the dunite, but only 7 grains of irarsite, which they considered insufficient to account for the whole-rock abundance. One PdBi selenide was also documented from this sample. In contrast, they located ~140 PGM grains in more altered samples, including froodite ($n = 44$), michenerite ($n = 24$), and padmaite (PdBiSe; $n = 24$). Other documented phases include 33 PGM of the irarsite–hollingworthite–platarsite solid solution series and minor (< 11% of the total PGM observed) Pt- and Pd-tellurides. Prichard et al. (2013b) concluded that Pd initially partitioned into base-metal sulfides, whereas early crystallization of irarsite and sperrylite may have occurred if As was present (explaining the paucity of Ir and Pt in base-metal sulfides). A second phase of metasomatism involving oxidizing fluids was invoked to explain the Se-bearing PGM. To explain the metasomatism, Prichard et al. (2013b) highlighted a general worldwide association between Pd-selenides and carbonates. They pointed toward the carbonate country rocks that host the Jinchuan intrusion and suggested that the interaction of low pH oxidizing fluids with the carbonates may have been the driver for precipitation of Pd and Se at Jinchuan.

The Duluth Complex, Minnesota, USA. The Duluth Complex is one of the largest known layered intrusions on Earth, occupying an area of >4,700 km^2. It was emplaced close to the unconformity between Archean supracrustal rocks and Proterozoic metasediments in the north and comagmatic Mesoproterozoic intrusions and lava flows in the south, at ~1.1 Ga (Hoaglund 2010). Mogessie et al. (1991) described PGM from drill core samples of the basal troctolites of Duluth, including sperrylite, taimyrite, froodite, michenerite, and moncheite. The PGM occur within a zone of Cu–Ni–PGE sulfide mineralization at or close to the base of the Duluth Complex, and are dominantly associated with serpentinized olivine and secondary magnetite, or with hydrous silicate phases (e.g., prehnite, actinolite, hornblende, chlorite), all interpreted as alteration products. Mogessie et al. (1991) suggested that a late hydrothermal magmatic event was responsible for mobilization and re-deposition of the PGM, with possible sourcing of the volatiles from assimilated metasedimentary country rocks. They noted relatively high Cl contents of some of the associated silicates (e.g., serpentine, biotite, apatite) and suggested that transport of the PGM in Cl-complexes may have been a viable mechanism of ore formation.

The Sudbury Igneous Complex, Canada. The Sudbury Igneous Complex has been an important source of global Pt and Pd and contains four different styles of mineralization (see also Barnes and Ripley 2016, this volume). Broadly, these include contact ores, offset ores, deep chalcopyrite-rich veins (occur beneath contact ores), and PGE-rich disseminated mineralization around the latter veins. The Sudbury body is an atypical igneous intrusion in that it is believed to have formed from a melt sheet produced after a boloid impact, at ~1.85 Ga. It has been suggested by a number of workers that the Sudbury PGE occur as PGM, rather than in solid solution in base-metal sulfides (Cabri and Laflamme 1976; Cabri 1981b, 1988; Cabri et al. 1984; Li et al. 1993; Farrow and Lightfoot 2002; Huminicki et al. 2005). Ford et al. (2011) carried out a grade recovery exercise utilizing samples from Sudbury's Coleman and Creighton mines as natural examples. The Coleman and Creighton samples are of 'sublayer' material lying immediately above the footwall (country rock) lithologies, on the North and South Range of the intrusion, respectively. Samples from the Coleman Mine yielded 2866 grains, which were fashioned into 26 mounts. The samples from the Creighton Mine yielded a total of 440 PGM grains in 40 thin sections. Both samples exhibit markedly

different PGM populations, attributed by Ford et al. (2011) and Farrow and Lightfoot (2002) to the interaction of the parental magmas with significantly different (sedimentary/volcanic vs. gneissic lithologies) country rocks. In the sample from the Coleman mine, six PGM account for 88% of the PGM and precious metals by total area, including Pt–Sn alloy (20%), maslovite (18%), froodite (17%), michenerite (15%), Au–Ag alloy (11%) and moncheite (7%). The Creighton sample exhibits less diversity, with three principal mineral phases accounting for ~90% of the total surface area of the PGM and precious metals, including michenerite (39%), sperrylite (32%), and Pt–Sn alloy (20%). The distribution of Pt from the Creighton sample is dominated by sperrylite, whereas Pt in the sample from Coleman is controlled by bismuthotellurides and Pt–Sn tellurides. The distribution of Pd at Creighton is dominated by michenerite (78% of Pd) whereas both michenerite (37%) and froodite (39%) dominate the Pd budget at Coleman. The results of the study by Ford et al. (2011) are generally in agreement with an earlier study by Farrow and Lightfoot (2002) which found that the Sudbury PGM population is dominated by tellurides, bismuthotellurides and arsenides, with a notable absence of PGE-sulfides or alloys.

However, the samples studied by Dare et al. (2010) suggested that PGE sulfarsenides (86%) dominated the PGM at Creighton, with sperrylite (9%), michenerite (5%) and electrum (0.1%) constituting only a minor proportion of the overall budget. This observation highlights that the PGM mineralogy can be highly heterogeneous at the hand specimen scale. Dare et al. (2010) reported that the PGE sulfarsenides are characteristically compositionally zoned, with irarsite cores, hollingworthite mantles, and a PGE-rich Ni cobaltite rim. The sulfarsenides and sperrylite thus concentrate Ir, Rh, Pt±Os, and Ru, such that accompanying mss accounts for <10% of the bulk rock Ir, Rh and Pt, and 50–90% of Os, Ru, and Pd. Dare et al. proposed that the PGE-sulfarsenides and sperrylite at Creighton crystallized from a high-temperature (1,200–900 °C) sulfide melt and were subsequently surrounded by the PGE-depleted mss cumulate. Thus, the observed mineralogy is predominantly a magmatic assemblage, with limited low-temperature modification. However, Dare et al. (2010) did suggest a degree of Pd mobility at lower temperatures, linking recrystallization of the base-metal sulfides to michenerite formation at <540 °C. At higher temperatures and an earlier stage of evolution, pentlandite may have been an important host for Pd (Cabri 1981b, 1988; Cabri et al. 1984).

EXAMPLES OF UNCONVENTIONAL PGM OCCURRENCES

Kimberlite- and Cu-porphyry-hosted PGM

Kimberlites. Kimberlites are the solidified remnants of volatile-rich ultrabasic potassic magmas that typically develop in cylindrical pipes and contain olivine phenocrysts, megacrysts, and pyroclasts (Sparks et al. 2006). Xenolithic materials in kimberlites can include a variety of mantle lithologies, including peridotites, pyroxenites, and eclogites. Their origin close to the interface between the cratonic continental lithosphere and underlying convecting asthenospheric mantle means that they can provide insights into the structure and composition of the deep mantle. An example of a PGM assemblage in a kimberlite setting is described by Stone and Fleet (1990). The intrusion occurs in Fayette County (Pennsylvania, USA). Two forsteritic olivine megacrysts contain composite (chalcopyrite–pentlandite) sulfide inclusions, two of which each host a single grain of isoferroplatinum. Although Stone and Fleet (1990) discussed the formation of the PGM within the kimberlite system, it also seems plausible that the olivine megacrysts are xenolithic and that these PGM have a mantle (SCLM) affinity.

Power et al. (2004) report PGE-mineralization associated with two dioritic sheet intrusions at Talnotry, southwest Scotland. The style of magmatism is broadly similar to kimberlite occurrences in that these sheets are lamprophyric. The intrusions are likely lower-mid Paleozoic in age. Power et al. (2004) recognized three distinct mineralogical assemblages in the Talnotry

ore deposit, including a pyrrhotite–chalcopyrite assemblage, a niccolite–gersdorffite assemblage, and a chalcopyrite–gersdorffite assemblage. Overall, the PGM assemblage is diverse, with abundant sperrylite, irarsite, and electrum, as well as minor merenskyite, michenerite, and froodite. In the pyrrhotite–chalcopyrite assemblage, > 100 PGM were reported in 19 thin sections. Almost 90% of the grains are sperrylite, irarsite or electrum (50%, 26%, and 13%, respectively; electrum was included as a PGM in this particular study). The remainder are Pd-bearing PGM, including merenskyite, michenerite, and froodite. A total of 63 PGM were observed in 17 thin sections in the niccolite–gersdorffite assemblage. Electrum is the dominant mineral (63%), with Pd–Bi–Te phases (21%), and sperrylite (13%) also significant. The chalcopyrite–gersdorffite assemblage contains sperrylite and electrum, but due to the diffuse and cross-cutting nature of this assemblage, the PGM are more difficult to isolate and identify. Power et al. (2004) proposed a paragenetic sequence where early sperrylite and gersdorffite crystallized first from metal-rich sulfide liquid. Exsolution of Pt and Ir occurred from the gersdorffite, whilst Rh remained in solid solution. Crystallization of mss from the sulfide liquid formed the pyrrhotite–chalcopyrite assemblage, accompanied by separation of the remaining IPGE in the solid fraction, whilst As, Pd, and some Pt remained in the sulfide liquid. Crystallization of the NiAs liquid to form the niccolite–gersdorffite assemblage was associated with removal of the remaining Pt and Pd from the sulfide liquid. A Cu- and Au-rich iss is the final crystallization product, and locally reacts with and cross-cuts the pre-existing ore assemblage.

Porphyry-Cu (±Au) deposits. Porphyry-Cu deposits can be significantly enriched in Au, but their potential for PGE enrichment has been less well studied (cf. Eliopoulos et al. 2014). Hanley (2005) suggests that moderately oxidized hypersaline fluids are capable of dissolving ppm quantities of Pt and Au, such that the arc magmas typically associated with porphyry-Cu deposits may have the potential to be PGE ore deposits. Examples of Pt+Pd enrichment associated with porphyry-Cu ores occur at Copper Mountain and Galore Creek (British Columbia), Allard Stock (Colarado; Werle et al. 1984), the Elatsite porphyry deposit (Chelopech, Bulgaria; Tarkian et al. 2003; Augé et al. 2005b), and the Skouries porphyry deposit (Greece; Economou-Elipoulos et al. 2000). However, detailed accounts of the PGM assemblages of many of these localities have not been reported. The Skouries Cu–Au deposit is ~18 Ma in age and hosted in the Vertiskos Formation of the Serbo-Macedonian massif. The dominant PGM phase at Skouries is merenskyite, which occurs as intergrowths with hessite, electrum and Cu-sulfides (bornite and chalcopyrite). The Elatsite porphyry-Cu deposit is related to multiple monzonitic and monzodioritic intrusions of Upper Cretaceous age (92.3 ± 1.4 Ma), along a portion of the so-called 'Tethyan Eurasian Metallogenic Belt'. Augé et al. (2005b) describe a PGM assemblage of merenskyite, moncheite, palladoarsenide, and a Pd–Ag–Te–Bi phase associated with base-metal sulfides including bornite and chalcopyrite. The latter authors attribute the PGM assemblage to initially high concentrations of PGE in the magma, subsequently concentrated in hydrothermal fluids, rather than early separation in high-temperature sulfides. As noted by Eliopoulos et al. (2014), an interesting feature of PGM occurrences in porphyry-Cu deposits is that they underline the potentially important roles of aqueous vapors and brines for PGE concentration, these being capable of scavenging the metals in evolved hydrothermal systems.

The Bon Accord Ni-deposit, South Africa. The ~3.5 Ga Bon Accord Ni-deposit was situated in the lowermost stratigraphic units of the Barberton greenstone belt of the Kaapvaal craton (South Africa). It was completely quarried out for smelting, never having comprised more than ~6.3 m^2 of material (Tredoux et al. 1989). The deposit is located in the Tjakastad subgroup of the Onverwacht Group and contained within serpentinized mafic and ultramafic rocks. It comprised a unique suite of Ni-rich minerals, including Ni-rich spinel (trevorite; $NiFe^{3+}{}_2O_4$) and Ni-rich silicates: liebenbergite (olivine; Ni_2SiO_4), nimite (chlorite; $[(Ni,Mg,Al)_6[(OH)_8(Si,Al)_4O_{10}]$) and népouite (serpentine; $[(Ni,Mg)_3[(OH)_4Si_2O_5]]$). There is also an abundance of accessory phases, such as Ni-rich sulfides, arsenides and antimonides, bunsenite (NiO), bonaccordite (Ni_2FeBO_5)

and gaspéite ([Ni,Mg]CO_3), some of which are likely unique to Bon Accord (Tredoux et al., in press). There is some controversy over the origin of the deposit, with two competing hypotheses emerging in the 1970's and 1980's. The first suggested that Bon Accord had an extraterrestrial provenance (an iron meteorite; De Waal 1978) whilst the second argued that the ore body represents an oxidized fragment of Fe–Ni alloy originating from the Earth's core (Tredoux et al. 1989). Other alternatives such as oxidation of either (a) podiform chromitite or (b) awaruite (Ni–Fe alloy stabilized during the highly reducing conditions associated with serpentinization) were dismissed (Tredoux et al. 1989). Although formation of the deposit as an oxidized volcanic massive sulfide (VMS) deposit or as a modified Ni–sulfide deposit was also ruled out by the latter authors, these possibilities have recently been revisited (O'Driscoll et al. 2014b).

Zaccarini et al. (2014) and Tredoux et al. (in press) have recently reported the presence of PGM in Bon Accord material. This is not surprising, since Tredoux et al. (1989) reported ppm levels of the PGE. Zaccarini et al. (2014) report a variety of Pd–Sb Pd–Sb, Pd–Sb–As, Pd–Cu–Sb, Pt–Sb, Pt–As–S, Ru–As–S, and Ru–S phases, as well as sperrylite and phases in the solid solution series sobolevskite–kotulskite. Electrum was also reported. Tredoux et al. (in press) report the presence of native Ru alloys (<1 μm in diameter) in their samples. Although heavy mineral separation techniques were used by Zaccarini et al. to isolate the PGM, they were able to provide some textural context for the PGM, which appear to be preferentially sited close to the edges of Ni-arsenide and Ni-antimonide grains, in turn typically encased in trevorite grains. Zaccarini et al. (2014) suggest that the observed assemblage was formed during a hydrothermal or low temperature metamorphic episode, possibly during exhumation of the body, but this plausibly lends support to the origin of Bon Accord as an altered Ni-sulfide deposit too. It is difficult to speculate much further than this on the petrogenesis of the PGM assemblage in the Bon Accord deposit. However, it is worth highlighting the importance of future study on what is one of the oldest (reported to date) PGM assemblages in the (terrestrial) geological record.

OUTLOOK AND FUTURE WORK

This chapter has described the occurrence and petrogenesis of the PGM in numerous natural examples, with an emphasis on settings where PGE-enrichment is known to occur. An important point arising from this review is that whilst many PGM may initially form under high-temperature (magmatic; 900–1200 °C) conditions, modification of such assemblages can occur down to much lower temperatures (e.g., ~300 °C). A good example of this is the Platinova reef of the Skaergaard intrusion, where the final PGM assemblage observed is the product of a range of processes, including low-temperature equilibration. It is worth concluding this chapter by mentioning some of the outstanding problems in the field of PGM petrogenesis, as well as highlighting areas for future work.

Assessing the mineralogical and textural complexity of PGM assemblages

It is evident that even well-characterized PGM assemblages exhibit features that are not well understood. For example, the Merensky Reef of the Bushveld contains one of the most intensely studied PGM assemblages on Earth, the observations on which raise as many issues as they resolve with respect to formation of the reef. The distribution of the PGM in the Merensky Reef varies from one locality to the next, and from pothole-style reef to normal reef, despite the relative (lithological) similarity of the host rock cumulates over 100's of km of strike (e.g., Table 2). Paradoxically, the overall grade of the PGE remains relatively consistent. Similarly, each of the Rum Layered Suite chromitites, which are typically ~2 mm thick, has a distinctive PGM assemblage that is relatively consistent over 100's m of strike. However, the PGM assemblages of the chromitites can vary considerably up or down stratigraphy. For example, the Unit 11/12 chromitite is dominated by arsenides (i.e., sperrylite), whereas the Unit 7/8 chromitite is dominated by Pt–Fe alloys and PGE sulfides. Despite this, the PGE

abundances of the chromitites vary by one order of magnitude or less (O'Driscoll et al. 2009a). These observations suggest that PGE grades may not be wholly dependent on the PGM mineralogy. Perhaps it is the high-temperature magmatic system that fixes the PGE budget of a reef, and the mineralogy is simply a consequence of the whole-rock PGE geochemistry.

Another complexity that has arisen in studies of PGM mineralogy is the presence of xenocrystic PGM in ophiolite chromitite. For example, González-Jiménez et al. (2014a) reported $^{187}Os/^{188}Os$ heterogeneities within single PGM grains, some of which yielded model ages that are older than the host chromitite. Thus it is clear, in upper mantle examples at least, that recycling of PGM may occur, complicating the interpretation of the observed assemblage. Establishing whether xenocrystic PGM form a statistically significant proportion of PGM in all ophiolite chromitites, and whether they exist in PGM assemblages in other settings, is therefore an important target for future study.

There is a clear, if not ubiquitous, link between the formation of chromitite seams and concentration of PGM in LMI (e.g., Fig. 4), the upper mantle and CUAAC. A critical factor here appears to be suppression of silicate phases on the magma liquidus, enabling the precipitation of non-silicates (such as chromite) only. An observation that seems to hold for many chromitite occurrences, irrespective of setting, is that IPGE-rich PGM (i.e., laurite) are preferentially hosted in inclusions in chromite, whereas PPGE-rich phases occur interstitially. An important advance in our understanding of this relationship was the work of Finnigan et al. (2008), which experimentally documented the nucleation of IPGE-rich PGM in boundary layers around growing chromite crystals. Given the importance of chromitite in studies of upper mantle Os isotope heterogeneity (e.g., Walker et al. 2002), placing further constraints on the distribution of the PGE in chromitite is a very useful goal.

In general, this review has shown that many published models favor the high-temperature separation and fractionation of sulfide melt, the subsequent crystallization of which may allow the PGE (together with As, Te, and Bi) to be concentrated in the residual melt fraction. However, early crystallization of PGM from the sulfide melt (e.g., Dare et al. 2010), or desulfurization of base-metal sulfides which fractionated with the PGE in solid solution (e.g., Fonseca et al. 2012; Bowles et al. 2013) have also been suggested. Looking forward, progress in our understanding of PGM petrogenesis will be made by consideration of the PGM in conjunction with their coexisting sulfide and silicate parageneses, rather than as an isolated mineral group.

Constraints on quantifying the distribution and grain size of PGM

A significant outstanding challenge to future investigations of the PGM is their small grain size. Indeed, the lower grain size limit for these minerals is quite poorly constrained. A good example of this problem is the Bon Accord deposit. Although Tredoux et al. (1989) reported ppm levels of all of the PGE, PGM have proven difficult to find and where present do not explain the observed whole-rock abundances (Zaccarini et al. 2014). In addition, the relevance of fully understanding the textural and compositional diversity and distribution of PGM present in a sample should not be underestimated. For example, Godel (2013) showed that small widely distributed PGM tend to be over-sampled relative to coarser-grained sparsely distributed grains. The latter may contain an abundance of some or all of the PGE, leading to problems in the interpretation of the whole-rock geochemistry.

Godel (2013) highlighted the utility of X-ray micro-CT scanning in addressing these problems (see also Godel et al. 2010). The advantage of this technique is that the composition and distribution of the PGM can be studied in 3D, although sub-μm grain sizes are still challenging to analyze. For example, König et al. (2015) carried out X-ray micro-CT scanning of PGM in a harzburgite from the Lherz peridotite (in material originally studied by Luguet et al. 2007). They reported IPGE-rich PGM inclusions in olivine that they interpreted as residual after mantle melting (sulfide exhaustion). These PGM are relatively abundant, compared to

the interstitial PGM, which were considered to be metasomatic. König et al. (2015) quoted a lower limit of 2.5 μm for the resolution of the micro-CT scanning technique, but were able to document grain sizes in the range 3–5 μm.

Advances in microbeam techniques such as LA-ICP-MS have highlighted the wealth of information that may be extracted from individual PGM and base-metal sulfides, for example where isotopic information (e.g., $^{187}Os/^{188}Os$ and $^{186}Os/^{188}Os$) can be derived (Coggon et al. 2011b; González-Jiménez et al. 2012a). Further progress will undoubtedly be made through increasing the resolution of existing approaches, such as *in situ* elemental mapping, and the application of new instrumentation. For example, the NanoSIMS offers the potential to investigate other isotope systems (i.e., S) in PGM and coexisting sulfide and arsenide phases, opening up avenues for investigation of the petrogenetic histories of these minerals by assessing isotopic heterogeneity in domain sizes of 10s–100s nm. In addition, field-emission SEMs are capable of analyzing samples at higher resolutions (10s–100s nm) than conventional SEMs and synchrotron-based XRF mapping and high-resolution transmission electron microscopy (HRTEM) also offer future potential in PGM investigations.

Advancing our understanding of the link between PGM assemblage and PGE geochemistry

In general, the whole-rock PGE budgets of natural samples from different environments vary. For example, ophiolite peridotites and especially chromitites are characterized by PGE patterns on chondrite-normalized diagrams that have negative slopes, signifying relative enrichments in the IPGE relative to the PPGE. By contrast, the distributions of the PGE from layered intrusion lithologies, including many chromitites, typically have patterns with a positive slope on similar diagrams. Exceptions do occur, such as the Cliff chromitites in the Shetland Ophiolite Complex (Prichard et al. 1986; Prichard and Lord 1993), which have anomalously high PPGE abundances (>250 ppm Pt+Pd; O'Driscoll et al. 2012) and strongly positive patterns on chondrite-normalized diagrams. The high abundances of the PPGE here can be linked to the abundant sperrylite at this locality. The typical 'M-shaped' PGE patterns of CUAAC-associated rocks reflect relatively positive anomalies of Pt and Ir, which likely indicate a mineralogical control on the fractionation of the PGE. However, as highlighted for the Merensky Reef above, the extent to which the PGE patterns are a function of the mineralogy or perhaps the mineralogy is the result of the whole-rock chemistry (allowing for down temperature processes to affect the mineralogy but not change the bulk chemistry drastically) for such samples is an important line of investigation for future studies.

One important conclusion that can be drawn from the majority of the studies described in this chapter is that, where present, PGM account for the whole-rock budget of most of the PGE. One key exception is Pd, and an important focus for additional study should be the ubiquity of Pd occurrences in solid solution in base-metal sulfide, vs. the occurrences of Pd-rich PGM. Junge et al. (2015) recently reported the presence of μm- and nm-sized PGM in pentlandite from the UG2 chromitite and the Platreef of the Bushveld Complex. They observed no orientation (crystallographic) relationship between some of the PGM nanoparticles and the sulfide host, leading them to suggest that the PGM were discrete phases trapped during pentlandite growth. However, they also suggested that Rh and Ir were present in the sulfide liquid. Palladium was observed as nanoparticles and also homogeneously distributed throughout pentlandite grains, suggesting both modes of occurrence are possible. Brenan et al. (2012) have shown experimentally that Ru may also partition into chromite, although this may not be significant for PGE-enriched chromitites where chromite has relatively low ferric iron contents. Additional experimental investigation will be invaluable in further elucidating our knowledge of PGE solubility in silicate and sulfide melts (cf. Mungall and Brenan 2014; Brenan et al. 2016, this volume). Although not the focus of this chapter and not an area where a large amount of research has been carried out, the basic solubilities of the PGE in aqueous solutions in the presence of As-bearing ligands (or Bi and Te) also has the potential to have implications for PGE mineralization in nominally high-temperature deposits (cf. Hanley 2005).

ACKNOWLEDGEMENTS

BO'D acknowledges research support from a NERC New Investigator grant NE/J00457X/1 during the early stages of writing this paper. Support for this study has also been provided by the FONDECYT #11140005 and 'Millenium Nucleus for Metal Tracing Along Subduction NC130065 to JMGJ. The following are thanked for their permission to use various images and illustrative material (in the case of published studies, the first author is listed): JFW Bowles, B Godel, G MacPherson, KN Malitch, T Oberthür, R Piña, D Schwander, RJ Voordouw. The authors are also grateful to Louis Cabri and Fernando Gervilla for discussion and feedback on early manuscript versions. Detailed reviews by Andrew McDonald and Steve Barnes as well as editorial handling and comments by Jason Harvey, James Day, and Ian Swainson helped improve the clarity and focus of the manuscript.

REFERENCES

Ahmed AH, Arai S (2003) Platinum-group minerals in podiform chromitites of the Oman ophiolite. Can Mineral 41:597–616

Ahmed AH, Hanghøj K, Kelemen PB, Hart SR, Arai S (2006) Osmium isotope systematics of the Proterozoic and Phanerozoic ophiolitic chromitites: in situ ion probe analysis of primary Os-rich PGM. Earth Planet Sci Lett 245:777–791

Alard O, Griffin WL, Lorand J-P, Jackson SE, O'Reilly SY (2000) Non-chondritic distribution of the highly siderophile elements in mantle sulphides. Nature 407:891–894

Alard O, Griffin WL, Pearson NJ, Lorand JP, O'Reilly SY (2002) New insights into the Re–Os systematics of sub-continental lithospheric mantle from in situ analyses of sulphides. Earth Planet Sci Lett 203:651–663

Alard O, Lorand JP, Reisberg L, Bodinier JL, Dutria JM, O'Reilly SY (2011) Volatile-rich metasomatism in Monteferrier xenoliths (Southern France): Implications for the abundances of chalcophile and highly siderophile elements in the subcontinental mantle. J Petrol 52:2009–2045

Amossé J, Piboule M, Allibert M (1990) Experimental study of the solubility of platinum and iridium in basic melts: implications for the differentiation of platinum-group elements during magmatic processes. Chem Geol 81:45–53

Amossé J, Dable P, Allibert M (2000) Thermo-chemical behavior of Pt, Ir, Rh and Ru vs f_{O_2} and f_{S_2} in a basaltic melt. Implications for the differentiation and precipitation of these elements. Miner Petrol 68:29–62

Andersen JCØ (2006) Postmagmatic sulphur loss in the Skaergaard Intrusion: Implications for the formation of the Platinova Reef. Lithos 92:198–221

Andrews DRA, Brenan JM (2002) Phase-equilibrium constraints on the magmatic origin of laurite + Ru–Os–Ir alloy. Can Mineral 40:1705–1716

Arndt NT (1994) Komatiites. *In*: Archean Crustal Evolution. Condie KC (ed) Elsevier, Amsterdam, p 11–44

Arndt NT (2008) Komatiite. Cambridge University Press, Cambridge

Arndt NT, Keer AC, Tarney J (1997) Dynamic melting in plume heads: the formation of Gorgona komatiites and basalts. Earth Planet Sci Lett 146:289–301

Augé T (1985) Platinum-group mineral inclusions in ophiolitic chromitite from the Vourinos Complex. Greece. Can Mineral 23:163–171

Augé T (1987) Chromite deposits in the northern Oman ophiolite: mineralogical constraints. Miner Deposita 22:1–10

Augé T (1988) Platinum-group minerals in the Tiébaghi and Vourinos ophiolitic complexes: genetic implications. Can Mineral 25:177–192

Augé T, Johan Z (1988) Comparative study of chromite deposits from Troodos, Vourinos, North Oman and New Caledonia ophiolites. *In*: Mineral Deposits within the European Community. Boissonnas J, Omenetto P (eds) Springer-Verlag, Berlin, p 267–288

Augé T, Maurizot P (1995) Stratiform and alluvial platinum mineralization in the New Caledonian ophiolite complex. Can Mineral 33:1023–1045

Augé T, Legendre O, Maurizot P (1998) The distribution of Pt and Ru–Os–Ir minerals in the New Caledonia ophiolite. *In*: Proc. 8th Int. Platinum. Laverov NP, Distler V (eds) Theophrastus Publications, St- Petersburg-Athens, p 129–132

Augé T, Genna A, Legendre O (2005a) Primary platinum group mineralization in the Nizhny Tagil and Kachkanar ultramafic complexes, Urals, Russia: a genetic model for PGE concentration in chromite-rich zones. Econ Geol 100:707–732

Augé T, Petrunov R, Bailly L (2005b) On the mineralization of the PGE mineralization in the Elatsite porphyry Cu–Au deposit, Bulgaria: Comparison with the Baula–Nuasahi Complex, India, and other alkaline PGE-rich porphyries. Can Mineral 43:1355–1372

Aulbach S, Mungall JE, Pearson DG (2016) Distribution and processing of highly siderophile elements in cratonic mantle lithosphere. Rev Mineral Geochem 81:239–304

Bacuta GC, Kay RW, Gibbs AK, Lipin BR (1990) Platinum-group element abundance and distribution in chromite deposits of Acoje block, Zambale ophiolite complex, Philippines. J Geochem Explor 37:113–145

Ballhaus C (1995) Is the upper mantle metal-saturated? Earth Planet Sci Lett 132:75–86

Ballhaus C, Ryan CG (1995) Platinum-group elements in the Merensky Reef. I. PGE in solid solution in base metal sulfides and the down temperature equilibration history of Merensky ores. Contrib Mineral Petr 122:241–251

Ballhaus C, Sylvester P (2000) Noble metal enrichment processes in the Merensky Reef, Bushveld Complex. J Petrol 41:545–561

Ballhaus C, Ulmer P (1995) Platinum-group elements in the Merensky Reef: II. Experimental solubilities of platinum and palladium in $Fe_{1-x}S$ from 950 to 450 °C under controlled f_{S_2} and f_{H_2}. Geochim Cosmochim Acta 59:4881–4888

Ballhaus C, Bockrath C, Wohlgemuth-Ueberwasser C, Laurenz V, Berndt J (2006) Fractionation of the noble metals by physical processes. Contrib Mineral Petr 152:667–684

Barkov AY, Fleet ME (2004) An unusual association of hydrothermal platinum-group minerals from the Imandra Layered Complex, Kola Peninsula, northwestern Russia. Can Mineral 42:455–467

Barkov AY, Fleet ME, Martin RF, Halkoaho TAA (2005) New data on "Bonanza"-type PGE mineralization in the Kirakkajuppura PGE deposit, Penikat Layered Complex, Finland. Can Mineral 43:1663–1686

Barnes SJ (2006) Komatiite-hosted nickel sulfide deposits: geology, geochemistry and genesis. Soc Econ Geol Spec Publ 13:51–118

Barnes S-J, Francis D (1995) The distribution of platinum group elements, nickel, copper, and gold in the Muskox layered intrusion, Northwest Territories, Canada. Econ Geol 90:135–154

Barnes SJ, Hoatson DM (1994) The Munni Munni Complex, Western Australia: Stratigraphy, structure and petrogenesis. J Petrol 35:715–751

Barnes S-J, Maier WD (2002) Platinum-group elements and microstructures of normal Merensky Reef from Impala Platinum Mines, Bushveld Complex. J Petrol 43:171–198

Barnes SJ, Naldrett AJ (1986) Geochemistry of the J-M Reef of the Stillwater Complex, Minneapolis Adit Area II. Silicate mineral chemistry and petrogenesis. J Petrol 27:791–825

Barnes S-J, Ripley EM (2016) Highly siderophile and strongly chalcophile elements in magmatic ore deposits. Rev Mineral Geochem 81:725–774

Barnes SJ, Naldrett AJ, Gorton MP (1985) The origin of the fractionation of platinum-group elements in terrestrial magmas. Chem Geol 53:303–323

Barnes SJ, Boyd R, Korneliussen A, Nilsson LP, Often M, Pedersen RB, Robins B (1988) The use of mantle normalization and metal ratios in discriminating between the effects of partial melting, crystal fractionation and sulfide segregation on platinum-group elements, gold, nickel and copper: examples from Norway. *In*: Geoplatinum 87. Prichard PJ, Potts, Bowles JFW, Cribb SJ (eds) Elsevier, London, p 113–143

Becker H, Dale CW (2016) Re–Pt–Os isotopic and highly siderophile element behavior in oceanic and continental mantle tectonite. Rev Mineral Geochem 81:369–440

Belousova EA, González-Jiménez JM, Graham I, Griffin WL, O'Reilly SY, Pearson N, Martin L, Craven S, Talavera C (2015) The enigma of crustal zircons in upper mantle rocks: clues from the Tumut ophiolite, SE Australia. Geol 43:119–122

Berlincourt LE, Hummel HH, Skinner BJ (1981) Phases and phase relations of the platinum-group elements. *In* Platinum-Group Elements: Mineralogy, Geology, Recovery. Cabri LJ (ed) Can Inst Min Metall Petrol Spec Vol 23, p 19–45

Berg T, Maul J, Schönhense G, Marosits E, Hoppe P, Ott U, Palme H (2009) Direct evidence for condensation in the early solar system and implications for nebular cooling rates. Astrophys J 702:L172–L176

Bezigov VK, Borisenko LF, Uskov YD (1975) Sulfides and natural solid solution of platinum metals from the ultrabasites of the Gusevogerskiy pluton, Urals. Dokl Acad Sci SSSR, Earth Sci Sect 225:1408–1411

Bézos A, Lorand J-P, Humler E, Gros M (2005) Platinum-group element systematics in mid-oceanic ridge basaltic glasses from the Pacific, Atlantic, and Indian Oceans. Geochim Cosmochim Acta 69:2613–2627

Blander M, Fuchs LH, Hurowitz C, Land R (1980) Primordial refractory metal particles in the Allende meteorite. Geochim Cosmochim Acta 44:217–223

Bockrath C, Ballhaus C, Holzheid A (2004a) Fractionation of the platinum-group-elements during mantle melting. Science 305:1951–1953

Bockrath C, Ballhaus C, Holzheid A (2004b) Stabilities of laurite RuS_2 and monosulphide liquid solution at magmatic temperature. Chem Geol 208:265–271

Borisov A, Palme H (1997) Experimental determination of the solubility of platinum in silicate melts. Geochim Cosmochim Acta 61:4349–4357

Borisov A, Palme H (2000) Solubilities of noble metals in Fe-containing silicate melts as derived from experiments in Fe-free systems. Am Mineral 85:1665–1673

Boudreau AE, McCallum IS (1992a) Infiltration metasomatism in layered intrusions-an example from the Stillwater Complex, Montana. J Volcanol Geoth Res 52:171–183

Boudreau AE, McCallum IS (1992b) Concentration of Platinum-group elements by magmatic fluids in layered intrusions. Econ Geol 87:1830–1848
Boudreau AE, Stewart MA, Spivack A (1997) Stable Cl isotopes and origin of high Cl/F magmas of the Stillwater Complex, Montana. Geol 25:791–794
Bowles JFW (1986) The development of platinum-group minerals in laterites. Econ Geol 81:1278–1285
Bowles JFW, Lyon IC, Saxton JM, Vaughan DJ (2000) The origin of platinum group minerals from the Freetown Intrusion, Sierra Leone, inferred from osmium isotope systematics. Econ Geol 95:539–548
Bowles JFW, Prichard HM, Suárez S, Fisher PC (2013) The first report of platinum-group minerals in magnetite-bearing gabbro, Freetown Layered Complex, Sierra Leone: occurrences and genesis. Can Mineral 51:455–473
Boyd R, Barnes SJ, Gronlie A (1988) Noble metal geochemistry of some Ni–Cu deposits in the Sveconorwegian and Caledonian orogens in Norway. *In*: Geoplatinum 87. Prichard HM, Potts PJ, Bowles JFW, Cribb SJ (eds) Elsevier, London, p 145–158
Brenan JM, Andrews DRA (2001) High-temperature stability of laurite and Ru–Os–Ir alloy and their role in PGE fractionation in mafic magmas. Can Mineral 39:341–360
Brenan JM, Mungall JE (2008) Platinum-group elements. Elements 4:227–232
Brenan JM, McDonough WF, Ash R (2005) An experimental study of the solubility and partitioning of iridium, osmium and gold between olivine and silicate melt. Earth Planet Sci Lett 237:855–872
Brenan JM, Finnigan CF, McDonough WF, Homolova V (2012) Experimental constraints on the partitioning of Ru, Rh, Ir, Pt and Pd between chromite and silicate melt: The importance of ferric iron. Chem Geol 302–303:16–32
Brenan JM, Bennett NR, Zajacz Z (2016) Experimental results on fractionation of the highly siderophile elements (HSE) at variable pressures and temperatures during planetary and magmatic differentiation. Rev Mineral Geochem 81:1–87
Brown AV, Page NJ, Love AH (1988) Geology and platinum-group element geochemistry of the Serpentinite Hill Complex, Dundas Trough, western Tasmania. Can Mineral 26:161–175
Brynard HJ, De Villiers JPR, Viljoen EA (1976) A mineralogical investigation of the Merensky Reef at the Western Platinum mine, near Marikana, South Africa. Econ Geol 71:1299–1307
Burton KW, Schiano P, Birck J-L, Allègre CJ (1999) Osmium isotope disequilibrium between mantle minerals in a spinel-lherzolite. Earth Planet Sci Lett 172:311–322
Burton KW, Abdelmouhcine G, Birck J-L, Allègre CJ, Schiano P, Clocchiatti R, Alard O (2002) The compatibility of rhenium and osmium in natural olivine and their behavior during mantle melting and basalt genesis. Earth Planet Sci Lett 198:63–76
Cabri LJ (1981a) The platinum-group minerals. *In:* Platinum-Group Elements: Mineralogy, Geology, Recovery. Cabri LJ (ed) Can Inst Min Metall Pet Spec Vol 23, p 84–15045
Cabri LJ (1981b) Mineralogy and distribution of the platinum-group in mill samples from the Cu-Ni deposits of the Sudbury, Ontario area. *In:* Precious Metals. McGachie RO, Bradley AG (eds), Pergamon Press, Toronto, p 23–34
Cabri LJ (1988) Overview on application of platinum mineralogy to mineral exploration and processing. *In:* Carson DJT, Vassilou AH (eds) Process Mineralogy VIII: Applications of mineralogy to mineral beneficiation technology, metallurgy, and mineral exploration and evaluation, with emphasis on precious metal ores. Miner Metals Mater Soc, p 23–31
Cabri LJ (2002) The platinum-group minerals. *In:* The Geology, Geochemistry, Mineralogy and Mineral Beneficiation of Platinum-Group Elements. Cabri LJ (ed) Can Inst Min Metall Pet Spec Vol 54, p 13–130
Cabri LJ, Feather CE (1975) Platinum-iron alloys: A nomenclature based on a study of natural and synthetic alloys. Can Mineral 13:117–126
Cabri LJ, Laflamme JHG (1976) The mineralogy of the platinum-group elements from some copper–nickel deposits of the Sudbury area, Ontario. Econ Geol 71:1159–1195
Cabri LJ, Blank H, El Goresy A, Laflamme JHG, Nobiling R, Sizgoric MB, Traxel K (1984) Quantitative trace-element analyses of sulfides from Sudbury and Stillwater by proton microprobe. Can Mineral 22:521–542
Cabri LJ, Stern R, Czamanske GK (1998) Osmium Isotope Measurements of PGM in Kondyor Pt–Fe Nuggets Using a SHRIMP II Ion Microprobe. 8th International Platinum Symposium, Extended Abstracts:55–58
Cameron WE, Nisbet EG (1982) Phanerozoic analogues of komatiitic basalts. *In*: Komatiites. Arndt NT, Nisbet EG (eds). Allen & Unwin, London, p 29–50
Cameron WE, Nisbet EG, Dietrich VJ (1979) Boninites, komatiites and ophiolitic basalts. Nature (London) 280:550–553
Campbell IH, Naldrett AJ (1979) The influence of silicate:sulfide ratios on the geochemistry of magmatic sulfides. Econ Geol 76:1503–1506
Campbell IH, Naldrett AJ, Barnes SJ (1983) A model for the origin of platinum-rich sulphide horizons in the Bushveld and Stillwater complexes. J Petrol 24:133–165
Campbell AJ, Humayun M, Meibom A, Krot AN, Keil K (2001) Origin of zoned metal grains in the QUE 94411 chondrite. Geochim Cosmochim Acta 65:163–180

Capobianco CJ (1998) Ruthenium solubility in hematite. Am Mineral 83:1152–1160
Capobianco CJ, Drake MJ (1990) Partitioning of ruthenium, rhodium, and palladium between spinel and silicate melt and implications for platinum-group element fractionation trends. Geochim Cosmochim Acta 54:869–874
Capobianco CJ, Hervig RL, Drake MJ (1994) Experiments on crystal/liquid partitioning of Ru, Rh and Pd for magnetite hematite solid solutions crystallized from silicate melt. Chem Geol 113:23–43
Carlson RW (2005) Application of the Pt–Re–Os isotopic systems to mantle geochemistry and geochronology. Lithos 82:249–272
Cawthorn RG, Lee CA, Schouwstra RP, Mellowship P (2002) Relationship between PGE and PGM in the Bushveld Complex. Can Mineral 40:311–328
Clark T (1975) Geology of an ultramafic complex on the Turnagain River, northwestern B.C. Unpublished PhD thesis, Queens University
Coggon JA, Nowell GM, Pearson DG, Lorand J-P, Oberthür T, Parman SW (2011a) The ^{190}Pt–^{186}Os decay system applied to dating platinum-group element mineralization of the Bushveld Complex, South Africa. Chem Geol 302–303:48–60
Coggon JA, Nowell GM, Pearson DG, Parman SW (2011b) Application of the ^{190}Pt–^{186}Os isotope system to dating platinum mineralization and ophiolite formation: an example from the Meratus Mountains, Borneo. Econ Geol 106:93–117
Constantinides CC, Kingston GA, Fisher PC (1980) The occurrence of platinum group minerals in chromitites of the Kokkinortsos chromite mine, Cyprus. *In*: Proc. Int. Ophiolite Symp. Panayiotou A (ed) Min of Ag Natur Resour, Geol Survey Dept, Cyprus, p 93–101
Cottrell E, Walker D (2006) Constraints on core formation from Pt partitioning in mafic silicate liquids at high temperatures. Geochim Cosmochim Acta 70:1565–1580
Croat TK, Stadermann F, Bernatowicz T (2008) Correlated isotopic and microstructural studies of turbostratic presolar graphites from the Murchison meteorite. Meteorit Planet Sci 43:1497–1516
Croat TK, Berg T, Bernatowicz T, Groopman E, Jhadav M (2013) Refractory metal nuggets within presolar graphite: first condensates from a circumstellar environment. Meteorit Planet Sci 48:686–699
Czamanske GK, Kunilov VE, Zientek ML, Cabri LJ, Likhachev AP, Calk LC, Oscarson RL (1992) A proton-microprobe study of magmatic sulfide ores from the Noril'sk-Talnakh district, Siberia. Can Mineral 30:249–287
Dare SAS, Barnes S-J, Prichard HM, Fisher PC (2010) The timing and formation of platinum-group minerals from the Creighton Ni–Cu–platinum-group element sulfide deposit, Sudbury, Canada: early crystallization of PGE-rich sulfarsenides. Econ Geol 105:1071–1096
Day JMD, Pearson DG, Hulbert LJ (2008) Rhenium–osmium isotope and platinum group element constraints on the origin and evolution of the 1.27 Ga Muskox layered intrusion. J Petrol 49:1255–1295
Day JMD, Brandon AD, Walker RJ (2016) Highly siderophile elements in Earth, Mars, the Moon, and asteroids. Rev Mineral Geochem 81:161–238
De Almeida CM, Olivo GR, De Carvalho SG (2007) The Ni–Cu–PGE sulfide ores of the komatiite-hosted Fortaleza De Minas deposit, Brazil: Evidence of hydrothermal remobilization. Can Mineral 45:751–773
De Waal SA (1978) The nickel deposit at Bon Accord, Barberton, South Africa-A proposed paleometeorite. *In*: Verwoerd WJ (ed) Mineralisation in Metamorphic Terranes. Spec Publ Geol Soc S Afr, Johannesburg, South Africa:87–98
Derbyshire EJ, O'Driscoll B, Lenaz D, Gertisser R, Kronz A (2013) Compositionally heterogeneous podiform chromitite in the Shetland Ophiolite Complex (Scotland): implications for chromitite petrogenesis and late-stage alteration in the upper mantle portion of a supra-subduction zone ophiolite. Lithos 162–163:279–300
Eales HV (2000) Implications of the chromium budget of the Western Limb of the Bushveld Complex. S Afr J Geol 103:141–150
Echeverria LM (1980) Tertiary or Mesozoic komatiites from Gorgona island, Colombia: field relations and geochemistry. Contrib Mineral Petr 73:253–266
Eckstrand OR, Hulbert LJ (2007) Magmatic nickel–copper–platinum group element deposits. *In*: Goodfellow WD (ed) Mineral deposits of Canada: a synthesis of major deposit types, district metallogeny, the evolution of geological provinces, and exploration methods. Geol Assoc Canada Spec Publ 5:205–222
Economou M (1983) Platinum-group metals in chromite ores from the Vourinos ophiolite complex, Greece. Ofioliti 8:339–356
Economou-Eliopoulos M (1993) Platinum-group element (PGE) distribution in chromite ores from ophiolite complexes of Greece: implications for chromite exploration. Ofioliti 18:83–98.
Economou M, Naldrett AJ (1984) Sulfides associated with podiform bodies of chromite at Tsangli Eretria, Greece. Miner Deposita 19:289–297
Economou-Eliopoulos M, Vacondios I (1995) Geochemistry of chromitites and host rocks from the Pindos ophiolite complex, northwestern Greece. Chem Geol 122:99–108
Economou-Eliopoulos M, Eliopoulos DG (2000) Palladium, platinum and gold concentrations in porphyry copper systems of Greece and their genetic significance. Ore Geol Rev 16:59–70
Economou-Eliopoulos M (2010) Platinum-group elements (PGE) in various geotectonic settings: opportunities and risks. Hell J Geosci 45:65–82

El Goresy A, Nagel K, Ramdohr P (1978) Fremdlinge and their noble relatives. Proc Lunar Planet Sci Conf 9:1279–1303
Eliopoulos DG, Economou-Eliopoulos M, Zelyaskova-Panayiotova M (2014) Critical factors controlling Pd and Pt potential in porphyry Cu–Au deposits: Evidence from the Balkan Peninsula. Geosciences 4:31–49
Farrow CEG, Lightfoot PC (2002) Sudbury PGE revisited: Toward an integrated model. *In:* The Geology, Geochemistry, Mineralogy and Mineral Beneficiation of Platinum-Group Elements. Cabri LJ (ed) Geol Soc CIM, Can Inst Min Metall Petrol Spec Vol 54, p 13–130
Fedortchouk Y, Lebarge W, Barkov AY, Fedele L, Bodnar RJ, Martin RF (2010) Platinum-group minerals from a placer deposit in Burwash Creek, Kluane Area, Yukon Territory, Canada. Can Mineral 48:583–596
Ferrario A, Garuti G (1990) Platinum-group mineral inclusions in chromitites of the Finero mafic–ultramafic complex (Ivrea-Zone, Italy). Miner Petrol 41:125–143
Findlay DC (1969) Origin of the Tulameen ultramafic–gabbro complex, southern British Columbia. Can J Earth Sci 6:399–425
Finnigan CS, Brenan JM, Mungall JE, McDonough WF (2008) Experiments and models bearing on the role of chromite as a collector of platinum group minerals by local reduction. J Petrol 49:1647–1665
Fiorentini ML, Stone WE, Beresford SW, Barley ME (2004) Platinum-group element alloy inclusions in chromites from Archean mafic–ultramafic units: Evidence from the Abitibi and the Agnew–Wiluna greenstone belts. Miner Petrol 82:341–355
Fiorentini ML, Beresford SW, Grguric B, Barnes SJ, Stone WE (2007) Atypical stratiform sulfide-poor platinum-group element mineralisation in the Agnew–Wiluna belt komatiites, Wiluna, Western Australia. Aust J Earth Sci 54:801–824
Fiorentini ML, Barnes SJ, Lesher CM, Heggie GJ, Keays RR, Burnham OM (2010) Platinum group element geochemistry of mineralized and nonmineralized komatiites and basalts. Econ Geol 105:795–823
Fleet ME, Chryssoulis SL, Stone WE, Weisener CG (1993) Partitioning of platinum-group elements and Au in the Fe–Ni–Cu–S system: experiments on the fractional crystallization of sulphide melt. Contrib Mineral Petr 115:36–44
Foley JY, Light TD, Nelson SW, Harris RA (1997) Mineral occurrences associated with mafic–ultramafic and related alkaline complexes in Alaska. *In:* Mineral deposits of Alaska. Goldfarb RA, Miller LD (eds.) Econ Geol Monogr 9, p 396–449
Fominykh VG, Yushko-Zakharova OE, Dubakina LS (1974) Platinum-group minerals of the Gusevogorsk deposit. Dokl Akad Nauk SSSR 217:663–666 (in Russian)
Fonseca ROC, Campbell IH, O'Neill HSC, Allen CM (2009) Solubility of Pt in sulfide mattes: implications for the genesis of PGE-rich horizons in layered intrusions. Geochim Cosmochim Acta 73:5764–5777
Fonseca ROC, Laurenz V, Mallmann G, Luguet A, Hoehne N, Jochum KP (2012) New constraints on the genesis and long-term stability of Os-rich alloys in the Earth's mantle. Geochim Cosmochim Acta 87:227–242
Foose MP (1985) The setting of a magmatic sulfide occurrence in a dismembered ophiolite, southwest Oregon. US Geol Surv Bull 1626a
Foose MP, Economou M, Panayiotou A (1985) Compositional and mineralogic constraints on the genesis of ophiolite hosted nickel mineralization in the Pevkos Area, Limassol Forest, Cyprus. Miner Deposita 20:234–240
Ford FD, Wercholaz CR, Lee A (2011) Predicting process outcomes for Sudbury platinum-group minerals using grade-recovery modeling from mineral liberation analyzer (MLA) data. Can Mineral 49:1627–1642
Fortenfant SS, Guenther D, Dingwell DB, Rubie DC (2003) Temperature dependence of Pt and Rh solubilities in a haplobasaltic melt. Geochim Cosmochim Acta 67:123–131
Gain SB (1985) The geological setting of the platiniferous UG-2 chromitite layer on the farm Maandagshoek, Eastern Bushveld Complex. Econ Geol 80:925–943
Gansser A, Dietrich VJ, Cameron WE (1979) Paleogene komatiites from Gorgona island. Nature 278:545–546
Garuti G, Rinaldi R (1986) Mineralogy of melonite-group and other tellurides from the Ivrea–Verbano basic complex, western Italian Alps. Econ Geol 81:1213–1217
Garuti G, Zaccarini F (1994) I minerali del gruppo del platino: primi ritrovamenti in Italia. Atti della Società dei Naturalisti e Matematici di Modena 125:11–28
Garuti G, Zaccarini F (1997) In situ alteration of platinum-group minerals at low temperature: evidence from serpentinized and weathered chromitite of the Vourinos complex, Greece. Can Mineral 35:611–626
Garuti G, Fershtater C, Bea F, Montero P, Pushkarev EV, Zaccarini F (1997) Platinum-group elements as petrological indicators in mafic–ultramafic complexes of the central and southern Urals: preliminary results. Tectonophys 276:181–194
Garuti G, Zaccarini F, Economou-Eliopoulos M (1999a) Paragenesis and composition of laurite from chromitites of Othrys (Greece): implications for Os–Ru fractionation in ophiolitic upper mantle of the Balkan peninsula. Miner Deposita 34:312–319
Garuti G, Zaccarini F, Moloshag V, Alimov V (1999b) Platinum-group elements as indicators of sulphur fugacity in ophiolitic upper mantle: an example from chromitites of the Ray-Iz ultramafic complex, Polar Urals, Russia. Can Mineral 37:1099–1115
Garuti G, Pushkarev EV, Zaccarini F (2002) Composition and paragenesis of Pt alloys from chromitites of the Uralian–Alaskan-type Kytlym and Uktus complexes, northern and central Urals, Russia. Can Mineral 40:357–376

Garuti G, Pushkarev EV, Zaccarini F, Cabella R, Anikina E (2003) Chromite composition and platinum-group mineral assemblage in the Uktus Uralian–Alaskan-type complex (central Urals, Russia): Miner Deposita 38:312–326

Gault HR (1945) The Salt Chuck copper–palladium mine, Prince of Wales Island, southeastern Alaska. US Geol Surv, Open-File Rep. 4Gl9

Gauthier M, Corrivaux L, Trottier LJ, Cabri J, Laflamme JH, Bergeron M (1990) Chromitites platinifères des complexes ophiolitiques de l'Estrie-Beauce, Appalaches du Sud du Québec. Miner Deposita 25:169–178

Genkin AD (1968) Minerals of the platinum metals and their associations in the copper–nickel ores of Noril'sk deposit: Moscow, Nauka (in Russian)

Genkin AD, Evstigneeva TL (1986) Associations of platinum-group minerals of the Noril'sk copper–nickel sulfide ores. Econ Geol 81:1203–1212

Genkin AD, Distler VV, Gladyshev GD, Filimonova AA, Evstigneeva TL, Kovalenker VA, Laputina IP, Smirnov AV, Grokhovskaya TL (1981) Sulfide copper–nickel ores of Noril'sk deposits: Moscow, Nauka (in Russian)

Gervilla F, Kojonen K (2002) The platinum-group minerals in the upper section of the Keivitsansarvi Ni–Cu–PGE deposit, northern Finland. Can Mineral 40:377–394

Gervilla F, Proenza JA, Frei, González-Jiménez JM, Garrido C, Melgarejo JC, Meibom A, Díaz-Martínez R, Lavaut W (2005) Distribution of platinum-group elements and Os isotopes in chromite ores from Mayarí-Baracoa Ophiolitic Belt (eastern Cuba). Contrib Mineral Petr 150:589–607

Gijbels RH, Millard HT, Deborough GA, Bartel AJ (1974) Osmium, ruthenium, iridium and uranium in silicates and chromite from the eastern Bushveld Complex, South Africa. Geochim Cosmochim Acta 38:319–337

Godel B (2013) High-resolution X-ray computed tomography and its application to ore deposits: From data acquisition to quantitative three-dimensional measurements with case studies from Ni–Cu–PGE deposits. Econ Geol 108:2005–2019

Godel B, Barnes S-J (2008a) Platinum-group elements in sulfide minerals and the whole rocks of the J-M Reef (Stillwater Complex): Implication for the formation of the reef. Chem Geol 248:272–294

Godel B, Barnes S-J (2008b) Image analysis and composition of platinum-group minerals in the J-M Reef, Stillwater Complex. Econ Geol 103:637–651

Godel B, Barnes S-J, Maier WD (2007) Platinum-group elements in sulphide minerals, platinum-group minerals, and whole rocks of the Merensky Reef (Bushveld Complex, South Africa): Implications for the formation of the reef. J Petrol 48:1569–1604

Godel B, Barnes SJ, Barnes S-J, Maier WD (2010) Platinum ore in three dimensions: Insights from high-resolution X-ray computed tomography. Geol 38:1127–1130

Godel B, González-Álvarez I, Barnes SJ, Barnes S-J, Parker P, Day J (2012) Sulfides and sulfarsenides from the Rosie Nickel Prospect, Duketon Greenstone Belt, Western Australia. Econ Geol 107:275–294

González-Jiménez JM, Gervilla F, Proenza JA, Augé T, Kerestedjian T (2009a) Distribution of platinum-group minerals in ophiolitic chromitites. Trans Inst Min Metal B118:101–110

González-Jiménez JM, Gervilla F, Proenza JA, Kerestedjian T, Augé T, Bailly L (2009b) Zoning of laurite (RuS_2)–erlichmanite (OsS_2): implications for the genesis of PGM in ophiolite chromitites. Eur J Mineral 21:419–432

González-Jiménez JM, Gervilla F, Kerestedjian T, Proenza JA (2010) Effects of metamorphism on platinum-group and base-metal mineral assemblages in ophiolite chromitites from the Dobromirtsi massif, Rhodope Mountains (SE Bulgaria). Resour Geol 60:315–334

González-Jiménez JM, Augé T, Gervilla F, Bailly L, Proenza JA, Griffin WL (2011a) Mineralogy and geochemistry of platinum-rich chromitites from the mantle–crust transition zone at Ouen Island, New Caledonia ophiolite. Can Mineral 49:1549–1570

González-Jiménez JM, Proenza JA, Gervilla F, Melgarejo JC, Blanco-Moreno JA, Ruiz-Sánchez R, Griffin WL (2011b) High-Cr and high-Al chromitites from the Sagua de Tánamo district, Mayarí-Cristal Ophiolitic Massif (eastern Cuba): constraints on their origin from mineralogy and geochemistry of chromian spinel and platinum-group elements. Lithos 125:101–121

González-Jiménez JM, Gervilla F, Griffin WL, Proenza JA, Augé T, O'Reilly SY, Pearson NJ (2012a) Os-isotope variability within sulfides from podiform chromitites. Chem Geol 291:224–235

González-Jiménez JM, Griffin WL, Gervilla F, Kerestedjian TN, O'Reilly SY, Proenza JA, Pearson NJ, Sergeeva I (2012b) Metamorphism disturbs the Re–Os signatures of platinum-group minerals in ophiolite chromitites. Geol 40:659–662

González-Jiménez JM, Marchesi C, Griffin WL, Gutiérrez-Narbona R, Lorand J-P, O'Reilly SY, Garrido CJ, Gervilla F, Pearson NJ, Hidas K (2013a) Transfer of Os isotopic signatures from peridotite to chromitite in the subcontinental mantle: insights from in situ analysis of platinum-group and base-metal minerals (Ojén peridotite massif, southern Spain). Lithos 164–167:74–85

González-Jiménez JM, Locmelis M, Belousova E, Griffin WL, Gervilla F, Kerestedjian T, O'Reilly SY, Sergeeva I, Pearson NJ (2013b) Genesis and tectonic implications of podiform chromitites in the metamorphosed Ultramafic Massif of Dobromirtsi (Bulgaria). Gondwana Res 27:555–574

González-Jiménez JM, Griffin WL, Gervilla F, Proenza JA, O'Reilly SY, Pearson NJ (2014a) Chromitites in ophiolites: how, where, when, why? Part I. Origin and significance of platinum-group minerals. Lithos 189:127–139

González-Jiménez JM, Griffin WL, Proenza JA, Gervilla F, O'Reilly SY, Akbulut M, Pearson NJ, Arai. S (2014b) Chromitites in ophiolites: how, where, when, why? Part II. The crystallisation of chromitites. Lithos 189:140–158

González-Jiménez JM, Villaseca C, Griffin WL, O'Reilly SY, Belousova E, Ancochea E, Pearson NJ (2014c) Significance of ancient sulfide PGE and Re–Os signatures in the mantle beneath Calatrava, Central Spain. Contrib Mineral Petr 168:1047

Gornostayev SS, Crocket JH, Mochalov AG, Laajoki KVO (1999) The platinum-group minerals of the Baimka placer deposits, Aluchin horst, Russian Far East. Can Mineral 37:1117–1129

Gornostayev SS, Dodatko AD, Laajoki KVO, Mochalov AG (2000) Origin of platinum-bearing placers in the Aluchin horst, Russian Far East. Econ Geol 95:549– 558

Gornostayev SS, Ohnenstetter M, Neziraj A, Ohnenstetter D, Laajoki KVO, Popovchenko SE, Kornienko PK (2001) New occurrence of anduoite $(Ru,Os)As_2$ from chromite deposits of Ukraine and Albania. Can Mineral 39:591–606

Graham IT, Franklin BJ, Marshall B (1996) Chemistry and mineralogy of podiform chromitite deposits, southern NSW, Australia: a guide to their origin and evolution. Miner Petrol 57:129–150

Grieco G, Diella V, Chaplygina NL, Savalieva GN (2006) Platinum group element zoning and mineralogy of chromitite from the cumulate sequence of the Nurali massif (Southern Urals, Russia). Ore Geol Rev 30:257–276

Griffin WL, Spetsius ZV, Pearson NJ, O'Reilly SY (2002) In situ Re–Os analysis of sulfide inclusions in kimberlitic olivine: New constraints on depletion events in the Siberian lithospheric mantle. Geochem Geophys Geosyst 3:1069, doi: 10.1029/2001GC000287

Griffin WL, Begg GC, O'Reilly SY (2013) Continental-root control on the genesis of magmatic ore deposits. Nat Geosci 6:905–910, doi: 10.1038/NGEO1954

Gutierrez-Narbona R, Lorand J-P, Gervilla F, Gros M (2003) New data on base-metal mineralogy and platinum-group minerals in the Ojen chromitites (Serranía de Ronda, Betic Cordillera, southern Spain). N Jb Miner Abh 179:143–173

Halkoaho TAA, Alapieti TT, Lahtinen JJ (1990) The Sompujärvi PGE Reef in the Penikat Layered Intrusion, Northern Finland. Mineral Petrol 42:39-55

Handler MR, Bennett VC (1999) Behavior of platinum-group elements in the subcontinental mantle of eastern Australia during variable metasomatism and melt depletion. Geochim Cosmochim Acta 63:3597–3618

Hanley JJ (2005) The Aqueous Geochemistry of the Platinum-Group Elements (PGE) in Surficial, Low-T Hydrothermal and High-T Magmatic Hydrothermal Environments. *In:* Exploration for Platinum-Group Element Deposits; Mungall JE (ed) Mineral Assoc Canada: Quebec, QC, Canada. p 35–56

Hanley JJ (2007) The role of arsenic-rich melts and mineral phases in the development of high-grade Pt–Pd mineralization within komatiite-associated magmatic Ni–Cu sulfide horizons at Dundonald Beach South, Abitibi Subprovince, Ontario, Canada. Econ Geol 102:305–317

Harries D, Berg T, Langenhorst F, Palme H (2012) Structural clues to the origin of refractory metal alloys as condensates of the solar nebula. Meteorit Planet Sci 47:2148–2159

Hart SR, Kinloch ED (1989) Osmium isotope systematics in Witwatersrand and Bushveld ore deposits. Econ Geol 84:1651–1655

Hart SR, Ravizza GE (1996) Os partitioning between phases in lherzolite and basalt. Earth Processes: Reading the Isotopic Code. Basu A, Hart SR (eds) Geophys Monogr 95: Amer Geophys Union. p 123–134

Harvey J, Gannoun A, Burton KW, Schiano P, Rogers NW, Alard O (2010) Unravelling the effects of melt depletion and secondary infiltration on mantle Re–Os isotopes beneath the French Massif Central. Geochim Cosmochim Acta 74:293–320

Harvey J, Dale CW, Gannoun A, Burton KW (2011) Osmium mass balance in peridotite and the effects of mantle-derived sulphides on basalt petrogenesis, Geochim Cosmochim Acta 75:5574–5596

Harvey J, Warren JM, Shirey SB (2016) Mantle sulfides and their role in Re–Os and Pb isotope geochronology. Rev Mineral Geochem 81:579–649

Hattori K, Cabri LJ, Hart SR (1991) Osmium isotope ratios of PGM grains associated with the Freetown layered complex, Sierra Leone, and their origin. Contrib Mineral Petr 109:10–18

Hattori KH, Takahashi Y, Augé T (2010) Mineralogy and origin of oxygen-bearing platinum–iron grains based on an X-ray absorption spectroscopy study. Am Mineral 95:622–630

Helmy HM (2004) Cu–Ni–PGE mineralization in the Genina Gharbia mafic–ultramafic intrusion, Eastern Desert, Egypt. Can Mineral 42:351–370

Helmy HM, Mogessie A (2001) Gabbro Akarem, Eastern Dessert, Egypt: Cu–Ni–PGE mineralization in a concentrically zoned mafic–ultramafic complex. Miner Deposita 36:58–71

Helmy HM, Ballhaus C, Fonseca ROC, Wirth R, Nagel T, Tredoux M (2013) Noble metal nanoclusters and nanoparticles precede mineral formation in magmatic sulphide melts. Nat Comm 4:2405

Hewins RH, Bourot-Denise M, Zanda B, Leroux H, Barrat J-A, Humayun M, Göpel C, Greenwood RC, Franchi IA, Pont S, Lorand J-P, Cournède C, Gattacceca J, Rochette P, Kugak M, Marrocchi Y, Marty B (2014) The Paris meteorite, the least altered CM chondrite so far. Geochim Cosmochim Acta 124:190–222

Heyse JV (1983) The mineralogy of the Stillwater platinum–palladium ore in the Frog Pond and Minneapolis adits: Chevron Research Company Report 41

Hiemstra SA (1985) The distribution of some platinum group elements in the UG2 chromitite layer of the Bushveld Complex. Econ Geol 80:944–957

Hill R, Roeder P (1974) The crystallization of spinel from basaltic magma as a function of oxygen fugacity. J Geol 82:709–729

Himmelberg GR, Loney RA, Craig JT (1986) Petrogenesis of the ultramafic complex at the Blashke Islands, southeastern Alaska. US Geol Surv Bull 1662, p 14

Himmelberg GR, Loney RA (1995) Characteristics and petrogenesis of Alaskan-type ultramafic–mafic intrusions, southeastern Alaska. US Geol Surv Prof Paper 1564. p 47

Hoaglund SA (2010) U–Pb geochronology of the Duluth Complex and related hypabyssal intrusions: investigating the emplacement history of a large multiphase intrusive complex related to the 1.1 Ga Midcontinent Rift. Unpublished PhD Thesis. Retrieved from the University of Minnesota Digital Conservancy, http://purl.umn.edu/93624

Holt SP, Shepard JG, Thorne RL, Tolonen AW, Fosse EL (1948) Investigation of the Salt Chuck copper mine, Kasaan Peninsula, Prince of Wales Island, southeastern Alaska. US Bur Mines Rep Invest 4358

Holwell DA, McDonald I, Armitage PEB (2006) Platinum-group mineral assemblages in the Platreef at the Sandsloot Mine, northern Bushveld Complex, South Africa. Mineral Mag 70:83–101

Holwell DA, Keays RR, Firth EA, Findlay J (2014) Geochemistry and mineralogy of platinum group element mineralization in the River Valley Intrusion, Ontario, Canada: a model for early-stage sulfur saturation and multistage emplacement and the implications for "contact-type" Ni–Cu–PGE sulfide mineralization. Econ Geol 109:689–712

Holzheid A (2010) Separation of sulphide melt droplets in sulphur saturated silicate liquids. Chem Geol 274:127–135

Holzheid A, Sylvester P, O'Neil HStC, Rubie DC, Palme H (2000) Evidence for a late chondritic veneer in the Earth's mantle from high-pressure partitioning of palladium and platinum. Nature 406:396–399

Horan MF, Morgan JW, Walker RJ, Cooper RW (2001) Re–Os isotopic constraints on magma mixing in the peridotite zone of the Stillwater complex, Montana, USA. Contrib Mineral Petr 141:446–457

Hudson DR (1986) Platinum-group minerals from the Kambalda nickel deposits, Western Australia. Econ Geol 81:1218–1225

Hudson DR, Donaldson MJ (1984) Mineralogy of platinum group elements in the Kambalda nickel deposits, Western Australia. *In:* Sulphide Deposits in Mafic and Ultramafic Rocks. Buchanan DL, Jones MJ (eds) The Inst Min Metall, p 55–61

Huminicki MAE, Sylvester PJ, Cabri LJ, Lesher CM, Tubrett M (2005) Quantitative mass balance of platinum group elements in the Kelly Lake Ni–Cu–PGE deposit, Copper Cliff Offset, Sudbury. Econ Geol 100:1631–1646

Hutcheon ID, Armstrong JT, Wasserburg GJ (1987) Isotopic studies of Mg, Fe, Mo, Ru and W in Fremdlinge from Allende refractory inclusions. Geochim Cosmochim Acta 51:3175–3192

Hutchinson D, Prichard HM, Macleod CJ (1999) Evidence for partial melting and melt impregnation of mantle peridotites leading to PGM deposition: a comparison of samples from the Lizard and Troodos ophiolites and the Tonga Trench [abs.]. *In:* Mineral deposits: Processes to processing. Stanley CJ et al. (eds) SGA London, Balkema, Rotterdam, p 729–732

Hutchinson D, Kinnaird JA, Schurmann LW (2004) Complex, multi-stage mineralization history in the southern sector of the Platreef, Bushveld Complex, RSA. Geoscience Africa 2004, Abstract Vol, University of the Witwatersrand, Johannesburg, South Africa. p 293–294

Irvine TN (1977a) Origin of chromitite layers in the Muskox intrusion and other stratiform intrusions: A new interpretation. Geol 5:273–277

Irvine TN (1977b) Chromite crystallisation in the join Mg_2SiO_4–$CaMgSi_2O_6$–$CaAl_2Si_2O_8$–$MgCr_2O_4$–SiO_2. Carnegie Institution of Washington Yearbook 76:465–472

Jackson-Brown S, Scoates JS, Nixon GT, Ames DE (2014) Mineralogy of sulphide, arsenide, and platinum group minerals from the DJ/DB Zone of the Turnagain Alaskan-type ultramafic intrusion, north-central British Columbia. Geological Fieldwork 2013, British Columbia Ministry of Energy and Mines, British Columbia Geol Surv Paper 2014–1

Johan Z (2002) Alaskan-type complexes and their platinum-group element mineralization. *In:* The Geology, Geochemistry, Mineralogy and Mineral Beneficiation of Platinum-Group Elements. Cabri LJ (ed) Geol Soc CIM, Can Inst Min Metall Petrol Spec Vol 54, p 669–719

Johan Z, Ohnenstetter D, Naldrett AJ (1989a) Platinum-group minerals and associated oxides and base metal sulphides of the Main Sulphide Zone, Great Dyke, Zimbabwe. *In*: Papunen H (ed) Proc 5th Int Platinum Symp, Bull Geol Soc Finland 61:53–54

Johan Z, Ohnenstetter M, Slansky E, Barron LM, Suppel D (1989b) Platinum mineralization in the Alaskan-type intrusive complexes near Fifield, New South Wales, Australia. Part 1. Platinum-group minerals in clinopyroxenites of the Kelvin Grove prospect, Owendale intrusion. Miner Petrol 40:289–309

Jones JH, Drake MJ (1986) Geochemical constraints on core formation in the earth. Nature 322:221–228

Junge M, Oberthür T, Melcher F (2014) Cryptic variation of chromite chemistry, platinum group element and platinum group mineral distribution in the UG-2 chromitite: an example from the Karee Mine, western Bushveld Complex, South Africa. Econ Geol 109:795–810

Junge M, Wirth R, Oberthür T, Melcher F, Schreiber A (2015) Mineralogical siting of platinum-group elements in pentlandite from the Bushveld Complex, South Africa, Miner Deposita 50:41–54

Karaj N (1992) Répartition des platinoides, chromites et sulfures dans le massif de Bulqiza, Albanie. Incidence sur les processus métallogéniques dans les ophiolites. Unpublished PhD Thesis, Université d'Orléans, France

Karup-Møller S, Mackovicky E, Barnes S-J (2008) The metal-rich portions of the phase system Cu–Fe–Pd–S at 1000 °C, 900 °C and 725 °C: implications for mineralization in the Skaergaard intrusion. Mineral Mag 72:941–951

Kelemen PB, Dick HJB, Quick JE (1992) Formation of harzburgite by pervasive melt rock reaction in the upper mantle. Nature 358:635–641

Kinloch ED (1982) Regional trends in the platinum-group mineralogy of the Critical Zone of the Bushveld Complex, South Africa: Econ Geol 77:1328–1347

Kinloch ED, Peyerl W (1990) Platinum-group minerals in various rock types of the Merensky Reef: genetic implications. Econ Geol 85:537–555

Kocks H, Melcher F, Meisel, T, Burgath KP (2007) Diverse contributing sources to chromitite petrogenesis in the Shebenik Ophiolitic Complex, Albania: evidence from new PGE- and Os-isotope data. Mineral Petrol 91:139–170

Kogiso T, Suzuki K, Suzuki T, Uesugi K (2008) Two- and three-dimensional imaging of platinum-group minerals at submicrometer scale with synchrotron X-ray. Goldschmidt 2008 Conf Abst, p 1212

König S, Lissner M, Lorand J-P, Bragagni A, Luguet A (2015) Mineralogical control of selenium, tellurium and highly siderophile elements in the Earth's mantle: Evidence from mineral separates of ultra-depleted mantle residues. Chem Geol 396:16–24

Lachize M, Lorand JP, Juteau T (1991) Cu–Ni–PGE magmatic sulfide ores and their host layered gabbros in the Haymiliyah fossil magma chamber (Haylayn block, Semail ophiolite nappe, Oman). *In*: Ophiolite Genesis and Evolution of Oceanic Lithosphere. Peters TJ, Nicolas A, Coleman RG (eds) Kluwer, Dordrecht, p 209–229

Latypov R, O'Driscoll B, Lavrenchuk A (2013) Towards a model for an in situ origin for PGE reefs in layered intrusions: insights from the chromitite seams of the Rum Eastern Layered Intrusion, Scotland. Contrib Mineral Petr 166:309–327

Leblanc M (1991) Platinum-group elements and gold in ophiolitic complexes: distribution and fractionation from mantle to oceanic floor. *In*: Ophiolite Genesis and Evolution of the Oceanic Lithosphere, Oman. Peters TJ, Nicolas A, Coleman RG (eds) Kluwer, Dordrecht, pp 231–260

Legendre O (1982) Minéralogie et Géochimie des platinoïdes dans les chromitites ophiolitiques. Thèse Doctoral 3º Cycle, Université de Paris, p 171

Legendre O, Augé T (1986) Mineralogy of platinum group mineral inclusions in chromitites from different ophiolitic complexes. *In*: Metallogeny of Basic and Ultrabasic Rocks. Gallagher MJ, Ixer RA, Neary CR (eds) The Inst Min Metall, London, UK, p 361–372

Lesher MC (1989) Komatiite-associated nickel sulfide deposits. Rev Econ Geol 4:44–101

Lesher CM, Keays RR (1984) Metamorphically and hydrothermally mobilized Fe–Ni–Cu sulphides at Kambalda, Western Australia. *In:* Buchanan DL, Jones MJ (eds) Sulphide Deposits in Mafic and Ultramafic Rocks, Inst Min Metall, London, p 62–69

Lesher CM, Keays RR (2002) Komatiite-associated Ni–Cu–PGE deposits: geology, mineralogy, geochemistry and genesis. *In:* The Geology, Geochemistry, Mineralogy and Mineral Beneficiation of Platinum-Group Elements. Cabri LJ (ed) Geol Soc CIM, Can Inst Min Metall Petrol Spec Vol 54, p 579–617

Lesher CM, Arndt NT, Groves DI (1984) Genesis of komatiite-associated nickel sulphide deposits at Kambalda Western Australia: A distal volcanic model. *In:* Sulphide Deposits in Mafic and Ultramafic Rocks. Buchanan DL, Jones MJ (eds) The Inst Min Metall, London, UK, p 70–80

Li C, Naldrett AJ, Rucklidge JC, Kilius LR (1993) Concentrations of platinum-group elements and gold in sulfides from the Strathcona deposit, Sudbury, Ontario. Can Mineral 30:523–531

Locmelis M, Barnes SJ, Pearson NJ, Fiorentini ML (2009) Anomalous sulfur-poor platinum group element mineralization in komatiitic cumulates, Mount Clifford, Western Australia: Econ Geol 104:841–855

Locmelis M, Pearson NJ, Barnes S-J, Florentini ML (2011) Ruthenium in komatiitic chromite. Geochim Cosmochim Acta 75:3645–3661

Locmelis M, Fiorentini ML, Barnes SJ, Pearson NJ (2013) Ruthenium variation in chromite from komatiites and komatiitic basalts-a potential mineralogical indicator for nickel sulfide mineralization. Econ Geol 108:355–364

Loney RA, Himmelberg GR (1992) Petrogenesis of the Pd-rich intrusion at Salt Chuck, Prince of Wales Island: an early Paleozoic Alaskan-type ultramafic body. Can Mineral 30:1005–1022

Lorand J-P, Alard O (2001) Platinum-group element abundances in the upper mantle: new constraints from in situ and whole rock analyses of Massif Central xenoliths (France). Geochim Cosmochim Acta 65:2789–2806

Lorand JP, Conquéré F (1983) Contribution à l'étude des sulfures dans les enclaves de lherzolites à spinelle des basaltes alcalins (Massif Central et du Languedoc, France). Bull de Minéral 106:585–606

Lorand J-P, Luguet A (2016) Chalcophile and siderophile elements in mantle rocks: Trace elements controlled by trace minerals. Rev Mineral Geochem 81:441–488

Lorand J-P, Luguet A, Alard O, Bézos A, Meisel T (2008) Abundance and distribution of platinum-group elements in orogenic lherzolites; a case study in a Fontete Rouge lherzolite (French Pyrenees) Chem Geol 248:174–194

Lorand JP, Alard O, Luguet A (2010) Platinum-group element micronuggets and refertilization process in Lherz orogenic peridotite (northeastern Pyrenees, France). Earth Planet Sci Lett 289:298–310

Lorand J-P, Barrat J-A, Chevrier V, Sautter V, Pont S (2012) Metal-saturated sulfide assemblages in NWA 2737: Evidence for impact-related sulfur devolatilization in Martian meteorites. Meteorit Planet Sci 47:1830–1841

Lorand J-P, Hewins RH, Remusat L, Zanda B, Pont S, Humayun M, Nemchin A, Grange M, Kennedy A, Göpel C (2014) Pyrite tracks late hydrothermal alteration in Martian regolith breccia NWA 7533. Meteorit Soc Meet Abstr, 5123

Luguet A, Reisberg L (2016) Highly siderophile element and 187Os signatures in non–cratonic basalt–hosted peridotite xenoliths: Unravelling the origin and evolution of the post-Archean lithospheric mantle. Rev Mineral Geochem 81:305–367

Luguet A, Lorand J-P, Seyler M (2003) Sulfide petrology and highly siderophile element geochemistry of abyssal peridotites: A coupled study of samples from the Kane Fracture Zone (45°W 23°20'N, MARK Area, Atlantic Ocean). Geochim Cosmochim Acta 67:1553–1570

Luguet A, Shirey SB, Lorand J-P, Horan MF, Carlson RW (2007) Residual platinum-group minerals from highly depleted harzburgites of the Lherz massif (France) and their role in HSE fractionation of the mantle. Geochim Cosmochim Acta 71:3082–3097

Mackovicky M, Mackovicky E, Rose-Hansen J (1986) Experimental studies and distribution of platinum-group elements in base metal sulfides in platinum deposits. *In*: Galagher MJ, Ixer RA, Neary CR, Prichard HM (eds) Metallogeny of Basic and Ultrabasic Rocks. Inst Min Metall, London, p 415–423

Makovicky M, Makovicky E, Rose-Hansen J (1988) Experimental evidence of the formation and mineralogy of platinum and palladium ore deposits. *In*: Mineral Deposits Within the European Community. Boissonnas J, Omenetto P (eds) Springer-Verlag, Berlin, p 303–317

Malitch KN (2004) Osmium isotope constraints on contrasting sources and prolonged melting in the Proterozoic upper mantle: evidence from ophiolitic Ru–Os sulfides and Ru–Os–Ir alloys. Chem Geol 208:157–173

Malitch KN, Kostoyanov AI (1999) Model Re–Os isotopic age of the PGE mineralization at the Gulinsk massif (at the Northern Siberian Platform, Russia). Geol Ore Deposit 41:126–135

Malitch KN, Thalhammer OAR (2002) Pt–Fe nuggets derived from clinopyroxenite–dunite massifs, Russia: a structural, compositional and osmium-isotope study. Can Mineral 40:395–418

Malitch KN, Melcher F, Mühlhans H (2001) Palladium and gold mineralization in podiform chromitite at Kraubath, Austria. Miner Petrol 73:247–277

Malitch KN, Junk SA, Thalhammer OAR, Melcher F, Knauf VV, Pernicka E, Stumpfl EF (2003) Laurite and ruarsite from podiform chromitites at Kraubath and Hochgrössen, Austria: new insights from osmium isotopes. Can Mineral 41:331–352

Malitch KN, Badanina IY, Kostoyanov AI (2011a) Initial Os-isotopic composition of Os–Ir–Ru alloys from ultramafic massifs of the Polar Siberia. Dokl Earth Sci 440:1343–1348

Malitch KN, Kadik AA, Badanina IY, Zharkova EV (2011b) Redox conditions of formation of osmium-rich minerals from the Guli massif, Russia. Geochem Int 49:726–730

Malitch KN, Efimov AA, Badanina IY (2011c) Contrasting platinum-group mineral assemblages from chromitites of the Nizhny Tagil and Guli massif (Russia): implications for composition, sources and age. Dokl Earth Sci 441:1514–1518

Malitch KN, Badanina I, Belousova E, Lord R, Meisel T, Murzin V, Pearson N (2014) Ru–Os–Ir alloys and Ru–Os sulfides from oceanic mantle: evidence of robustness of Os-isotope system. Goldschmidt Conf Abstr 2014, p 1575

Marchesi C, Griffin WL, Garrido CJ, Bodinier J-L, O'Reilly SY, Pearson N (2010) Persistence of mantle lithospheric Re–Os signature during asthenospherization of the subcontinental lithospheric mantle: insights from in situ isotopic analysis of sulfides from the Ronda peridotite (Southern Spain). Contrib Mineral Petr 159:315–330

Marchesi C, González-Jiménez JM, Gervilla F, Garrido CJ, Griffin WL, O'Reilly SY, Proenza JA, Pearson NJ (2011) In situ Re–Os isotopic analysis of platinum-group minerals from the Mayarí–Cristal ophiolitic massif (Mayarí–Baracoa Ophiolitic Belt, eastern Cuba): implications for the origin of Os-isotope heterogeneities in podiform chromitites. Contrib Mineral Petr 161:977–990

Marchetto CML (1990) Platinum-group minerals in the O'Toole (Ni–Cu–Co) deposit, Brazil. Econ Geol 85:921–927

Matveev S, Ballhaus C (2002) Role of water in the origin of podiform chromitite deposits. Earth Planet Sci Lett 203:235–243

McCallum IS (1996) The Stillwater Complex. *In*: Cawthorn RG (ed) Layered Intrusions, Developments in Petrology 15, Elsevier, Amsterdam, p 441–483

McDonald AM, Cabri LJ, Rudashevsky NS, Stanley CJ, Rudashevsky VN, Ross KC (2008) Nielsenite, $PdCu_3$, a new platinum-group mineral intermetallic mineral species from the Skaergaard Intrusion, Greenland. Can Mineral 46:709–716
McElduff B, Stumpfl EF (1990) Platinum-Group Minerals from the Troodos Ophiolite, Cyprus. Miner Petrol 42:211–232
McGowan NM, Griffin WL, González-Jiménez JM, Belousova E, Afonso JC, Shi R, McCammon CA, Pearson NJ, O'Reilly SY (2015) Tibetan chromitites: excavating the slab graveyard. Geol 43:179–182
McLaren CH, De Villiers JPR (1982) The platinum-group chemistry and mineralogy of the UG-2 chromitite layer of the Bushveld Complex. Econ Geol 77:1348–1366
Melcher F, Grum W, Simon G, Thalhammer TV, Stumpfl EF (1997) Petrogenesis of the ophiolitic giant chromite deposits of Kempirsai, Kazakhstan: a study of solid and fluid inclusions in chromite. J Petrol 38:1419–1458
Merkle RKW (1992) Platinum-group minerals in the middle group of chromitite layers at Marikana, western Bushveld Complex: indications for collection mechanisms and post-magmatic modification. Can J Earth Sci 29:209–221
Mernagh TP, Hoatson DM (1995) A laser-raman microprobe study of platinum-group minerals from the Munni Munni layered intrusion, west Pilbara Block, western Australia. Can Mineral 33:409–417
Mertie JB Jr (1969) Economic geology of the platinum metals. US Geol Surv Prof Paper 630
Mitchell RH, Keays RR (1981) Abundance and distribution of gold, palladium and iridium in some spinel and garnet lherzolites – implications for the nature and origin of precious metal-rich intergranular components in the upper mantle. Geochim Cosmochim Acta 45:2425–2442
Mogessie A, Stumpfl EF, Weiblen PW (1991) The role of fluids in the formation of platinum-group-minerals, Duluth Complex, Minnesota; Mineralogic, textural and chemical evidence. Econ Geol 86:1506–1518
Mondal SK, Mathez EA (2007) Origin of the UG-2 chromitite layer, Bushveld Complex. J Petrol 48:495–510
Moreno T, Prichard HM, Lunar R, Monterrubio S, Fisher PC (1999) Formation of a secondary PGM assemblage in chromitites from the Herbeira ultramafic massif, Cabo Ortegal, NW, Spain. Eur J Mineral 11:363–378
Moreno T, Gibbons W, Prichard H, Lunar R (2001) Platiniferous chromitite and the tectonic setting of ultramafic rocks in Cabo Ortegal NW Spain. J Geol Soc London 158:601–614
Morgan JW (1986) Ultramafic xenoliths: clues to the Earth's late accretionary history. J Geophys Res 91B:12375–12387
Mostert AB, Hofmeyr PK, Potgieter GA (1982) The platinum-group mineralogy of the Merensky Reef at Impala Platinum Mines, Bophuthatswana. Econ Geol 77:1385–1394
Mudd GM (2012) Key trends in the resource sustainability of platinum group elements. Ore Geol Rev 46:106–117
Mungall JE (2005) Magmatic geochemistry of the platinum-group elements. *In*: Exploration for platinum-group elements deposits. Short Course Ser Vol 35, Mungall JE (ed) Mineral Assoc Canada, p 1–34
Mungall JE, Brenan JM (2014) Partitioning of platinum-group elements and Au between sulfide liquid and basalt and the origins of mantle–crust fractionation of the chalcophile elements. Geochim Cosmochim Acta 125:265–289
Mungall JE, Naldrett AJ (2008) Ore deposits of the platinum-group elements. Elements 4:253–258
Mungall JE, Andrews DRA, Cabri LJ, Sylvester PJ, Tubrett M (2005) Partitioning of Cu, Ni, Au, and platinum-group elements between monosulfide solid solution and sulfide melt under controlled oxygen and sulfur fugacities. Geochim Cosmochim Acta 69:4349–4360
Naldrett AJ (1989) Stratiform PGE deposits in layered intrusions. Rev Econ Geol 4:135–166
Naldrett AJ (2004) Magmatic Sulfide Deposits: Geology, Geochemistry and Exploration. Springer, Berlin
Naldrett AJ, Cabri LJ (1976) Ultramafic and related mafic rocks: their classification and genesis with special reference to the concentration of nickel sulfides and platinum-group elements. Econ Geol 71:1131–1158
Naldrett AJ, Duke JM (1980) Platinum metals in magmatic sulfide ores. Science 208:1417–1424
Naldrett A, Kinnaird J, Wilson A, Yudovskaya M, Chunnett G (2011) Genesis of the PGE-enriched Merensky Reef and chromitite seams of the Bushveld Complex. *In*: Li C, Ripley EM (eds) Review in Economic Geology: Magmatic Ni–Cu and PGE Deposits: Geology, Geochemistry and Genesis 17:235–296
Nazimova YV, Zaytsev VP, Petrov S (2011) The Galmoenan massif, Kamchatka, Russia: Geology, PGE mineralization, applied mineralogy and beneficiation. Can Mineral 49:1433–1453
Neigishi H, Arai S, Yurimoto H, Ito S, Ishimaru S, Tamura A, Akizawa N (2013) Sulfide-rich dunite within a thick Moho transition zone of the northern Oman ophiolite: implications for the origin of Cyprus-type sulfide deposits. Lithos 164–167:22–35
Nielsen TFD, Rasmussen H, Rudashevsky NS, Kretser YuL, Rudashevsky VN (2003a) PGE and sulphide phases of the precious metal mineralisation of the Skaergaard intrusion. 1. Sample 90–23A, 807. Geol Surv Denmark and Greenland: 2003/47
Nielsen TFD, Rasmussen H, Rudashevsky NS, Kretser YuL, Rudashevsky VN (2003b) PGE and sulphide phases of the precious metal mineralisation of the Skaergaard intrusion. 2. Sample 90–24, 1057. Geol Surv Denmark and Greenland: 2003/48
Nielsen TFD, Rasmussen H, Rudashevsky NS, Kretser YuL, Rudashevsky VN (2003c) PGE and sulphide phases of the precious metal mineralisation of the Skaergaard intrusion. 3. Sample 90–18, 1010. Geol Surv Denmark and Greenland: 2003/52

Nielsen TFD, Rasmussen H, Rudashevsky NS, Kretser YuL, Rudashevsky VN (2003d) PGE and sulphide phases of the precious metal mineralisation of the Skaergaard intrusion. 4. Sample 90–23A, 806. Geol Surv Denmark and Greenland: 2003/53

Nielsen TFD, Rasmussen H, Rudashevsky NS, Kretser YuL, Rudashevsky VN (2003e) PGE and sulphide phases of the precious metal mineralisation of the Skaergaard intrusion. 5. Sample 90–23A, 808. Geol Surv Denmark and Greenland: 2003/54

Nixon GT (1997) Ni–Cu sulfide mineralization in the Turnagain Alaskan-type complex: a unique magmatic environment. Geological Fieldwork 1997, British Columbia Min Energy Mines, BC Geol Surv Paper 1998–1

Nixon GT, Cabri LJ, Laflame JHF (1990) Platinum-group element mineralization in lode and placer deposits associated with the Tulameen Alaskan-type complex, British Columbia. Can Mineral 28:503–535

Noble JA, Taylor HPJr (1960). Correlation of the ultramafic complexes of southeastern Alaska with those of other parts of North America and the world. 21st International Geological Congress Report, Part XIII, p 188–197

O'Driscoll B, Day JMD, Daly JS, Walker RJ, McDonough WF (2009a) Rhenium–osmium isotope and platinum-group elements in the Rum Layered Suite, Scotland: Implications for Cr-spinel seam formation and the composition of the Iceland mantle anomaly. Earth Planet Sci Lett 286:41–51

O'Driscoll B, Donaldson CH, Daly JS, Emeleus CH (2009b) The roles of melt infiltration and cumulate assimilation in the formation of anorthosite and a Cr-spinel seam in the Rum Eastern Layered Intrusion. Lithos 111:6–20

O'Driscoll B, Emeleus CH, Donaldson CH, Daly JS (2010) Cr-spinel seam petrogenesis in the Rum Layered Suite, NW Scotland: cumulate assimilation and in situ crystallisation in a deforming crystal mush. J Petrol 51:1171–1201

O'Driscoll B, Day JMD, Walker RJ, Daly JS, McDonough WF, Piccoli PM (2012) Chemical heterogeneity in the upper mantle recorded by peridotites and chromitites from the Shetland Ophiolite Complex, Scotland. Earth Planet Sci Lett 333–334:226–237

O'Driscoll B, Butcher A, Latypov R. (2014a) New insights into precious metal enrichment on the Isle of Rum, Scotland. Geol Today Feat 30:134–141

O'Driscoll B, Clay PL, Cawthorn RG, Lenaz D, Adetunji J, Kronz A (2014b) Trevorite: Ni-rich spinel formed by metasomatism and desulphurization processes at Bon Accord, South Africa? Mineral Mag 78:145–163

Oberthür T (2011) Platinum-group element mineralization of the Main Sulfide Zone, Great Dyke, Zimbabwe. Rev Econ Geol 17:329–349

Oberthür T, Cabri LJ, Weiser ThW, McMahon G, Müller P (1997) Pt, Pd and other trace elements in sulfides of the Main Sulfide Zone, Great Dyke, Zimbabwe-a reconnaissance study. Can Mineral 35:597–609

Oberthür T, Weiser ThW, Müller P, Lodziak J, Cabri LJ (1998) New observations on the distribution of platinum group elements (PGE) and minerals (PGM) in the MSZ at Hartley Mine, Great Dyke, Zimbabwe. *In*: Proc 8th Int Platinum Symp. S Afr Inst Mining Metall Symp Ser S18:293–296

Oberthür T, Weiser ThW, Gast L, Wittich C, Kojonen K (2000) Mineralogy applied to the evaluation and processing of platinum ores of the Main Sulfide Zone, Great Dyke, Zimbabwe. *In*: Rammlmair D, Mederer J, Oberthür T, Heimann RB, Pentinghaus H (eds) Applied Mineralogy. Balkema, Rotterdam, p 379–382

Oberthür T, Davis DW, Blenkinsop TG, Höhndorf A (2002) Precise U–Pb mineral ages, Rb–Sr and Sm–Nd systematics for the Great Dyke, Zimbabwe-constraints on late Archean events in the Zimbabwe Craton and Limpopo Belt. Precambrian Res 113:293–305

Oberthür T, Weiser ThW, Gast L, Kojonen K (2003) Geochemistry and mineralogy of the platinum-group elements at Hartley platinum mine, Zimbabwe. Pt. 1: Primary distribution patterns in pristine ores of the Main Sulfide Zone of the Great Dyke. Miner Deposita 38:327–343

Ohnestetter M (1992) Platinum-group element enrichment in the upper mantle peridotites of the Monte Maggiore ophiolitic massif (Corsica, France): Mineralogical evidence for ore-forming metasomatism. Miner Petrol 46:85–107

Okrugin AV (2011) Origin of platinum-group minerals in mafic and ultramafic rocks: from dispersed elements to nuggets. Can Mineral 49:1397–1412

Orberger B, Friedrich G, Woermann E (1988) Platinum-group element mineralisation in the ultramafic sequence of the Acoje ophiolite block, Zambales, Philippines. *In*: Geoplatinum 87. Prichard PJ, Potts, Bowles JFW, Cribb SJ (eds) Elsevier, London, p 361–380

Ortega L, Lunar R, García-Palomero F, Moreno T, Martín Estévez JR, Prichard HM, Fisher PC (2004) The Aguablanca Ni–Cu–PGE deposit, southwestern Iberia: magmatic ore-forming processes and retrograde evolution. Can Mineral 42:325–335

Pagé P, Barnes S-J, Bédard JH, Zientek ML (2012) In situ determination of Os, Ir, and Ru in chromites formed from komatiite, tholeiite and boninite magmas: implications for chromite control of Os, Ir and Ru during partial melting and crystal fractionation. Chem Geol 302–303:3–15

Palme H (2008) Platinum-group elements in cosmochemistry. Elements 4:234–238

Palme H, Wlotzka F (1976) A metal particle from a Ca,Al-rich inclusion from the meteorite Allende, and the condensation of refractory siderophile elements. Earth Planet Sci Lett 33:45–60

Palme H, Hutcheon ID, Spettel B (1994) Composition and origin of refractory-metal-rich assemblages in a Ca,Al-rich Allende inclusion. Geochim Cosmochim Acta 58:495–513

Paraskevoupoulos GM, Economou MI (1986) Komatiite-type ultramafic lavas from the Agrilia Formation, Othrys Ophiolite complex, Greece. Ofioliti 11:293–304
Patton Jr. WW, Box SE, Grybeck DJ (1994) Ophiolites and other mafic–ultramafic complexes in Alaska. *In:* The Geology of North America Vol. G1, The Geology of Alaska: Boulder Colorado. Plafker G, Berg HC (eds), Geol Soc North Amer, p 671–685
Pattou L, Lorand J-P, Gros M (1996) Non-chondritic platinum-group element ratios in the Earth's mantle. Nature 379:712–715
Pearson NJ, Alard O, Griffin WL, Jackson SE, O'Reilly SY (2002) In situ measurement of Re–Os isotopes in mantle sulfides by Laser Ablation Multi-Collector Inductively- Coupled Mass Spectrometry: analytical methods and preliminary results. Geochim Cosmochim Acta 66:1037–1050
Pearson DG, Parman SW, Nowell GM (2007) A link between large mantle melting events and continent growth seen in osmium isotopes. Nature 449:202–205
Peck DC, Keays RR (1990) Insights into the behavior of precious metals in primitive, S-undersaturated magmas: Evidence from the Heazlewood River Complex, Tasmania. Can Mineral 28:553–577
Penberthy CJ, Merkle RKW (1999) Lateral variations in the platinum- group element content and mineralogy of the UG-2 chromitite layer, Bushveld Complex. S Afr Jour Geol 102:240–250
Pedersen, RB, Johannesen GM, Boyd R (1993) Stratiform platinum-group element mineralizations in the ultramafic cumulates of the Leka ophiolite complex, central Norway. Econ Geol 88:782–803
Peregoedova A, Ohnenstetter M (2002) Collectors of Pt, Pd, and Rh in S-poor Fe–Ni–Cu sulfide system at 760 ºC: experimental data and application to ore deposits. Can Mineral 40:527–561
Peregoedova A, Barnes S-J, Baker DR (2004) The formation of Pt–Ir alloys and Cu–Pd-rich sulfide melts by partial desulfurization of Fe–Ni–Cu sulfides: results of experiments and implications for natural systems. Chem Geol 208:247–264
Peyerl W (1982) The influence of the Driekop dunite pipe on the platinum-group mineralogy of the UG2 chromitite in its vicinity. Econ Geol 77:1432–1438
Piña R, Lunar L, Ortega L, Gervilla F, Alapieti T, Martinez C (2004) Origen de los fragmentos maficos–ultramaficos de la brecha mineralizada del yacimiento de Ni–Cu–EGP de Aguablanca (Badajoz). Revista Soc Españ Mineral 2:19–20
Piña R, Gervilla F, Ortega L, Lunar R (2008) Mineralogy and geochemistry of platinum-group elements in the Aguablanca Ni–Cu deposit (SW Spain). Miner Petrol 92:259–282
Piña R, Romeo I, Ortega L, Lunar R, Capote R, Gervilla F, Tejero R, Quesada C (2010) Origin and emplacement of the Aguablanca magmatic Ni–Cu–(PGE) sulfide deposit, SW Iberia: a multidisciplinary research. Geol Soc Am Bull 122:915–925
Piña R, Gervilla F, Barnes S-J, Ortega L, Lunar R (2012) Distribution of platinum-group and chalcophile elements in the Aguablanca Ni–Cu sulfide deposit (SW Spain): Evidence from a LA-ICP-MS study. Chem Geol 302–303:61–75
Pirrie D, Power MR, Andersen JCØ, Butcher AR (2000) Platinum-group mineralization in the Tertiary Igneous Province: new data from Mull and Skye, Scottish Inner Hebrides, UK. Geol Mag 137:651–658
Podlipskiy MYU, Sidorov EG, Tolstykh ND, Krivenko AP (1999) Cobalt-bearing malanite and other Pt-thiospinels from the Maior River placers. Geol Geofiz 40:629–633
Power MR, Pirrie D, Anderson JCØ, Butcher AR (2000) Stratigraphical distribution of platinum-group minerals in the Eastern Layered Series, Rum, Scotland. Miner Deposita 35:762–775
Power MR, Pirrie D, Andersen JCØ (2003) Diversity of platinum-group element mineralisation in the North Atlantic Igneous Province: new evidence from the Sgaorishal plugs, Rum, U.K. Geol Mag 144:499–512
Power MR, Pirrie D, Jedwab J, Stanley CJ (2004) Platinum-group element mineralization in an As-rich magmatic sulphide system, Talnotry, southwest Scotland. Mineral Mag 68:395–411
Prichard HM, Neary CR, Potts PJ (1986) Platinum-group minerals in the Shetland Ophiolite. *In*: Metallogeny of Basic and Ultrabasic Rocks. Gallagher MJ, Ixer RA, Neary CR (eds) Inst Min Metall, London, UK, p 395–412
Prichard HM, Lord RA (1993) An overview of the PGE concentrations in the Shetland ophiolite complex. *In*: Magmatic Processes and Plate Tectonics. Prichard HM, Alabaster T, Harris NBW, Neary CR (eds) Geol Soc Spec Publ 76:273–294
Prichard HM, Ixer RA, Lord RA, Maynard J, Williams, N (1994) Assemblages of platinum-group minerals and sulfides in silicate lithologies and chromite-rich rocks within the Shetland ophiolite. Can Mineral 32:271–294
Prichard HM, Barnes S-J, Maier WD, Fisher PC (2004) Variations in the nature of the platinum-group minerals in a cross section through the Merensky Reef at Impala platinum: implications for the mode of formation of the reef. Can Mineral 42:423–437
Prichard HM, Neary CR, Fisher FC, O'Hara MJ (2008) PGE-rich Podiform chromitites in the Al'Ays ophiolite complex, Saudi Arabia: an example of critical mantle melting to extract and concentrate PGE. Econ Geol 103:1507–1529
Prichard HM, Fisher PC, McDonald I, Knight R, Sharp D, Williams J (2013a) The distribution of PGE and the role of arsenic as a collector of PGE in the Spotted Quoll nickel ore deposit in the Forrestania Greenstone Belt, Western Australia. Econ Geol 108:1903–1921

Prichard HM, Knight RD, Fisher PC, McDonald I, Zhou M-F, Wang CY (2013b) Distribution of platinum-group elements in magmatic and altered ores in the Jinchuan intrusion, China: an example of selenium remobilisation by postmagmatic fluids. Miner Deposita 48:767–786

Proenza JA, Gervilla F, Melgarejo JC, Bodinier JL (1999) Al- and Cr-rich chromitites from the Mayarí–Baracoa Ophiolitic Belt (Eastern Cuba): consequence of interaction between volatile-rich melts and peridotites in suprasubduction mantle. Econ Geol 94:547–566

Proenza JA, Gervilla F, Melgarejo JC, Vera O, Alfonso P, Fallick A (2001) Genesis of sulfide-rich chromite ores by the interaction between chromitite and olivine-norite dikes in the Potosí Mine (Moa-Baracoa ophiolitic massif, eastern Cuba). Miner Deposita 36:658–669

Proenza JA, Zaccarini F, Escayola M, Cábana C, Shalamuk A, Garuti G (2008) Composition and textures of chromite and platinum-group minerals in chromitites of the western ophiolitic belt from Córdoba Pampeans Ranges, Argentine. Ore Geol Rev 33:32–48

Razin LV, Yurkina KV (1971) Platinum-group minerals in ores of the Gusevogorsk titanomagnetite deposit, (the Middle Urals). Geol Rudnych Mestorozh 2:102–109 (in Russian)

Reich M, Utsunomiya S, Kesler S, Wang L, Ewing RC, Becker U (2006) Thermal behavior of metal nanoparticles in geologic materials. Geol 34:1033–1036

Riches AJV, Rogers NW (2011) Mineralogical and geochemical constraints on the origin, ancient veining, and multi-stage modification of the Lherz peridotite. Geochim Cosmochim Acta 75:6160–6182

Righter K, Downs RT (2001) The crystal structures of synthetic Re- and PGE-bearing magnesioferrite spinels: implications for impacts, accretion and the mantle. Geophys Res Lett 28:619–622

Righter K, Campbell AJ, Humayun M, Hervig RL (2004) Partitioning of Ru, Rh, Pd, Re, Ir, and Au between Cr-bearing spinel, olivine, pyroxene and silicate melts. Geochim Cosmochim Acta 68:867–880

Rose D, Viljoen F, Knoper M, Rajesh H (2011) Detailed assessment of platinum-group minerals associated with chromitite stringers in the Merensky Reef of the eastern Bushveld Complex, South Africa. Can Mineral 49:1385–1396

Roy-Barman M, Wasserburg GJ, Papanastassiou DA, Chaussidon M (1998) Osmium isotope compositions and Re–Os concentrations in sulfide globules from basaltic glasses. Earth Planet Sci Lett 154:331–347

Rudashevsky NS, Mochalov AG, Orlova MP (1982) Silicate inclusions in natural iron–platinum alloys of the Konder massif. Dokl Akad Nauk SSSR 266:977–981 (in Russian)

Rudashevsky NS, McDonald AM, Cabri LJ, Nielsen TDF, Stanley CJ, Kretser YuL, Rudashevsky VN (2004) Skaergaardite, PdCu, a new platinum-group intermetallic mineral from the Skaergaard intrusion, Greenland. Mineral Mag 68:615–632

Rudashevsky NS, Kretser YL, Rudashevsky VN, Nielsen TFD (2009) Gold, PGE and sulfide phases of the precious mineralization of the Skaergaard intrusion, parts 6 and 7. Geol Surv Denmark and Greenland Reports 54 and 68

Rudraswami NG, Shyam Prasad M, Plane JMC, Berg T, Feng W, Balgar S (2014) Refractory metal nuggets in different types of cosmic spherules. Geochim Cosmochim Acta 131:247–266

Sattari P, Brenan JM, Horn I, McDonough WF (2002) Experimental constraints on the sulphide– and chromite–silicate melt partitioning behavior of rhenium and platinum-group elements. Econ Geol 97:385–398

Scheel JE (2007) Age and Origin of the Turnagain Alaskan type Intrusion and Associated Ni-Sulphide Mineralization, North-Central British Columbia, Canada. M.Sc. thesis, Univ. British Columbia, Vancouver, British Columbia

Scheel JE, Scoates JS, Nixon GT (2009) Chromian spinel in the Turnagain Alaskan-type ultramafic intrusion, Northern British Columbia, Canada. Can Mineral 47:63–80

Shcheka GG, Lehmann B, Gierth E, Gömann K, Wallianos A (2004) Macrocrystals of Pt–Fe alloy from the Kondyor PGE placer deposit, Khabarovskiy Kray, Russia: trace-element content, mineral inclusions and reaction assemblages. Can Mineral 42:601–6176

Schoenberg R, Kruger FJ, Nagler TF, Meisel T, Kramers JD (1999) PGE enrichment in chromitite layers and the Merensky Reef of the Bushveld complex; a Re–Os and Rb–Sr isotope study. Earth Planet Sci Lett 172: 49–64

Schouwstra RP, Kinloch ED, Lee CA (2000) A short geological review of the Bushveld Complex. Plat Metal Rev 44:33–39

Schwander D, Berg T, Ott U, Schönhense G, Palme H (2011) Refractory metal nuggets in carbonaceous chondrites and early solar nebula condensates. Lunar Planet Sci #9070 (abstr)

Schwander D, Berg T, Ott U, Schönhense G, Palme H (2012) Formation of refractory metal alloys and their occurrence in CAIs. Meteorit Planet Sci 47: A348 #5203 (abstr)

Schwander D, Berg T, Ott U, Schönhense G, Palme H (2013) Clues to formation of refractory metal nuggets. Lunar Planet Sci XLIV Lunar Planet Inst Houston. #1959 (abstr)

Schwander D (2014) Extraktion und nanoanalytische Charakterisierung refraktärer Nanometallpartikel frühester solarer Materie und Synthese metallischer Nanopartikel aus dotierten Ca–Mg–Al–Si Schmelzen. Unpublished PhD thesis, University of Mainz, Germany

Scoates JS, Friedman RM (2008) Precise age of the platiniferous Merensky Reef, Bushveld Complex, South Africa, by the U–Pb Zircon chemical abrasion ID-TIMS technique. Econ Geol 103:465–471

Scoon RN, Teigler B (1994) Platinum-group element mineralization in the Critical Zone of the Western Bushveld Complex: I. Sulphide-poor chromitites below the UG-2, Econ Geol 89:1094–1121

Seabrook CL, Prichard HM, Fisher PC (2004) Platinum-group minerals in the Raglan Ni–Cu–(PGE) sulfide deposit, Cape Smith, Quebec, Canada. Can Mineral 42:485–497

Shi R, Alard O, Zhi X, O'Reilly, SY, Pearson NJ, Griffin WL, Zhang M, Chen X (2007) Multiple events in the Neo-Tethyan oceanic upper mantle: evidence from Ru–Os–Ir alloys in the Luobusa and Dongqiao ophiolitic podiform chromitites, Tibet. Earth Planet Sci Lett 261:33–48

Sideek S, El Goresy A (1996) Phase relations of sulphide minerals at Akarem area and platinum-group minerals in chromites from Abu Seifein chromite. Abstr Centennial Geol Surv Egypt, Cairo, p 168–169

Simon JI, Young ED, Russell SS, Tonui EK, Dyl KA, Manning CE (2005) A short timescale for changing oxygen fugacity in the solar nebula revealed by high-resolution ^{26}Al–^{26}Mg dating of CAI rims. Earth Planet Sci Lett 238:272–283

Slansky E, Johan Z, Ohnenstetter M, Barron LM, Suppel D (1991) Platinum mineralization in the Alaskan- type intrusive complexes near Fifield, N.S.W., Australia. 2. Platinum-group minerals in placer deposits at Fifield. Miner Petrol 43:161–180

Sparks RSJ, Baker L, Brown RJ, Field M, Schumacher J, Stripp G, Walters A (2006) Dynamical constraints on kimberlite volcanism. J Volcanol Geoth Res 155:18–48

Stockman HW, Hlava PF (1984) Platinum-group minerals in Alpine chromitites from southwestern Oregon. Econ Geol 79:492–508

Stone WE, Fleet ME (1990) Platinum–iron alloy (Pt_3Fe) in kimberlite from Fayette County, Pennsylvania. Am Mineral 75:881–885

Stone WE, Fleet ME, Crocket ME, Kingston DM (1992) Platinum-group minerals in pyroxenite from the Boston Creek Flow basaltic komatiite, Abitibi greenstone belt, Ontario. Can Mineral 30:109–119

Suppel D, Barron LM (1986) Platinum in basic to ultrabasic intrusive complexes at Fifield: A preliminary report. Quat notes, Geol Surv New S Wales 65:1–8

Sylvester PJ, Ward BJ, Grossman L, Hutcheon ID (1990) Chemical compositions of siderophile element-rich opaque assemblages in an Allende inclusion. Geochim Cosmochim Acta 54:3491–3508

Talkington RW, Lipin BR (1986) Platinum-group minerals in chromite seams of the Stillwater Complex, Montana. Econ Geol 81:1179–1186

Talkington W, Watkinson DH, Whittaker PJ, Jones PC (1983) Platinum-group mineral inclusions in chromite from the Bird River Sill, Manitoba. Miner Deposita 18:245–255

Tarkian M, Hunken U, Tokmakchieva M, Bogdanov K (2003) Precious-metal distribution and fluid-inclusion petrography of the Elatsite porphyry copper deposit, Bulgaria. Miner Deposita 38:261–281

Taylor HP (1967) The zoned ultramafic complexes of southeastern Alaska. *In:* Ultramafic and Related Rocks. Wylie, PJ (ed) New York-London-Sydney, p 97–121

Thalhammer OAR, Stumpfl E, Panayiotou A (1986) Postmagmatic, hydrothermal origin of sulfide and arsenide mineralization at Limassol Forest, Cyprus. Miner Deposita 21:95–105

Thalhammer OAR, Prochaska W, Mühlhans HW (1990) Solid inclusions in chrome-spinels and platinum group element concentration from the Hochgrössen and Kraubath Ultramafic Massifs (Austria). Contrib Mineral Petr 105:66–80

Tistl M (1994) Geochemistry of platinum-group elements of the zoned ultramafic Alto Condoto complex, northwest Colombia. Econ Geol 89:158–167

Todd SG, Keith DW, LeRoy LW, Schissel DJ, Mann EL, Irvine TN (1982) The J-M platinum–palladium reef of the Stillwater Complex, Montana: I. Stratigraphy and petrology. Econ Geol 77:1454–1480

Tolstykh ND, Sidorov EG, Kozlov AP (2004) Platinum-group minerals in lode and placer deposits associated with the Ural–Alaskan-type Gal'Moenan complex, Koryak–Kamchatka Platinum belt, Russia. Can Mineral 42:619–630

Torres-Ruiz J, Garuti G, Gazzotti M, Gervilla F, Fenoll Hach-Alí P (1996) Platinum-group minerals in chromitites from the Ojen lherzolite massif (Serranía de Ronda, Betic Cordillera, Southern Spain). Miner Petrol 56:25–50

Tredoux M, de Wit MJ, Hart RJ, Armstrong RA, Lindsay NM, Sellschop JPF (1989) Platinum group elements in a 3.5 Ga nickel–iron occurrence: Possible evidence of a deep mantle origin. J Geophys Res 94(B1):795–813

Tredoux M, Lindsay NM, Davies G, McDonald I (1995) The fractionation of platinum-group elements in magmatic systems with the suggestion of a novel causal mechanism. S Afr J Geol 98:157–167

Tredoux M, Zaccarini F, Garuti G, Miller DE (In Press) Phases in the Ni–Sb–As system which occur in the Bon Accord oxide body, Barberton greenstone belt, South Africa. Mineral Mag

Tsikouras B, Pe-Piper G, Piper DJW, Hatzipanagiotou K (2008) Triassic rift-related komatiite, picrite and basalt, Pelagonian continental margin, Greece. Lithos 104:199–215

Ukhanov AV, Mochalov AG, Ustinov VI (1997) Fluid-driven PGE redistribution in the alkaline–ultrabasic Konder massif: Oxygen isotope data. Geokhimiya 4:443–450 (in Russian)

Uysal I, Sadiklar MB, Tarkian M, Karsli O, Aydin F (2005) Mineralogy and composition of the chromitites and their platinum-group minerals from Ortaca (Mugla-SW Turkey): evidence for ophiolitic chromitite genesis. Miner Petrol 83:219–242

Vermaak CF, Hendricks LP (1976) A review of the mineralogy of the Merensky Reef, with specific reference to new data on the precious metal mineralogy. Econ Geol 71:1244–1269

Viljoen MJ, Schürmann LW (1998) Platinum group metals. *In*: The Mineral Resources of Southern Africa, Wilson MGC, Anhaeusser CR (eds) Council for Geoscience, p 532–568

Voordouw R, Gutzmer J, Beukes NJ (2010) Zoning of platinum group mineral assemblages in the UG-2 chromitite determined through in situ SEM-EDS-based image analysis. Miner Deposita 45:147–159

Vuorelainen Y, Häkli TA, Hänninen E, Papunen H, Reino J, Törnroos R (1982) Isomertieite and other platinum-group minerals from the Konttijärvi layered mafic intrusion, northern Finland. Econ Geol 77:1511–1518

Vymazalová A, Laufek F, Drábek M, Haloda J, Sidorinová T (2009) Pašavaite, $Pd_3Pb_2Te_2$, A new platinum-group mineral species from the Noril'sk-Talnakh Ni–Cu Cample, Russia. Can Mineral 47:53–62

Vymazalová A, Laufek F, Drábek M, Stanley CJ, Baker RJ, Bermejo R, Garuti G, Thalhammer O, Proenza JA, Longo F (2012) Application of synthetic material for characterization of new PGM: Zaccariniite. *In:* Uysal I, Zaccarini F, Vymazalová A (eds) Workshop Abstract book s. 15. Karadeniz Technical University. Trabzon

Wager LR, Brown GM (1968) Layered igneous rocks. Edinburgh: Oliver and Boyd

Walker RJ (2009) Highly siderophile elements in the Earth, Moon and Mars: Update and implications for planetary accretion and differentiation. Chem Erde 69:101–125

Walker RJ, Hanski E, Vuollo J, Liip J (1996) The Os isotopic composition of Proterozoic upper mantle: evidence for chondritic upper mantle from the Outokumpu ophiolite, Finland. Earth Planet Sci Lett 141:161–173

Wang KL, O'Reilly SY, Griffin WL, Pearson NJ, Zhang M (2009) Sulfides in mantle peridotites from Penghu Island, Taiwan: Melt percolation, PGE fractionation, and the lithospheric evolution of the South China block. Geochim Cosmochim Acta 73:4531–4557

Wark DA, Lovering JF (1978) Refractory platinum metals and other opaque phases in Allende Ca–Al-rich inclusions. Lunar Planet Sci Meeting abstracts, 1421

Watkinson DH, Melling DR (1989) Genesis of Pd–Pt–Au–Ag–Hg minerals in Cu-rich sulfides; Salt Chuck mafic–ultramafic rock complex, Alaska. Geol Assoc Can Mineral Assoc Can Program Abstr 14, A48

Werle JI, Ikramuddin M, Mutschler FE (1984) Allard stock, La Plata Mountains, Colorado-An alkaline rock hosted porphyry copper precious metal deposit. Can J Earth Sci 21:630–641

Wirth R, Reid D, Schreiber A (2013) Nanometer-sized platinum-group minerals (PGM) in base metal sulfides: new evidence for an orthomagmatic origin of the Merensky Reef PGE ore deposit, Bushveld Complex, South Africa. Can Mineral 51:143–155

Yang J-S, Robinson PT, Dilek Y (2014) Diamonds in ophiolites. Elements 10:127–130

Yang K, Seccombe PK (1993) Platinum group minerals in the chromitites from the Great Serpentinite Belt, NSW, Australia. Miner Petrol 47:263–286

Yokoyama T, Walker RJ (2016) Nucleosynthetic isotope variations of siderophile and chalcophile elements in the Solar System. Rev Mineral Geochem 81:107–160

Yuan C (2001) Parageneses of platinum-group minerals. Geoscience 15:131–142

Zaccarini F, Anikina E, Pusharev E, Rusin I, Garuti G (2004a) Palladium and gold minerals from the Baronskoe-Kluevsky ore deposit (Volkovsky complex, Central Urals, Russia). Miner Petrol 82:137–156

Zaccarini F, Pushkarev EV, Fershtater GB, Garuti G (2004b) Composition and mineralogy of PGE-rich chromitites in the Nurali lherzolite-gabbro complex, southern Urals Russia. Can Mineral 42:545–562

Zaccarini F, Garuti G, Pushkarev EV (2011) Unusually PGE-rich chromitite in the Butyrin vein of the Kytlym Uralian-Alaskan complex, northern Urals, Russia. Can Mineral 49:1413–1431

Zaccarini F, Tredoux M, Miller DE, Garuti G, Aiglsperger T, Proenza JA (2014) The occurrence of platinum-group element and gold minerals in the Bon Accord Ni-oxide body, South Africa. Am Mineral 99:1774–1782

Zhang M, Kamo SL, Li C, Hu P, Ripley EM (2010) Precise U–Pb zircon–baddeleyite age of the Jinchuan sulfide ore-bearing ultramafic intrusion, western China. Miner Deposita 45:3–9

Zhou MF, Malpas J, Song XY, Robinson PT, Sun M, Kennedy AK, Lesher CM, Keays RR (2002) A temporal link between the Emeishan large igneous province (SW China) and the end-Guadalupian mass extinction. Earth Planet Sci Lett 196:113–122

Zientek ML (2012) Magmatic ore deposits in layered intrusions - Descriptive model for reef-type PGE and contact-type Cu–Ni–PGE deposits. US Geol Surv Open File, 2012–1010

Zientek ML, Czamanske GK, Irvine TN (1985) Stratigraphy and nomenclature for the Stillwater Complex. *In*: The Stillwater Complex, Montana: Geology and Guide. Butte, Montana. Czamanske GK, Zientek ML (eds) Montana Bur Min Geol Spec Publ 92, p 21–32

Zientek ML, Oscarson RL (1986) Textural association of platinum-group minerals from the J-M Reef, Stillwater Complex, Montana. US Geol Surv Circ 995, p 75–76

Zientek ML, Cooper RW, Corson SR, Geraghty EP (2002) Platinum-group element mineralization in the Stillwater Complex, Montana. *In*: Geology, Geochemistry, Mineralogy and Mineral Benefication of Platinum Group Element. Cabri LJ (ed) Can Inst Min Metall Petrol Spec Vol 54, p 459–481

APPENDIX

PGM in placers associated with ophiolite complexes

Platinum-group minerals have been reported in many placer deposits derived from ophiolites (*Supplementary Table* 2). These detrital PGM have generally been sampled in chromite-rich beach sands associated with river terraces or coastline fans, formed as a result of mechanical erosion of chromite-bearing peridotites (e.g., Meibom et al. 2002 and references therein). The vast majority of ophiolite-derived PGM-bearing placers are uneconomic but some of them were mined using artisanal methods for their associated gold in the Middle Ages (e.g., Krstić and Tarkian 1997 and references therein). Platinum-group mineral bearing placers are associated with ophiolites in Papua New Guinea (Harris and Cabri 1991; Weiser and Bachmann 1999), Adamsfield in Tasmania (Hattori and Hart 1991; Brandon et al. 1998, 2006; Pearson et al. 2007), Meratus-Bobaris in Borneo (Harris and Cabri 1991; Hattori et al. 2004; Coggon et al. 2011), Samar in the Philippines (Nakagawa and Franco 1997), Hokkaido in Japan (Hattori and Hart 1991; Nakawaga and Franco 1997; Hirata et al. 1998), Veluce in Yugoslavia (Krstić and Tarkian 1997), the Rhodope Complex (Tsintsov and Damayanov 1994; Tsintsov 2000, 2003, 2004), Sagua de Tánamo in eastern Cuba (Díaz-Martínez et al. 1998), southwestern Oregon and northern California (Walker et al. 1997; Bird et al. 1999; Meibom and Frei 2002; Meibom et al. 2004; Walker et al. 2005; Pearson et al. 2007), and in the ophiolites of Karaginsky in the Kamchatka peninsula (Tolstykh et al. 2009). Additionally, placer PGM have been found in laterites developed on the ophiolites of Samar and Dinagat islands (Franco et al. 1993; Nakawaga and Franco 1997) and the Pirogues River in New Caledonia (Augé and Legendre 1994).

Ophiolite placer PGM occurrences. Approximately 80% of PGM in placers associated with ophiolites are Os–Ru–Ir alloys (*Supplementary Table* 2), comprising many of the possible mineral species. Other significant phases, in order of abundance, are laurite, sulfarsenides of Ir–Pt–Rh (irarsite, platarsite, and hollingworthite), arsenides (sperrylite) and Pt–Fe–Cu alloys (isoferroplatinum, tetraferroplatinum, and tulameenite). Other accessory PGM in these types of placer deposits include Pt-sulfides (cooperite, cuproiridsite), Pt-tellurides (moncheite) and rare chengdeite (Ir_3Fe). The Os–Ir–Ru alloys show a variety of grain sizes (from a few μm up to a few mm in the largest dimension) and morphologies (from rounded to angular). The Os–Ir–Ru alloys may be homogeneous, zoned or porous. The intergrowth or exsolution patterns of the different IPGE may result in complex internal structures, which have been used to distinguish these types of alloys. For example, Bird et al. (1999) and Walker et al. (2005) differentiated the Os–Ir–Ru alloys in the southwestern Oregon placers as being portions of either lamellae or host matrix (see Figs. 1 and 2 of Walker et al. 2005). Inclusions of other PGM, base-metal sulfides or silicates in the Os–Ir–Ru alloys are not uncommon, but are much less frequent than observed in Pt–Fe alloys of CUAAC. They typically consist of other micro-PGM alloys that are co-genetic, exsolution products or silicates.

In addition to the alloy phases, other PGM in ophiolite-derived placers may show a range of morphologies and sizes. Hattori et al. (2004) reported different grain morphologies in placer-hosted laurite from Borneo; '*…including euhedral grains with conchoidal fractures and pits, and spherical grains with no crystal faces, probably because of abrasion…*'. Placer laurites often contain inclusions of silicates (amphibole, epidote, clinopyroxene, serpentine, olivine, anorthite), BMS (base-metal sulfide; pyrite, pyrrhotite, pentlandite and chalcopyrite) and composite inclusions of silicate + sulfide + alloy (Coggon et al. 2011). Similarly, Tsintsov (2004) recognized two types of placer sperrylite based on '*…the degree of mechanical processing during the exogenic transport: very strongly or relatively weakly processed…*'. According to the latter author, sperrylite that undergoes abrasion during transport exhibits smooth grain surfaces; these grains partially preserve crystal faces but the edges and apices between them are considerably smoothed. In contrast, sperrylite that was

transported over short distances has undergone less mechanical abrasion, resulting in better preservation of crystal faces but with pitted surfaces and/or mechanical defects formed by breakages during transport.

In addition to mechanical alteration of placer PGM, chemical alteration is also observed. Augé and Legendre (1994) reported abundant PGM oxides in the placers of the Pirogues River (New Caledonia), including Pt–Fe oxides, Ir–Fe–Pt–Rh oxides (Ir–Fe–Rh, Fe–Rh–Pt, Pt–Ir–Fe–Rh) and Ru–Mn–Fe oxides. These oxide grains show large infilled cracks, suggesting volume loss by replacement of a precursor mineral as well as bands concentrically arranged around partly desulfurized PGM (e.g., laurite). Augé and Legendre (1994) interpreted these microstructures as evidence that the remobilization of PGE in the supergene environment may facilitate growth of secondary PGM. More recently Hattori et al. (2010) analyzed these oxides using X-ray absorption spectroscopy and confirmed that these minerals are not true PGE-oxides, but likely comprise a sub-microscopic intergrowth of native PGE with Fe-oxides. Krstić and Tarkian (1997) also reported the presence of RuO_2 in placers associated with the Veluce ophiolite (Serbia). Another example of remobilization of the PGE in placers was provided by Díaz-Martínez et al. (1998) who described composite PGM nuggets in the Sagua de Tánamo River with at least three generations of laurite and Ir-arsenide. These particles consist of an early generation of Os-rich laurite (magmatic) replaced by a network of veins of secondary Os-free laurite; the contact between these two types of laurites is marked by a third variety having a composition intermediate between both.

Pt–Re–Os and S isotope systematics of ophiolite-derived placer PGM. The examination of the Re–Os–Pt isotopic compositions of detrital ophiolite PGM has greatly contributed to establishing fundamental constraints on the Os isotopic composition and heterogeneity of the convecting upper mantle. A number of studies have reported Os isotopic analyses of detrital Os–Ir–Ru alloys and laurites from placer deposits derived from ophiolites. Hattori and Hart (1991) observed significant dispersion of the $^{187}Os/^{186}Os$ ratios (1.022 ± 0.006 to 1.050 ± 0.006; $^{187}Os/^{188}Os = 0.1229 \pm 0.0007$ to 0.1263 ± 0.0007) in five Os-rich iridium grains from two massifs (Teshio and Onnabetsu) on Hokkaido, Japan. One osmium grain analyzed by Hirata et al. (1998) in the Horonobe ophiolitic massif of Hokkaido Island yielded $^{187}Os/^{188}Os = 0.12611 \pm 0.00028$). The latter authors noted that there were no significant variations in the $^{187}Os/^{188}Os$ isotopic ratios within the grain but important changes in the $^{183}W/^{188}Os$ ratio (0.002–0.006), which they interpreted as due to zoning or multi-stage growth. An analysis of one osmium grain in the same study yielded $^{187}Os/^{186}Os = 1.066 \pm 0.006$ ($^{187}Os/^{188}Os = 0.1282 \pm 0.0007$). In the placers associated with ophiolites on Kalimantan (Borneo), the Os–Ir–Ru alloys (including iridium, osmium and ruthenium) yield $^{187}Os/^{186}Os$ ratios between 1.041 ± 0.006 ($^{187}Os/^{188}Os = 0.1252 \pm 0.0007$) and 1.084 ± 0.006 ($^{187}Os/^{188}Os = 0.1304 \pm 0.0007$), less radiogenic than laurite (1.044 ± 0.10 to 1.088 ± 0.10; Hattori and Hart 1991; $^{187}Os/^{188}Os = 0.1256 \pm 0.0120$ to 0.1304 ± 0.0120). More recently, Coggon et al. (2011) analyzed the Pt–Re–Os isotopes of 260 PGM grains, including laurite, Pt–Fe alloys and one sperrylite from the Meratus Mountains (Borneo). Laurite yields $^{187}Os/^{188}Os$ between 0.13445 ±0.000014 and 0.122117 ± 0.000035 ($n = 81$); a much more restricted range than that shown by the Pt–Fe alloys (0.125063 ± 0.000042 to 0.140674 ± 0.000056; $n = 178$). Collectively, the PGM yield a Pt–Os isochron age of 197.8 ± 8.1 Ma (2σ), which fits well with published age constraints for the ophiolite in question. Hattori and Hart (1991) analyzed the Os isotope compositions of five grains of osmium from the placers of Adamsfield (Tasmania) that yielded $^{187}Os/^{186}Os$ isotopic ratios between 1.013 ± 0.006 and 1.028 ± 0.006 ($^{187}Os/^{188}Os = 0.1219 \pm 0.0007$ to 0.1237 ± 0.0007). Walker et al. (1997) and Brandon et al. (1998) carried out repeat analyses of an iridium grain from 19 Mile Creek (Tasmania) and obtained $^{186}Os/^{188}Os = 0.1198346$–$0.119841$ and $^{187}Os/^{188}Os = 0.123801$–$0.123824$. Pearson et al. (2007) analyzed 72 osmium grains from different localities worldwide that yielded a wide range of $^{187}Os/^{188}Os$ ratios between 0.11965 ± 0.00003 and 0.12234 ± 0.00002.

Several detrital Os–Ir alloys from different placers (southwestern Oregon and northern California) have been examined for Re–Os isotopes by different authors. For example, Hirata et al. (1998) carried out five spot analyses on one grain of Ir from Lower River (California), which yielded variable $^{186}Os/^{188}Os$ (0.12047 ± 0.00012 to 0.12060 ± 0.00002) and $^{187}Os/^{188}Os$ (0.12127 ± 0.00007 to 0.121322 ± 0.00007). Walker et al. (1997) and Brandon et al. (1998) analyzed the Os isotopic composition of Os-rich Ir grains derived from different ophiolitic massifs of California and Oregon and revealed relatively homogeneous $^{186}Os/^{188}Os$ (0.119829–0.1198361) but heterogeneous $^{187}Os/^{188}Os$ (0.119940–0.12329) isotopic ratios. The Ir and Os grains analyzed by Bird et al. (1999) from the same locality yield roughly similar $^{186}Os/^{188}Os$ (0.1195563–0.1198489) but more radiogenic $^{187}Os/^{188}Os$ (0.124787–0.129307) isotopic ratios. More recently, Meibom and Frei (2002), Meibom et al. (2002, 2004), Walker et al. (2005) and Pearson et al. (2007) have used N-TIMS and LA-ICP-MS to provide a more complete picture of the Os isotopic composition of the placer iridium and osmium grains derived from tectonic peridotites in northwestern California and southwest Oregon. A total of 739 Os–Ir alloy grains reveal large heterogeneities of $^{187}Os/^{188}Os$ (0.10953 ± 0.000003 to 0.18703 ± 0.0003) and yield T_{RD} model ages as old as 2.7 Ga (Pearson et al. 2007). Malitch et al. (2011) also used N-TIMS and LA-ICP-MS to analyze Re–Os isotopes on 19 detrital Ru–Os–Ir alloy grains from the Kunar massif in the Chelyuskin ophiolite (northeastern Taimyr, Russia). The $^{187}Os/^{188}Os$ ratios of the studied alloys ranged from 0.1094 ± 0.0004 to 0.1241 ± 0.0004, with corresponding model ages (relative to the present-day chondritic uniform reservoir, 0.12863 ± 0.00046; Chen et al. 1998) calculated between 0.64 and 2.6 Ga.

Hattori et al. (2004) analyzed the sulfur isotopes of 14 placer laurites from Tambanio (Borneo). They noted that '*…the values of all grains show a narrow spread in* $\delta^{34}S$ *values (+1.16 ± 0.36 ‰) and minor enrichment in* ^{34}S*, but they are very close to the meteorite standard value 0. The values are independent of the morphology and the composition of the grains…*'.

The origin of ophiolite-derived placer PGM. The origin of PGM found in placers associated with ophiolites is subject to debate, and two principal models exist as follows: (1) they simply represent magmatic grains that were liberated from their primary bedrock; (2) they are grains formed in the supergene setting as a result of remobilization of the PGE under appropriate conditions.

The placer PGM studied by Hattori et al. (2004) and Coggon et al. (2011) in Borneo are a good example for illustrating the first hypothesis. The placer laurite grains described by these authors contain euhedral and droplet-like inclusions of BMS (made up of aggregates of chalcopyrite + bornite + pentlandite + heazlewoodite) identical to those found in primary laurites hosted in the chromitites of the Sagua de Tánamo ophiolite (eastern Cuba; González-Jiménez et al. 2012). The nature of the BMS and the shape of the inclusions suggest that these inclusions crystallized contemporaneously with laurite at high (magmatic)-temperatures. This interpretation is consistent with the fact that these placer laurites also yield S isotopic ratios typical of mantle sulfides, as opposed to the fractionated and variable S isotope signatures expected from grains formed in the supergene environment (Hattori et al. 2004). These sulfides, like the coexisting Pt–Fe alloys in the placers, also contain a suite of silicates typically precipitated at high *T* from a magma, clearly indicating that these grains are primary in origin. Coggon et al. (2011) interpreted the similar $^{187}Os/^{188}Os$ ratios in these placer and *in situ* chromitite-hosted PGM to be additional evidence for the primary origin of the placer PGM. Their placer PGM yielded a relatively precise $^{186}Os/^{188}Os$ vs. $^{190}Pt/^{188}Os$ isochron age (197.8 ± 8.1 Ma (2σ); MSWD = 0.90), fitting well with the published age of the ophiolite. They concluded that the Pt–Os isotopic system is unaffected in single PGM during surficial processes and can be used to track the origin of the detrital PGM. These results confirm the previous observation of Malitch et al. (2003), who interpreted the similar 'unradiogenic' $^{187}Os/^{188}Os$ ratios in placer PGM in the Chelyuskin ophiolite and *in-situ* PGM in chromitites

of the Kraubath ophiolite, as evidence that the Re–Os system '*…remains unchanged from the time of formation of the PGM until now, despite later thermal events, which occurred in the vicinity of ophiolite-type complexes…*'.

The second hypothesis for the origin of placer PGM is illustrated by so-called PGM oxides from the laterites of the Pirogues River (Augé and Legendre 1994). The PGM oxides replace pre-existing magmatic sulfides and Pt–Fe alloys, providing clear evidence that PGM can grow in the supergene environment (e.g., Aiglsperger et al. 2014). Platinum–Re–Os isotopic data for these PGM do not exist, so evaluating how robust the isotopic systems are under these specific conditions of alteration is difficult. However, it might be expected that PGM precipitation from (or interaction with) surficial solutions may have significantly modified $^{187}Os/^{188}Os$ ratios, as these solutions typically contain both crustal ^{187}Re and common ^{187}Os. The recent results of González-Jiménez et al. (2012) have shown that metamorphic fluids are able to disturb the Re–Os isotopic system within single PGM grains and more importantly, the secondary PGM that have precipitated from these fluids yield $^{187}Os/^{188}Os$ ratios within the range of typical mantle values. If this situation applies to secondary PGM in placers, then only detailed petrographic study will reveal the true origin of the PGM grains. Interestingly, alluvial 'lamellae'-type Os–Ir alloy grains from southwestern Oregon are richer in Fe and more radiogenic than 'matrix'-type alloys (Walker et al. 2005), suggesting the possible contribution of common Os by secondary oxidizing (i.e., magnetite-bearing) solutions. The very radiogenic compositions of some PGM found in placers associated with the Freetown Complex (Bowles et al. 2000) are also worth considering in this regard (see main text).

PGM mineralization in CUAAC placer deposits

The CUAAC are usually associated with placer deposits that contain PGM (Weiser, 2002). Some of the most important are associated with the massifs of the Russian Platinum Belts in the Urals (Nizhny Tagil and Uktus) and Koryak-Kamchatka (Galmoenan), the margins of the Aldan Shield (Inagli, Guli, Zolotaya and Fadeevka), Tulameen (British Columbia), Alto Condoto (Colombia), Fifield (Australia) and Red Mountain (southern Goodnews Bay, southwestern Alaska) (*Supplementary Table* 3). Placer deposit PGM similar to those found in the aforementioned CUAAC have also been reported in river systems draining poorly exposed mafic and ultramafic rocks of the Yukon (i.e., Florence and Burwash Creeks) and British Columbia (island-arc terrane of Quesnellia) territories in Canada, the Esmeraldas Province (Ecuador), Atonambao-Manamposty (Madagascar), Kompiam (Papua New Guinea), the Serpentinite Hill Complex (Dundas Trough, western Tasmania) and with the laterite of the Yubdo Deposit in Ethiopia (*Supplementary Table* 3).

Occurrences of CUAAC placer-hosted PGM. Weiser (2002) presented a list of PGM associated with selected placer deposits worldwide. He showed that PGM in placers associated with CUAAC are typically in the size range of several tens of μm to a few mm, with a few exceptional grains reaching up to several kilograms (e.g., 11.641 kg for a Pt–Fe alloy from Colombia and 5 kg for a Pt–Fe alloy found in Nizhny Tagil in the Urals). In these types of placer deposit, the PGM are rarely single homogeneous grains but they commonly form heterogeneous nuggets made up of extensive PGM intergrowths with smaller inclusions and/or exsolution of other PGM, silicates, base-metal sulfides or oxides. Some exotic nuggets may contain large euhedral inclusions of chromite or magnetite with diameters of up to a few tens of μm, totally surrounded by interstitial platinum (e.g., Tulameen, Nixon et al. 1990; Nizhny Tagil, Augé et al. 2005).

Most placer deposits associated with CUAAC have a PGM assemblage dominated by large grains of isoferroplatinum or Pt characterized by rounded shapes and/or well-preserved crystal faces, which often contain bleb-like inclusions or crystallographically oriented exsolution lamellae of Os, Ir, and (rarely) Ru (*Supplementary Table* 3). Where present, such

exsolution textures are interpreted as evidence for a high temperature origin of the PGM. Other smaller PGM trapped by the Pt-alloy at high temperatures are euhedral grains of the laurite–erlichmanite solid solution series and a variety of sulfides of Ir–Pt–Rh ± base metals (bowieite, xingzhongite, kashinite, and thiospinels such as cuproiridsite, malanite, and cuprorhodsite), and Pt–Pd (cooperite–braggite). The sulfides are accompanied by sulfarsenides (platarsite, hollingworthite and irarsite), arsenides (cherepanovite and vincentite), keithconnite and tolovkite. Other Pt–Fe alloys such as tetraferroplatinum, tulameenite, ferroanplatinum or hongshiite may also comprise the main part of the nugget or occur as intergrowths with isoferroplatinum. The placer deposits associated with the Atonambao-Manamposty CUAAC in Madagascar contain a PGM assemblage dominated by a diversity of unidentified Pd, Pt, Rh, Ir, and Os sulfides that coexist with keithconnite, vincentite, and unnamed Pt_3Cu. A further example of a placer deposit with a peculiar PGM assemblage has been reported from the Guli Massif (Aldan Shield), which contains abundant PGM of Os, Ir, and Ru, including large grains of osmium (Malitch and Kostoyanov 1999; Malitch and Badanina 2011; Malitch et al. 2011; Merkle et al. 2012; *Supplementary Table* 3).

In addition to minerals interpreted as high-temperature phases, placer nuggets may contain PGM assemblages formed at low-temperature. The high-temperature PGM assemblage comprising placer nuggets is commonly subjected to lower temperature modification during metamorphism, serpentinization and alteration. The resultant secondary PGM typically form rims around, or fill fractures penetrating into, the primary PGM. In the CUAAC placers that drain the Urals and Koryak–Kamchatka platinum belts, the secondary PGM assemblage is dominated by Pt–Fe–Cu alloys (i.e. tulameenite, Pt-rich copper and unnamed Pt–Fe–Cu compounds), sulfarsenides and/or Ir–Rh–Os such as irarsite, hollingworthite, and osarsite. Other rare secondary PGM found in the placers of Nizhny Tagil include Pd and Pd_2S_7. Overall, this assemblage is similar to that observed in placers associated with the Tulameen Complex, comprising native platinum and Pt–Fe–Cu alloys (undefined Pt–Cu and Pt–Cu), antimonides (genkinite, geversite), sulfantimonides (tolokvite and undefined RhSbS) hollingworthite, sperrylite, and kotulskite. Secondary PGM found in the placers of Goodnews Bay (Alaska) are also Pt–Fe–Cu alloys (tetraferroplatinum and tulameenite) and sulfarsenides (irarsite, platarsite, and osarsite). The only secondary PGM identified in the Atonambao-Manamposty CUAAC is an Ir oxide. Shcheka and Lehmann (2007) have reported superfine (3–5 μm) discontinuous Au films on Pt–Fe alloys grains often overgrown by cooperite rims in the placer nuggets of Fadeevka (eastern Russia); these authors interpreted that the Au rims formed via selective Pt–Fe leaching during low-temperature alteration and/or weathering of the PGM alloy.

Large Pt–Fe or Os–Ir alloy nuggets from placers typically contain numerous inclusions of silicates, which may have been formed before (imposing their crystal morphology on the surrounding alloys) or after (by exsolution during cooling) their host alloy (Johan 2002). In some cases the silicate inclusions are monomineralic but more commonly they are polyphase, preserving an approximation of the composition of the original mineralizing fluid/melt. Primary silicates trapped at high temperature by the alloy include both anhydrous (olivine, pyroxene, plagioclase, K-feldspar, quartz, silicate-glass) and hydrous (amphibole, phlogopite, biotite, vermiculite) phases. Frequently observed secondary silicates in placer PGM nuggets are talc and chlorite (Johan et al. 2000; Johan 2002; Malitch and Thalhammer 2002; Tolstykh et al. 2004, 2005; Okrugin 2011). Other inclusions hosted in the alloy nuggets are oxides (chromite, spinel, magnetite, titanite, ilmenite, corundum), diamond and apatite (cf. Weiser 2002 and references therein).

Re–Os-isotopes in PGM from CUAAC-associated placer deposits. In their pioneering work, Hattori and Cabri (1992) used an ion microprobe to analyze the Os isotopic compositions of Os–Ir alloys and laurite–erlichmanite grains included in larger Pt–Fe alloys from a suite of placers, including those associated with the Tulameen (British Columbia), Chocó (Colombia),

Niznhy Tagil (Russia), Yubdo (Ethiopia) and Goodnews Bay (Alaska) CUAAC. The nuggets from Yubdo yield very homogeneous $^{187}Os/^{186}Os$ ratios that range between 1.019 ± 0.010 and 1.034 ± 0.008 ($^{187}Os/^{188}Os = 0.1226 \pm 0.0012$ to 0.1244 ± 0.0010). Hattori and Cabri (1992) also note that the PGM from the Niznhy Tagil have an average $^{187}Os/^{186}Os$ value of 1.029 ± 0.006 ($^{187}Os/^{188}Os = 0.1238 \pm 0.0007$). The latter value is the same, within error, as the average $^{187}Os/^{186}Os$ value of 1.035 ± 0.006 ($^{187}Os/^{188}Os = 0.1245 \pm 0.0007$) measured for a PGM nugget from the Omutnaya River that drains the Omutnaya Dunite Massif, considered to be part of the same ultramafic belt as the Niznhy Tagil Massif and situated 180 km to the south. More recently, Malitch and Kostoyanov (1999) and Malitch and Thalhammer (2002) used N-TIMS to analyze the $^{187}Os/^{188}Os$ ratios of Os–Ir alloys recovered from placer deposits associated with the Guli, Kondyor and Inagli CUAAC. All of the alloys are characterized by low Re (<0.05 wt.%) and homogeneous $^{187}Os/^{188}Os$; ranging between 0.1248 ± 0.0003 and 0.1252 ± 0.0003 at Kondyor, between 0.1249 ± 0.0003 and 0.1250 ± 0.0003 at Inagli and between 0.1246 ± 0.0003 and 0.1260 ± 0.0003 at Guli. In a subsequent study, Malitch and Badanina (2011) used LA-MC-ICP-MS to analyze another set of Os–Ir alloy nuggets from Guli and obtained $^{187}Os/^{188}Os$ values between 0.12433 ± 0.00010 and 0.12472 ± 0.00034. The latter authors also analyzed several laurite grains from the Guli placer deposits that have $^{187}Os/^{188}Os$ compositions that range between 0.12432 ± 0.00029 and 0.12463 ± 0.00009.

Origins of PGM in placers associated with CUAAC. As noted by Weiser (2002) '*…the complete history of the platinum-bearing placer deposits and their origin is not always known with certainty*'. Evidently this statement is still valid, given the lively debate on the origin of PGM found in placers associated with CUAAC. Hattori and Cabri (1992) reviewed the ideas on the origin of PGM in placers and stated that by the mid-1960s, the prevailing view was that these minerals were originally present in ultramafic rocks and subsequently released to the placers by weathering and transportation processes. This hypothesis was largely based on studies of PGM from placer deposits of the Urals (Betekhtin 1961), Tulameen (Rice 1947) and Yubdo (Molly 1959). One of the well-accepted theories at the time was that large PGM placer nuggets were formed '*by element agglutination under a phase of hydration (low temperature) of the ultrabasic rocks*' (Ottemann and Augustithis 1967). These ideas were later used to propose the hypothesis of 'chemical accretion' that was defended by several other authors (e.g., Cousins 1973; Cousins and Kinloch 1976; Stumpfl 1974, Cabri and Genkin 1991). The observation that PGM might crystallize in lateritic soils (e.g., Bowles 1986; Barker and Lamal 1989) led Cabri and Genkin (1991) to interpret the rounded shape and colloform habits exhibited by some PGM placer nuggets as evidence of the growth of PGM in a sedimentary environment.

In their evaluation of the potential source of PGM in the placers of the Tulameen Complex, Nixon et al. (1990) concluded '*…the mineralogical and compositional discrepancies between the PGM in chromitites and placers are perhaps not as striking as certain differences in grain size and texture…*'. Hattori (2002) observed that the Os isotopic data of placer PGM are similar to primary mantle-derived PGM, and refuted their formation during sedimentary processes at low temperature. It was maintained that the isotopic data are not consistent with models invoking the dissolution and precipitation of the PGE in sediments and residual soils, as proposed by Bowles (1986). A primary origin for placer-hosted PGM, as proposed by Cabri and Genkin (1991), Cabri et al. (1996) and Nixon et al. (1990) was advocated instead. A significant body of data published subsequently demonstrate fairly convincingly that PGM found in lode mineralization and in placers share a common heritage (e.g., Razin 1976; Nixon et al. 1990; Malitch and Lopatin 1997; Malitch and Kostoyanov 1999; Garuti et al. 2002). However, it is worth noting that the grains analyzed by Hattori and co-workers were Os-rich PGM included within larger Pt–Fe alloys; significantly different to those PGM exhibiting low temperature growth habits interpreted to have been precipitated in the sedimentary environment.

Garuti et al. (2002) studied the PGM assemblages of chromitites from Kytlym and Uktus and compared them with PGM from other Ural CUAAC placers, proposing that '*…the paragenetic relationships of the Pt-alloys that we have observed in the chromitites of Kytlym and Uktus are practically the same as those reported from the alluvial nuggets of the Urals…*'. Garuti et al. (2002) also stressed the difference in grain size between the PGM (< 100 μm) locked in chromitite and the alluvial nuggets reported from the Urals; the latter may be > 2 mm in diameter. Although a few placer-hosted Pt–Fe alloys associated with CUAAC have been reported to be relatively heavy (up to ~11 kg; Weiser 2002), Garuti et al. (2002) ruled out the hypothesis that these alloys precipitated or grew in the surficial environment by either physical or chemical agglutination (e.g., Ottemann and Augustithis 1967; Cabri and Genkin 1991). According to Garuti et al. (2002), the differences in PGM grain sizes are simply an artefact produced by several concomitant factors, including (1) inability of panning techniques to recover very small particles < 20–40 μm and (2) inherent difficulty liberating small (1–35 μm) grains from their chromite host during erosion of the bedrock or crushing during laboratory processing. Garuti et al. (2002) also noted that PGM with grain sizes from several tens of μm to a few mm occur in chromite interstices or associated with interstitial silicates in massive chromitites; such grains are comparable to those recovered as nuggets in placers. This is consistent with the observation of Augé et al. (2005), who described euhedral chromite grains totally surrounded by interstitial platinum in a PGM concentrate obtained from placer samples of Nizhny Tagil. Garuti et al. (2002) concluded that large PGM in lode chromitites could be more frequent than indicated by the study of polished sections and are therefore the best source material candidates for placer nuggets. The above arguments notwithstanding, many placer-hosted PGM show coatings of other PGM ± lower-temperature silicates, indicating that a solely residual origin for placer PGM (as grains liberated from ultramafic source rocks and later concentrated by mechanical processes) is not completely sufficient to explain all natural occurrences (e.g., Shcheka and Lehmann 2007).

REFERENCES

Aiglsperger T, Proenza JA, Lewis JF, Longo F (2014) Is microbial activity causing PGM neoformation in Ni-laterites? Evidence from Falcondo (Dominican Republic). Macla 19:1–2

Augé T, Legendre O (1994) Platinum-group element oxides from the Pirogues ophiolitic mineralization, New Caledonia: Origin and Significance. Econ Geol 89:1454–1468

Augé T, Genna A, Legendre O (2005) Primary Platinum Mineralization in the Nizhny Tagil and Kachkanar Ultramafic Complexes, Urals, Russia: A genetic model for PGE concentration in chromite-rich zones. Econ Geol 100:707–732

Barker JC, Lamal K (1989) Offshore extension of platiniferous bedrock and associated sedimentation of the Goodnews Bay ultramafic complex, Alaska. Mar Mining 8:365–390

Betekhtin AG (1961) Mikroskopische Untersuchungen and Platinerzen aus dem Ural. Neues Jahrb Miner Abh 97:1–34

Bird JM, Meibom A, Frei TF, Nägler TF (1999) Osmium and lead isotopes and rare OsIrRu minerals: derivation from the core–mantle boundary region? Earth Planet Sci Lett 170:83–92

Bowles JFW (1986) The development of platinum-group minerals in laterites. Econ Geol 81:1278–1285

Bowles JFW, Lyon IC, Saxton JM, Vaughan DJ (2000) The origin of platinum group minerals from the Freetown Intrusion, Sierra Leone, inferred from osmium isotope systematics. Econ Geol 95:539–548

Brandon AD, Walker RJ, Morgan JW, Norman MD, Prichard HM (1998) Coupled ^{186}Os and ^{187}Os evidence for core–mantle interaction. Science 280:1570–1573

Brandon AD, Walker RJ, Puchtel IS (2006) Platinum–osmium isotope evolution of the Earth's mantle: constraints from chondrites and Os-rich alloys. Geochim Cosmochim Acta 70:2093–2103

Cabri LJ, Genkin AD (1991) Re-examination of Pt alloys from lode and placer deposits, Urals. Can Mineral 29:419–425

Cabri LJ, Harris DC, Weiser TW (1996) Mineralogy and distribution of the platinum-group mineral (PGM) placer deposits of the world. Explor Min Geol 5:73–167

Chen JH, Papanastassiou DA, Wasserburg GJ (1998) Re–Os systematics in chondrites and the fractionation of the platinum group elements in the early solar system. Geochim Cosmochim Acta 62:3379–3392

Coggon JA, Nowell GM, Pearson DG, Parman SW (2011) Application of the ^{190}Pt–^{186}Os isotope system to dating platinum mineralization and ophiolite formation: an example from the Meratus Mountains, Borneo. Econ Geol 106:93–117

Cousins CA (1973) Notes on the geochemistry of the platinum-group elements. Trans Geol Soc S Afr 76:77–81

Cousins CA, Kinloch ED (1976) Some observations on textures and inclusions in alluvial platinoides. Econ Geol 71:1377–1398

Díaz-Martínez R, Proenza JA, Comas J, Fernández-Bellon, Fabra JM, Guinart O, Melgarejo JC (1998) El placer lateral de playa Mejias (noreste de Cuba Oriental): un ejemplo de interacción de procesos aluviales y marinos en la concentración de minerals de elementos preciosos. Acta Geológica Hispánica 33:351–371

Franco HEA, Nakawaga M, Esguerra E, Lazo FB, Domingo EG, Togashi Y (1993) Platinum-group minerals in laterite overlying the ultramafic massif in Eastern Samar and Dinagat Island, Philippines. Res Geol Spec Issue 15:149–156

Garuti G, Pushkarev EV, Zaccarini (2002) Composition and paragenesis of Pt alloys from chromitites of the Uralian–Alaskan-type Kytlym and Uktus complexes, Northern and Central Urals, Russia. Can Mineral 40:357–376

González-Jiménez JM, Gervilla F, Griffin WL, Proenza JA, Augé T, O'Reilly SY, Pearson NJ (2012) Os-isotope variability within sulfides from podiform chromitites. Chem Geol 291:224–235

Harris DC, Cabri LJ (1991) Nomenclature of platinum-group element alloys: review and revision. Can Mineral 29:231–237

Hattori K, Hart S (1991) Osmium-isotope ratios of platinum-group minerals associated with ultramafic intrusions: Os-isotopic evolution of the oceanic mantle. Earth Planet Sci Lett 107:499–514

Hattori K, Cabri LJ (1992) Origin of platinum-group mineral nuggets inferred from an osmium-isotope study. Can Mineral 30:289–301

Hattori K (2002) A review of rhenium–osmium isotope geochemistry of platinum-group minerals and platinum mineralization, *In:* Cabri LJ (ed) The Geology, Geochemistry, Mineralogy and Mineral Beneficiation of Platinum-Group Elements. Can Inst Min Metall Petrol Spec Vol 54, p 251–271

Hattori KH, Cabri LJ, Johanson B, Zientek ML (2004) Origin of placer laurite from Borneo: Se and As contents, and S isotopic compositions. Mineral Mag 68:353–368

Hattori KH, Takahashi Y, Augé T (2010) Mineralogy and origin of oxygen-bearing platinum–iron grains based on X-ray absorption spectroscopy study. Am Mineral 95:622–630

Hirata T, Hattori M, Tanaka T (1998) In-situ osmium isotope ratio analyses of iridosmines by laser ablation-multiple collector-inductively coupled plasma mass spectrometry. Chem Geol 144:269–280

Johan Z (2002) Alaskan-type complexes and their platinum-group element mineralization. *In:* Cabri LJ (ed) The Geology, Geochemistry, Mineralogy and Mineral Beneficiation of Platinum-Group Elements. Can Inst Min Metall Petrol Spec Vol 54, p 669–719

Johan Z, Slansky E, Kelly DA (2000) Platinum nuggets from the Kompiam area, Enga Province, Papua New Guinea: evidence for an Alaskan-type complex. Miner Petrol 68:159–176

Krstić S, Tarkian M (1997) Platinum-group minerals in gold-bearing placers associated with the Veluće Ophiolite Complex, Yugoslavia. Can Mineral 35:1–21

Malitch KN, Lopatin GG (1997) New data on the metallogeny of the unique Guli clinopyroxenite–dunite massif (northern Siberia, Russia) Geol Ore Deposit 39:209–218

Malitch KN, Kostoyanov AI (1999) Model Re–Os isotopic age of the PGE mineralization at the Gulinsk massif (at the Northern Siberian Platform, Russia). Geol Ore Deposit 41:126–135

Malitch K, Thalhammer OAR (2002) Pt–Fe nuggets derived from clinopyproxenite–dunite massifs, Russia: A structural, compositional and osmium-isotope study. Can Mineral 40:395–418

Malitch KN, Junk SA, Thalhammer OAR, Melcher F, Knauf VV, Pernicka E, Stumpfl EF (2003) Laurite and ruarsite from podiform chromitites at Kraubath and Hochgrössen, Austria: New insights from osmium isotopes. Can Mineral 41:331–352

Malitch KN, Badanina IY (2011) Laurite and Osmium from the Guli Massif, Siberian Craton, Russia: New Insights from Osmium Isotopes for the Origin of PGE-Mineralization in Ultramafic Complexes. *In:* 9th Int Plat Symp Abst

Malitch KN, Badanina IY, Kostoyanov AI (2011) Initial Os-isotopic composition of Os–Ir–Ru alloys from ultramafic massifs of the Polar Siberia. Dokl Eart Sci 440:1343–1348

Meibom A, Frei R (2002) Evidence for an ancient osmium isotopic reservoir in Earth. Science 296:516–518

Meibom A, Sleep NH, Chamberlain CP, Coleman RG, Frei R, Hren MT, Wooden JL (2002) Re–Os isotopic evidence for long-lived heterogeneity and equilibration processes in the Earth's upper mantle. Nature 419:705–708

Meibom A, Frei R, Sleep NH (2004) Osmium isotopic compositions of Os-rich platinum group element alloys from the Klamath and Siskiyou Mountains. J Geophys Res 109: B02203, doi: 10.1029/2003JB002602

Merkle RKW, Malitch KN, Gräser PPH, Badanina IY (2012) Native osmium from the Guli massif, Northern Siberia, Russia. Miner Petrol 104:115–127

Molly EW (1959) Platinum deposits in Ethiopia. Econ Geol 54:467–477
Nakawaga M, Franco H (1997) Placer Os–Ir–Ru alloys and sulfides: indicators of sulfur fugacity in an ophiolite? Can Mineral 35:1441–1452
Nixon GT, Cabri LJ, Laflamme JHG (1990) Platinum-group element mineralization in lode and placer deposits associated with the Tulameen Alaskan-type complex, British Columbia. Can Mineral 28:503–535
Okrugin AV (2011) Origin of platinum-group minerals in mafic and ultramafic rocks: from dispersed elements to nuggets. Can Mineral 49:1397–1412
Ottemann J, Augustithis SS (1967) Geochemistry and origin of 'platinum-nuggets' in lateritic covers from ultrabasic rocks and birbirites of W. Ethiopia. Miner Deposita 1:269–277
Pearson DG, Parman SW, Nowell GM (2007) A link between large mantle melting events and continent growth seen in osmium isotopes. Nature 449:202–205
Razin LV (1976) Geologic and genetic features of forsterite dunites and their platinum-group mineralization. Econ Geol 71:1371–1376
Rice HMA (1947) Geology and mineral deposits of the Princeton map-area, British Columbia. Geol Surv Can Mem 243
Shcheka GG, Lehmann B (2007) Gold overprint of PGE alloy: an example from the Fadeevka Au–PGE placer, Russian Far East. Miner Petrol 89:275–282
Stumpfl EF (1974) The genesis of platinum deposits: further thoughts. Mineral Sci Eng 6:120–141
Tolstykh ND, Sidorov EG, Kozlov AP (2004) Platinum-group minerals in lode and placer deposits associated with the Ural–Alaskan-type Gal'Moenan Complex, Koryak–Kamchatka Platinum Belt, Russia. Can Mineral 42:619–630
Tolstykh N, Sidorov EG, Krivenko AP (2005) Platinum-group element placers associated with Ural– Alaska type complexes. *In:* Exploration for Platinum-Group Element Deposits. Mungall, JE (ed) Mineral Assoc Can Short Course 35:113–143
Tolstykh ND, Sidorov E, Kozlov A (2009) Platinum-group minerals from the Olkhovaya-1 placers related to the Karaginsky ophiolite complex, Kamchatskiy Mys Peninsula, Russia. Can Mineral 47:1057–1074
Tsintsov Z (2000) Platinum-group minerals in sediments from Gotse Delchev graben, SW Bulgaria. Compt Rend Acd Bulg Sci 53:73–76
Tsintsov Z (2003) Platinum-Group Minerals (PGM) from the alluvial sediments of Samokov region, West Bulgaria. Rev Bulg Geol Society 64
Tsintsov Z (2004) Sperrylite from alluvial placers of Vurbitsa River, SE Rhodopes. Bulgarian Geological Society, Annual Scientific Conference Geology, 16–17.12.2004, p 92–94
Tsintsov Z, Damyanov Z (1994) Sperrylite from Struma River alluvial placers, Blagoevgrad graben, SE Bulgaria. N Jb Miner Mh 11:518–528
Walker RJ, Morgan JW, Beary ES, Smoliar MI, Czamanske GK, Horan MF (1997) Applications of the ^{190}Pt–^{186}Os isotope system to geochemistry and cosmochemistry. Geochim Cosmochim Acta 61:4799–4807
Walker RJ, Brandon AD, Bird JM, Piccoli PM, McDonough WF, Ash RD (2005) ^{187}Os–^{186}Os systematics of Os–Ir–Ru alloy grains from southwestern Oregon. Eart Planet Sc Lett 230:211–226
Weiser TW, Bachmann HG (1999) Platinum-group minerals from the Aikora rivers area, Papua New Guinea. Can Mineral 37:1131–1145
Weiser TW (2002) Platinum-group minerals (PGM) in placer deposits. *In:* Cabri LJ (ed) The Geology, Geochemistry, Mineralogy and Mineral Beneficiation of Platinum-Group Elements. Can Inst Min Metall Petrol Spec Publ Vol 54, p 721–756